STITCHES: creating new scenarios of climate model output by stitching together pieces of existing simulations

Claudia Tebaldi[1], Abigail Snyder[1], and Kalyn Dorheim[1]

[1]Joint Global Change Research Institute, Pacific Northwest National Laboratory and University of Maryland, College Park, MD, USA

Correspondence: Claudia Tebaldi (claudia.tebaldi@pnnl.gov)

Abstract. Climate model output emulation has long been attempted to support impact research, mainly to fill-in gaps in the scenario space. Given the computational cost of running coupled Earth System Models (ESMs), which are usually the domain of super computers and require on the order of weeks to complete a century-long simulation, only a handful of different scenarios are usually chosen to externally force ESM simulations. An effective emulator, able to run on standard computers in times of the order of minutes, rather than days, could therefore be used to derive climate information under scenarios that were not run by ESMs. Lately, the necessity of accounting for internal variability has also made the availability of initial condition ensembles, under a specific scenario, important, increasing further the computational demand. At least so far, emulators have been limited to simplified ESM-like output, either seasonal, annual or decadal averages of basic quantities, like temperature and precipitation, often emulated independently of one another. With this work, we propose a more comprehensive solution to ESM output emulation. Our emulator, STITCHES, uses existing archives of Earth System Models' (ESMs) scenario experiments to construct ESM-like output under new scenarios, or enrich existing initial condition ensembles, which is what other emulators also aim to do. Importantly, however, STITCHES' output has the same characteristics of the ESM output it sets out to emulate: multivariate, spatially resolved and high frequency, representing both the forced component and the internal variability around it. STITCHES extends the idea of time-sampling - according to which climate outcomes are stratified by the global warming level at which they manifest themselves, irrespective of the scenario and time at which they occur - to the construction of a continuous history of ESM-like output over the whole 21st century, consistent with a 21st century trajectory of Global Surface Air Temperature (GSAT) derived from the scenario that has been chosen as the target of the emulation. STITCHES does so by first splitting the target GSAT trajectory into decade-long windows, then matching each window in turn to a decade-long window within an existing model simulation from the available scenario runs according to its proximity to the target in absolute size of the temperature anomaly and its rate of change. A look-up table is therefore created of a sequence of existing experiments/time windows that, when stitched together, create a GSAT trajectory "similar" to the target. Importantly, we can then stitch together much more than GSAT from these windows, i.e., any output that the ESM has saved for these experiments/time windows, at any frequency and spatial scale available in its archive. We show that the stitching does not introduce artifacts, in the great majority of cases (we look at temperature and precipitation at monthly frequency and on the native grid of the ESM, and at an index of ENSO activity, the Southern Oscillation Index). This is true even if the criteria for the identification of the decades to be stitched together are chosen to work for a smoothed time series of annual GSAT, a result we expect given the larger amount of noise affecting most other variables at finer spatial scales and higher frequencies, which therefore are more "forgiving" of the stitching. We successfully test the method's performance over many ESMs and scenarios. Only a few exceptions surface, but these less-than-optimal outcomes are always associated with a scarcity of the archived simulations from which we can gather the decade-long windows that form the building blocks of the emulated time series. In the great majority of cases, STITCHES performance is satisfactory according to metrics that reward consistency in trends, inter-annual and inter-ensemble variance, and autocorrelation structure of the time series stitched together. The method therefore can be used to create ESM-like output according to new scenarios, on the basis of a trajectory of GSAT produced according to that scenario, which could be easily obtained by a simple climate model. It can also be used to increase the size of existing initial condition ensembles. There are aspects of our emulator that will immediately disqualify it for specific applications, like when climate information is needed whose characteristics result from accumulated quantities over windows of times longer than those used as pieces by STITCHES, droughts longer than a decade for example. But for many applications, we argue that a stitched product can satisfy the climate information needs of impact researchers. STITCHES cannot emulate ESM output from scenarios that result in GSAT trajectories outside of the envelope available in the archive, neither can it emulate trajectories with shapes different from existing ones (overshoots with negative derivative, for example). Therefore, the size and characteristics of the available archives of ESM output are the principal limitations for STITCHES deployment. Thus, we argue for the possibility of designing scenario experiments within, for example, the next phase of the Coupled Model Intercomparison Project according to new principles, relieved of the need to produce a number of similar trajectories that vary only in radiative forcing strength, but more strategically covering the space of temperature anomalies and rates of change.

1 Introduction

In this paper, we introduce a novel and comprehensive solution to climate model emulation. Our principal motivation is to support the climate information needs of the impact research community under arbitrary future scenarios of anthropogenic forcings, but we believe that our proposal may potentially benefit the scenario development, integrated assessment and climate modeling communities.

The overarching problem that our method seeks to resolve stems from the computational and human labor costs of running climate model experiments according to plausible future scenarios (as opposed to idealized forcings, e.g., 1% CO_2 increase pathways) with complex Earth System Models (ESMs). High costs are involved in translating emission and land-use scenarios produced by Integrated Assessment Models (IAMs) into inputs for ESMs. Running these experiments on super-computers is also very expensive, and considerable labor costs are involved in setting them up, launching them and attending to their completion. Lastly, significant effort is involved in translating ESM output into datasets that can be used in impact analysis, for example through statistical downscaling and bias-correction (Lange, 2019).

The latest phase of the Coupled Model Intercomparison Project, Phase 6, CMIP6 (Eyring et al., 2016) prescribed standardized experiments that a large international community of modeling centers performed in order to answer a wide range of scientific questions. CMIP6 used a decentralized structure composed of self-organized MIPs, among which ScenarioMIP coordinated future scenario projections. ScenarioMIP's experimental design (O'Neill et al., 2016) had to negotiate the trade-off between ensuring that the impact, adaptation and vulnerability (IAV) research community obtained ESM output from future scenarios of relevance to their analysis framework, and respecting the competing demands on ESMs' time and resources that the larger CMIP6 effort posed. Despite the latter, the modeling community signed up almost unanimously for the ScenarioMIP request – at a minimum, running the four scenarios in its Tier 1. Each experiment involved a complex set of forcing inputs (e.g., greenhouse gases and other atmospheric element concentrations, land use change trajectories) harmonized to corresponding historical estimates and downscaled from the aggregated trajectories produced by the IAMs (Gidden et al., 2019; Hurtt et al., 2020; Meinshausen et al., 2020). The computation, preparation and provision of these forcings required a complementary community effort (https://esgf-node.llnl.gov/projects/input4mips/). ESM outcomes from ScenarioMIP experiments form the basis for myriads of studies of the physical climate system, starting from basic characterizations of scenarios ranges and differences (Tebaldi et al., 2021) to complex and focused process-based analyses. Importantly, the same results are being used to conduct integrated IAV analyses, often within the Shared Socioeconomic Pathways-Representative Concentration Pathways (SSPs-RCPs) framework (van Vuuren et al., 2014) that matches qualitative and quantitative assumptions about future societal trends (like population and GDP – the SSP part) to outcomes from simulations forced by GHG trajectories consistent with those (the RCP part).

The range of radiative forcing at 2100 covered by the experiments in Tier 1 of ScenarioMIP, when complemented by the Paris-inspired low warming scenario reaching only $1.9\mathrm{Wm}^{-2}$ by 2100, can be considered well representative of the range of future plausible outcomes, reaching up to $8.5\mathrm{Wm}^{-2}$. Ideally, however, impact analyses should be able to use an arbitrary set of scenarios within this range, not just the handful run by ESMs. This freedom from specific (CMIP6) experiments is particularly relevant when impact analyses are conducted within an IAM framework, i.e., when the integrated assessment model endogenously produces its own trajectory of emissions and therefore global temperature changes, which should be translated into consistent resolved climate information driving impacts within the same integrated modeling ecosystem. Another desirable aspect for impact risk assessment, one that also imposes a trade-off on resources, is the availability of initial condition ensembles (sometimes simply called "large ensembles") under each scenario, in order to explore the contribution of internal variability to future changes and their impacts (Hawkins and Sutton, 2009; Lehner et al., 2020).

Thus far, the need for additional scenarios not available in ESM output archives has been addressed – when at all – by simple emulators of ESM output, usually producing multi-decadal averages of temperature and – separately – precipitation change fields. Most popular has been simple pattern scaling, starting from its initial conception (Santer et al., 1990), popularized by the software MAGICC-SCENGEN (http://www.magicc.org/, Meinshausen et al. (2011)), and made more sophisticated by the possibility of producing higher frequency fields, thus representing internal variability, for example by Link et al. (2019) and Nath et al. (2022). More complex emulators have also been proposed departing from pattern scaling (Castruccio et al., 2014), or extensions of pattern scaling that use zonal averages to drive the emulation (Schlosser et al., 2013), or that emulate other metrics besides average temperature and precipitation (Huntingford and Cox, 2000), even extremes (Tebaldi et al., 2020; Quilcaille et al., 2022). In many cases, however, specific applications challenge the use of emulators in place of ESM output: impact models have evolved so to require coherent multivariate input (i.e., multiple variables that preserve their spatial and temporal correlations), often at relatively high temporal frequencies (annual or monthly, when not higher), often spanning multidecadal periods, not just time slices. It is difficult to imagine any emulator, short of having the same complexity of an ESM, able to satisfy these requirements exhaustively.

Our approach, STITCHES, emulates an ESM by using its own output as building blocks, thus reproducing by construction the high-dimensionality, complexity and multiple frequencies of original ESM output. Working with existing scenario experiments run by an individual ESM, we stitch together output from time windows/experiments that we extract from the available archive on the basis of the corresponding value of global average temperature in those time windows/experiments.

The idea of using existing simulations' output over a window when global average temperature reaches a given warming level of interest, often called time-sampling, has been frequently and prominently used in recent years (King et al., 2018; James et al., 2017). In fact, it constitutes the foundation of an entire special assessment report of the Intergovernmental Panel on Climate Change (Masson-Delmotte et al., 2018), which assessed the consequences of reaching a global warming level of 1.5°C versus higher levels. That report's impact chapter made extensive use of this approach in the absence – at the time of its writing – of ESM experiments that simulated low warming scenarios consistent with the Paris targets of 1.5°C or 2°C. Rather, windows of time within experiments run under higher scenarios were isolated when global average temperature reached 1.5°C or 2°C, and the corresponding ESM output was extracted and analyzed to describe climate at those levels, and the ensuing impacts. Here we extend this approach, which only used individual time windows, to the emulation of ESM output for entire transient scenarios, i.e., trajectories of greenhouse gases and other anthropogenic forcings evolving continuously over the 21st century (Manabe et al., 1991; King et al., 2020). We first translate the target transient scenario into its GSAT time series over the century. We then split the GSAT trajectory into decade-long windows, and we identify for each of them a "nearest neighbor" among decade-long windows from GSAT trajectories available from existing ESM experiments. Nearest neighbors are defined in terms of the level of GSAT warming, but also the warming rate in the window. The sequence of nearest neighbors, identifying time-windows and experiments from the archive that constitute the building blocks of the emulation, becomes in practice a sequence of pointers that can be used to extract and stitch together any variable available in the ESM archive for those time windows and experiments, not just GSAT. We will show that our synthetic time series created by stitching together discrete windows are for most purposes (i.e., variables, time and spatial scales) acceptable surrogates of continuous ESM output. In other words, we show that the stitching in most cases does not introduce significant discontinuities at the seams, or otherwise spurious behavior, for most application we can envision.

In the next sections, we first describe our method in detail (Sect. 2), then present results of the emulator and document the ability of the method to reproduce output for the two intermediate scenarios of ScenarioMIP Tier 1 (SSP2-4.5 and SSP3-7.0) given only output from the two scenarios that bracket the targets, SSP1-2.6 and SSP5-8.5. This is the case for many of the ESMs that contributed to ScenarioMIP (Sect. 3.1.1). We also show how the method can be used to form additional initial condition ensemble members on the basis of the existing simulations (Sect. 3.1.2). In closing (Sect. 4), we summarize the strengths and value of our proposed emulation and discuss its limitations, highlighting what needs to be considered before applying STITCHES in place of true ESM output. We also discuss the challenges that STITCHES encounters when targeting scenarios of shapes other than regularly increasing forcings, like stabilized scenarios and overshoots, besides the obvious limitations to scenarios that produce warming levels intermediate to the existing ones. Therefore we suggest that a concerted effort could be made to facilitate the application of the emulator by choosing scenarios of different shapes, rather than scenarios that only vary in the strength of the radiative forcing, when ESM experiments are prescribed. If climate model output emulators, possibly used in a complementary fashion, become part of the overall strategy in providing climate information to the impact research community, we argue that the next ScenarioMIP design may follow different priorities from the current ones.

2 Methods

We here describe the emulator rationale and its main aspects, and discuss our validation approach.

Many applications have in the recent past focused on a window, along the length of an ESM simulation, when global average temperature change conforms to a given criterion (e.g., is on average 1.5°C with respect to a pre-industrial baseline). Climate in this window as represented by the multivariate ESM output is taken to be representative of conditions at that global temperature, no matter the scenario under which the global temperature is reached, or the time in the simulation when that happens. This "scenario-independence" assumption is valid for most atmospheric variables, which have a short memory and whose behavior depends on the instantaneous warming level. However, any quantity that is defined as an integral over time, like severe mega-droughts, or behaves in a way that is related to such integral, like sea-level change, cannot be accurately represented by this method. These caveats should not be overlooked, but for many aspects of the climate system that can be well represented by so-called time-sampling, this approach has obviated the need of running scenarios stabilizing at low warming levels through ESMs ((Masson-Delmotte et al., 2018)). It has also been instrumental for presenting climate outcomes at a range of discrete warming levels, even as recently as the latest assessment report by working group 1, the Physical Science Basis, of the IPCC, which used global warming levels as an alternative to scenarios to organize the discussion of future projections (Chen et al., 2021; Lee et al., 2021; Seneviratne et al., 2021; Gutiérrez et al., 2021).

Our method, that we suggestively call STITCHES, extends the time-sampling approach to an entire century-long global average temperature trajectory, rather than just individual and discrete global average temperature levels. Our hypothesis is that we can devise stringent enough criteria in matching successive pieces of a time series of global temperature (GSAT) generated under a target scenario to pieces chosen from available GSAT time series generated by ESMs according to the scenarios run and archived in community databases (e.g., through the CMIP6 database[1], or the CLIVAR SMILES collection[2], etc.). After matching we can stitch together these available pieces forming a time series of GSAT that appears as if it was produced by the ESM according to the new scenario. If the stitching works for GSAT, we show that we can also stitch together the corresponding pieces of simulations for many other impact-relevant variables that are in essence slaved to GSAT, at a range of time and spatial scales, without introducing artifacts and discontinuities of consequence for most application in impact research, especially in the context of the uncertainties that climate or impact models are well known to introduce.

[1] https://esgf-node.llnl.gov/projects/esgf-llnl/

[2] https://www.cesm.ucar.edu/projects/community-projects/MMLEA/

Our algorithm is applied separately to each individual ESM, as stitching together different models' lengths of simulations would almost certainly introduce spurious behavior. Within a single ESM universe, we can envision two distinct types of application of our algorithm, both of which would build from existing simulations under future scenarios by that model. In one case, the goal is to minimize the number of scenarios run by that ESM, supplementing the existing ones with stitched ones. To demonstrate the utility of STITCHES in this case, we will show the effectiveness of the method in emulating ESM output under intermediate scenarios to existing ones. This application benefits impact research, enriching the choice of scenarios whose impacts can be evaluated and compared; it also translates into saving resources by lowering the number of scenarios to be simulated by the ESMs, in no small measure when considering the large effort involved in preparing forcing inputs. (We repeat here, however, that by construction our algorithm does not allow extrapolating to levels of warming above those of the highest scenario available in the archive, or below the lowest. We will elaborate further on the limiting factors of the archive characteristics for the creation of new scenarios.) In the other case, the goal is to enrich the number of ensemble members available for existing scenarios. To this effect, STITCHES can be deployed on available simulations of the target scenario and neighboring scenarios, all potential sources of usable time samples. In this context however we also see promising complementarity with recently developed emulators that focus specifically on estimating the statistical characteristics of an ESM internal variability, and randomly generating new realizations of it (Beusch et al., 2020, 2021; Nath et al., 2022; Quilcaille et al., 2022; Liu et al., 2022).

We now describe the steps of the STITCHES algorithm. See also Figure A1 for a graphic illustration of the algorithm.

1. Time series of annual GSAT from all available simulations of the 21$^{\text{st}}$ century by a given model (all scenarios and initial condition ensemble members) are computed; the time series are made into anomalies with respect to a baseline period of 1995-2014 (we refer to GSAT time series in the following for brevity, but in all cases what we mean is GSAT *anomalies* time series);

2. a X-year running mean is applied to the GSAT time series and "pieces" are separated at a regular interval of X years (we use $X = 9$ in our demonstration). We label these pieces derived from the existing ESM simulations as "available". They identify the potential building blocks for our stitching procedure;

3. for each available piece i of smoothed, annual GSAT we compute its median value, T_i and, as a measure of the rate of temperature change within the piece, the linear trend within the piece, dT_i;

4. the same smoothing and splitting procedure is applied to the trajectory of GSAT for the target scenario to be emulated; we call the result "target pieces". Note that in the examples of this paper, we derive the target GSAT trajectory from the same ESM, run under a scenario that we choose as target of the emulation. Therefore, we apply the smoothing procedure to the target GSAT time series as well. Often the real application of the algorithm will target a time series of GSAT that is produced by a simple model, like MAGICC (http://www.magicc.org/, Meinshausen et al. (2011)) or Hector (Hartin et al., 2015), on the basis of a target scenario. These simple models do not simulate internal variability and therefore their output is in no need to be smoothed. Also, in these cases the moving average window X may be adjusted by narrowing or

extending X until the muted year-to-year variability of the smooth target series produced by the simple model is closely matched;

5. each target piece and each available piece can now be represented by a point in the two-dimensional space $(T, X * dT)$ (See Figure 1). In this space, we apply Euclidean distance (d_{l2}) to determine, for each of the target pieces its neighbors among the available pieces, within a tolerance Z, used to define a heterogeneous matching neighborhood around each target point of radius $r_i = d_{l2}\big((T_i, X * dT_i), nearest\, neighbor\big) + Z$. The choice of Z could be tailored to the characteristics of each ESM/scenario considered, but, importantly, is also directly relevant for the number of matches found and therefore the number of emulated scenarios constructed. Modification of the algorithm could also apply a differential weight to the two dimensions;

6. for each of the target pieces in the sequence spanning the 21st century, one of the neighbors within its Z radius is chosen, and the sequence of chosen available pieces is stitched together sequentially, to form the emulated GSAT trajectory. We can randomize the choice of matches, or choose nearest neighbors; importantly we do not choose the same piece more than once along the same emulated trajectory (one available piece may be neighbor of more than one target piece along the same target scenario) to avoid unrealistic repetitions, and we do not choose the same piece for the same window in time when constructing more than one ensemble member for the same scenario, to avoid what we call "collapsed" ensembles or "envelope collapse", i.e. trajectories that pass through the same values year after year over a window of time. We apply this restriction both within a single generated trajectory (once an archive window has been used for a target-year, it can not be used again for other target-years in that trajectory), and across ensemble members (if two target ensemble members match to the same archive-window for the same target-year, only one of the ensemble members may keep the match). All these constraints could of course be relaxed.

7. So far the algorithm has produced a new GSAT trajectory, emulating the target one. Importantly, however, the algorithm delivers in essence an ordered series of pointers to the time-windows and specific experiments in the archived output from which the chosen neighboring pieces were extracted. Any output from the model (any variable, in isolation or jointly, at any archived frequency, and on the native grid of the ESM) can be stitched together according to this sequence, recreating the climate outcome of the desired variable(s) consistent with the emulated scenario.

As pointed out in the description of the algorithm, its parameters (X, Z) are subject to tuning. However, they both have an interpretable function, and only small variations should be acceptable as alternative setting. In particular,

– X is the size of the smoothing window and the length of the pieces used as building blocks of the synthetic time series. Producing a time series from the available ESM GSAT series whose smoothness matches that of the target series should be the first aim of this parameter, when the target series does not contain internal variability. The use of about 9 years for GSAT has shown in our tests to be a good first guess, but trial and error for the specific simple model used may be in order. When starting from a time series that contains internal variability as our target, the same rule of thumb can be a starting point for the application of the smoothing to both target and available GSAT trajectories. Naturally the time window also dictates the size of the piece: if the window is long enough to erase internal variability, it will prevent any piece from reflecting a single phase of a mode of variability, and therefore, when stitched together, the pieces will not systematically give rise to unrealistic sequences of the phases of those modes. (This may of course fail for the longest multi-decadal modes, like NAO or PDO, so if the impact analysis is focusing on the sensitivity of the analyzed system to the phases of these modes, STITCHES may not be the best choice of emulator for this type of impacts.)

– Z is the tolerance radius within which we identify neighbors in the two-dimensional space $(T, X * dT)$. The distance along each dimension is immediately interpretable and comparable to the magnitude of the yearly values of GSAT within a piece of the smoothed series (in the T direction) and to the size of its variation within the piece, i.e., a measure of the rate of temperature change within the piece (in the $X * dT$ direction) providing guidance in choosing the size of the tolerance. The specific application may allow increasing the tolerance if a "jump" between pieces is not a concern for the application envisioned, a beneficial choice in enlarging the number of synthetic series that can be constructed from a finite archive of "building blocks". We also note here that fixing this tolerance in the space of the *smoothed* GSAT time series leaves open the possibility that the original, i.e., *non-smoothed*, yearly values can present the occasional large "jump" at the seams where the stitching is performed. This is of course also possible for the additional variables, besides GSAT, that we emulate. Our expectation is that the noise of annual or monthly variability for most variables and spatial scales is large enough to overwhelm the occasional jump at the seam. We will show that this is in fact the case in the large majority of cases, so, unless the application is particularly sensitive to year-to-year variations, it might not be considered a fatal defect. Section 3.1.3 presents some results specifically addressing the trade-off between Z and the number of replicates that STITCHES can create. We also note here that in our version of the algorithm we chose a simple Euclidean distance thus weighing the two dimensions equally, but a user may decide to have give larger weight to one of the two.

At the time of writing, STITCHES is built to integrate with (and depends on) the PANGEO CMIP6 archive of results[3]. From available runs on PANGEO, we have selected all models, all experiments and all ensemble members with reported monthly gridded data for surface air temperature and precipitation, (we will consider a smaller subset that also provides monthly gridded sea level pressure for one particular validation exercise). Model-specific archives are created separately for each ESM. Figure 1 plots the model-specific archive of $(T, X * dT)$ for six ESMs with various size ensembles for each of the scenarios (see Table 1). In the following, we either use a portion of the archive to emulate a left-out portion of the simulations, or we use all the archive to add new "ensemble members" to some scenarios. The former set-up simulates the situation where non-existing scenarios are created from existing ones, but here we also gain the prerogative of validating the emulated scenarios against their true realizations. When the goal instead is to enrich the ensemble size of existing scenarios, one has the option of using also the members of an existing initial condition ensemble, thus producing trajectories that repeat existing ensemble members' windows, but in a difference sequence, and mixed with other scenarios' windows. PANGEO contains files where both the historical period and the future have been connected under the label of a specific SSP. Our emulation applies to the entire period (1850-2100), but for brevity in most of the following we will label the various cases simply under the corresponding SSP. In fact,

[3] http://gallery.pangeo.io/repos/pangeo-gallery/cmip6/

most of the ESMs have branched different scenarios from the same historical simulations, so a strict out-of-sample construction of the historical period is in most cases impossible, and the effect is to produce emulated trajectories of the historical period that may use identical pieces to the target from the available. STITCHES main purpose remains the construction of future scenarios, though, so we do not worry about this detail as we do not predicate our assessment of performance on the historical period.

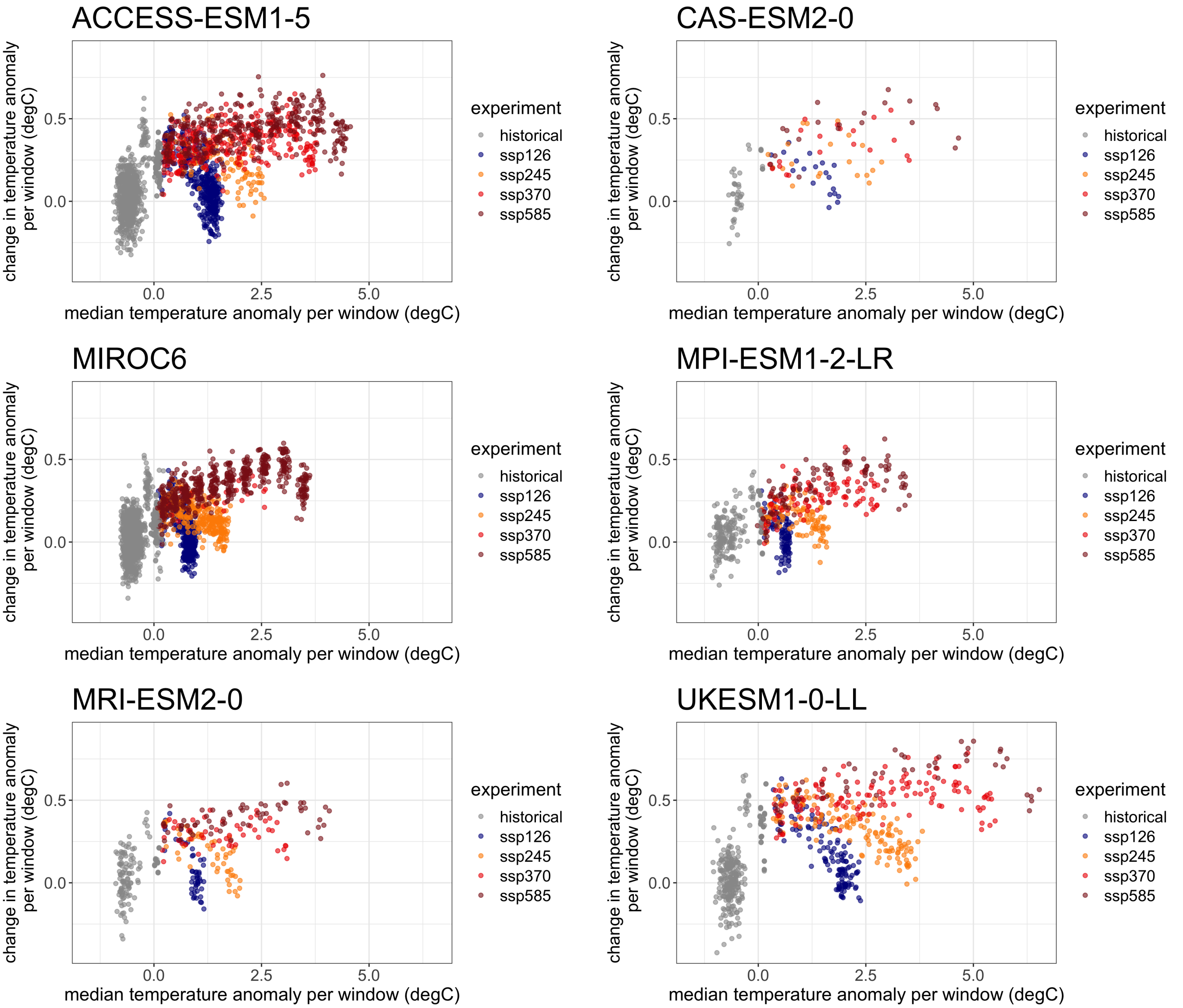

Figure 1. GSAT archive content, plotted in the space of $(T, X * dT)$, i.e., the warming level with respect to the period 1995-2014 (as represented by te median value of the X annual values in the window) and the within window rate of warming (as represented by a linear trend fitted to the X values), for six of the ESMs used in our emulation exercises. Each point corresponds to a $X = 9$-year-long window in the GSAT time series from an existing scenario simulation, indicated by the color legend.

3 Results

3.1 General tests and validation of the synthetic series

We now show results for several test cases. Table 1 details the models, experiments and ensemble sizes from the CMIP6 archive available through the PANGEO interface as of March 15, 2022.

Table 1. The ESMs, experiments from ScenarioMIP (O'Neill et al., 2016) and ensemble sizes from the PANGEO archive (as of 03/15/2022) used to derive test cases for our emulator.

Model	SSP1-2.6	SSP2-4.5	SSP3-7.0	SSP5-8.5
ACCESS-CM2	5	5	5	5
ACCESS-ESM1-5	40	10	30	35
BCC-CSM2-MR	1	1	1	1
CAMS-CSM1-0	2	2	2	2
CanESM5	25	25	25	25
CAS-ESM2-0	2	2	2	2
CMCC-CM2-SR5	1	1	1	1
CMCC-ESM2	1	1	1	1
FGOALS-g3	4	4	4	4
FIO-ESM-2-0	3	3	0	3
GISS-E2-1-G	4	5	9	4
HadGEM3-GC31-LL	1	4	0	4
MCM-UA-1-0	1	1	1	1
MIROC-ES2L	10	30	10	10
MIROC6	50	50	3	50
MPI-ESM1-2-HR	2	2	10	2
MPI-ESM1-2-LR	10	10	10	10
MRI-ESM2-0	5	5	5	6
NESM3	2	2	0	2
NorESM2-LM	1	3	3	1
NorESM2-MM	1	2	1	1
TaiESM1	1	1	1	1
UKESM1-0-LL	13	14	13	5

3.1.1 Validation of emulated intermediate scenarios

Table 2. The number of emulated trajectories produced to assess the performance of STITCHES in recreating intermediate scenarios (SSP2-4.5 and SSP3-7.0) from the two "bracketing" scenarios (SSP1-2.6 and SSP5-8.5).

Model	SSP2-4.5	SSP3-7.0
ACCESS-CM2	4	3
ACCESS-ESM1-5	5	5
BCC-CSM2-MR	1	1
CAMS-CSM1-0	2	2
CanESM5	3	1
CAS-ESM2-0	2	1
CMCC-CM2-SR5	1	1
CMCC-ESM2	1	1
FGOALS-g3	4	4
FIO-ESM-2-0	3	-
GISS-E2-1-G	4	5
HadGEM3-GC31-LL	1	-
MCM-UA-1-0	1	1
MIROC-ES2L	3	5
MIROC6	-	3
MPI-ESM1-2-HR	2	2
MPI-ESM1-2-LR	5	4
MRI-ESM2-0	1	3
NESM3	2	-
NorESM2-LM	1	1
NorESM2-MM	1	1
TaiESM1	1	1
UKESM1-0-LL	3	4

Our first goal is to test the ability of STITCHES to reconstruct ESM-like output for new scenarios using ESM output from existing scenarios. We do so for all available ESMs in the PANGEO CMIP6 archive that provide at least one member under SSP1-2.6 and one member under SSP5-8.5, targeting the two intermediate scenarios SSP2-4.5 and SSP3-7.0 (See Table 1). As already mentioned, when the goal is emulating ESM output for non-existing scenarios, our targets need to be trajectories that reach warming levels within the ones available in the archive, as our algorithm does not allow extrapolating. Similarly, STITCHES cannot emulate overshoot scenarios, given that the archive does not offer a large sample of overshoot experiments from which we can piece out our building blocks (obviously, the cooling behavior of GSAT in an overshoot experiment cannot be sampled from increasing, or flat, GSAT trajectories.) These considerations could be useful to keep in mind when designing the next phase of ScenarioMIP. Intentionally, we fix the values of the two parameters $(X, Z) = (9, 0.075)$, independently of the specific ESM targeted. A specific choice could only ameliorate the performance of our emulator for any given model used as test case. However, our common choice is the result of considering the behavior of many ESMs and finding values that are consistent with most, so, de facto, these parameters are tailored to some ESMs and less tailored to others. The best performance that we document could be regarded as what is expected when tailoring the parameter values to the specific ESM that we want to emulate.

Table 2 lists the number of emulated trajectories for each of the intermediate scenarios targeted, and for each of the models. Since this exercise is not about producing many replicates, but simply reproducing a target trajectory, for each model we set out to reproduce as many targets trajectory as there are ensemble members available under SSP2-4.5 or SSP3-7.0 if such number is less than or equal to five, capping at five the number of targets also for those models with more ensemble members potentially available as targets (see Table 1).

As mentioned in Sect. 2 our emulation approach produces the same complex, multidimensional output as an ESM does. Thus, validation could take a practically infinite number of forms, over a range of variables in isolation or jointly, and over arbitrary space and time scales. To simplify the task, however, we rely here on the well known result that – among atmospheric variables that are commonly used for impact modeling – surface air temperature has, relatively speaking, a lower amount of internal variability, and this variability becomes lower the larger the averages taken in the time and space domains. Thus, our validation will start by considering the behavior of *annual average* GSAT trajectories from STITCHES.

Our first concern is to not *systematically* introduce significant discontinuities when stitching together separate windows of ESM output, often from altogether different experiments (if always from the same ESM). To this end, we consider the year-to-year difference in the annual GSAT trajectories stitched together. The tolerance allowed for the match ($Z = 0.075$) is responsible for keeping the stitched-together pieces of the *smoothed trajectories* within a narrow interval of one another, but cannot directly control what happens when we recover the stitched-together original trajectories of (non-smoothed) annual values for this validation exercise. These could differ by a larger amount if, by chance, the 9-year pieces happen to end/begin with widely different values. Our concern is that this does not happen systematically. Table 3 reports, for each ESM, how many of these seams (as many for each trajectory as there are 9-year intervals) produce a year-to-year variation that is larger than twice the standard deviation of the real year-to-year variations. The latter are taken as either those from the archive simulations used as building blocks within the stitched trajectories (thus addressing the question "do the seams stand out from the rest of the series within which they appear?") or those in the target series (thus addressing the question "do the seams stand out compared to the year-to-year variations of the trajectories we want to emulate?"). As can be assessed, this behavior emerges only very sporadically, with most cases well below 10% of the seams. In fact the mean of these values is just above 5%, which could be the expected outcome by chance of such an exercise, even if those outliers came from the same distributions used as comparison.

Table 3. For all the models used in our emulation of ESM output under SSP2-4.5 and SSP3-7.0 we report the number of "seams" at which annual GSAT presents a jump that is larger than twice the inter-annual standard deviation. The latter is computed either from the inter-annual variations of the archive simulations used in the stitching (in practice, the inter-annual standard deviations of the stitched trajectories without including the seams in its computation), or from the target experiments (the inter-annual standard deviations of the real series that we are emulating). We also show the total number of seams from which percentages are computed.

Model	SSP2-4.5			SSP3-7.0		
	fraction (vs. archive)	fraction (vs. target)	total seams	fraction (vs. archive)	fraction (vs. target)	total seams
ACCESS-CM2	9	11	108	4	6	81
ACCESS-ESM1-5	1	1	135	9	10	270
BCC-CSM2-MR	2	2	27	2	2	27
CAMS-CSM1-0	3	3	54	3	3	54
CanESM5	2	3	81	0	0	27
CAS-ESM2-0	0	0	54	2	2	27
CMCC-CM2-SR5	0	0	27	3	2	27
CMCC-ESM2	1	1	27	1	1	27
FGOALS-g3	2	5	108	5	5	108
FIO-ESM-2-0	1	3	81			
GISS-E2-1-G	1	2	108	4	4	135
HadGEM3-GC31-LL	1	1	27			
MCM-UA-1-0	3	2	27	4	4	27
MIROC-ES2L	3	3	81	3	4	135
MIROC6	1	1	108	1	1	81
MPI-ESM1-2-HR	2	3	54	2	4	54
MPI-ESM1-2-LR	5	6	135	3	3	108
MRI-ESM2-0	3	1	27	5	5	81
NESM3	3	3	54			
NorESM2-LM	3	3	27	1	1	27
NorESM2-MM	3	4	27	2	2	27
TaiESM1	2	2	27	3	3	27
UKESM1-0-LL	3	3	81	4	5	108

We then compare linear trends fitted to the stitched trajectories to linear trends fitted to the target series, by separately
310 fitting a linear trend to the historical period (1850-2014) and the future period, 2015-2100. The trends are defined as the angular coefficient of a linear regression of annual mean values of GSAT onto years, and we consider central estimates (by

ordinary least squares) and 95% confidence intervals. We find that in all cases (109 stitched trajectories across the models and the two scenarios) historical trend central estimates for the stitched series fall comfortably within the confidence intervals of the historical trends of the target series. For the future trends, the confidence intervals of the stitched series overlap with the confidence intervals of the trends from the target series in all cases. There are 21 trajectories out of the 109 for which the central estimates fall outside those confidence intervals. In all these cases, the difference between the central estimate and the closest bound of the confidence interval is a very small value: in one single case, the central estimate is outside the confidence intervals by 0.056°C per decade. In two more cases, the values are between 0.04°C and 0.05°C; six more cases miss by 0.01-0.023°C per decade, with the remaining 12 cases falling outside the respective confidence intervals only by 0.01°C per decade or less.

We also compute inter-annual standard deviations for target and stitched trajectories, finding that once again, historical simulations remain within the ranges of the target trajectories in all cases. For the future period, in 78% of cases, the stitched series show inter-annual variability within 20% of that of the target series. The remaining 24 cases, out of the 109 tested, whose interannual variations fall outside the range of the target series show discrepancies that amount to less than 0.2°C in all cases, with a median value of 0.004°C and a third quartile of 0.05°C. Last, we compute autocorrelation and partial autocorrelation to determine the frequency characteristics of the time series. The results confirm the similarities of stitched and target series, i.e, the emulated trajectories do not show spurious behavior, with discrepancies in the AR order estimated only for lags at the margin of statistical significance (not shown).

Even if for a large majority of cases the performance of the emulator seems acceptable, and in many cases indistinguishable from the target cases, we underline that some model/experiment combinations appear to be challenging for this uniform set up. Most of these cases coincide with models providing only one ensemble member per scenario, and the spurious behavior is often found at the higher end of the warming range within the scenario emulated, where the only possible matches come from the model's only SSP5-8.5 available trajectory. It is not unlikely that the matches from the higher scenario result in less than optimal windows, given the limited choice available for the higher temperature levels. Likely, fixing the tolerance parameter to a tighter value could improve these specific emulation cases, or simply fail to create an emulated trajectory, so that the user would have an outright warning of the difficulty in matching. Here we remain within a generic setting in order to show the trade-offs at play, and identify lessons. We show in Figure 2 some examples of target (in black) and stitched (colored lines) GSAT trajectories for the two intermediate scenarios and three of the ESMs we test, differing from one another in the size of the archive available and their climate sensitivities (see caption). Additional examples are shown in Figure B1 through B7 in the appendix. From these additional figures one can also assess that the behaviors that appear to deviate from the expected are all at the tail end of the simulations, and only for those models that offer only one pair of scenarios in the archive to sample from. This is particularly true when the target scenario is SSP2-4.5, which adds the extra challenge of a trajectory that stabilizes ($dT \approx 0$) and needs to find matches among windows that, at those levels of warming, can only come from SSP5-8.5, a scenario of steadily increasing forcing. (As already mentioned, stabilization scenarios together with overshoots pose a challenge to STITCHES given the content of the CMIP6 archive from which we construct our emulations.) In these figures we use a range of colors, from cool to warm hues, to give a sense of the number of trajectories plotted in these spaghetti diagrams: while the target ensemble is always drawn in black lines, the emulated trajectories are in color, with cases showing warmer colors being those where we have created a larger number of stitched trajectories (see also Table 2).

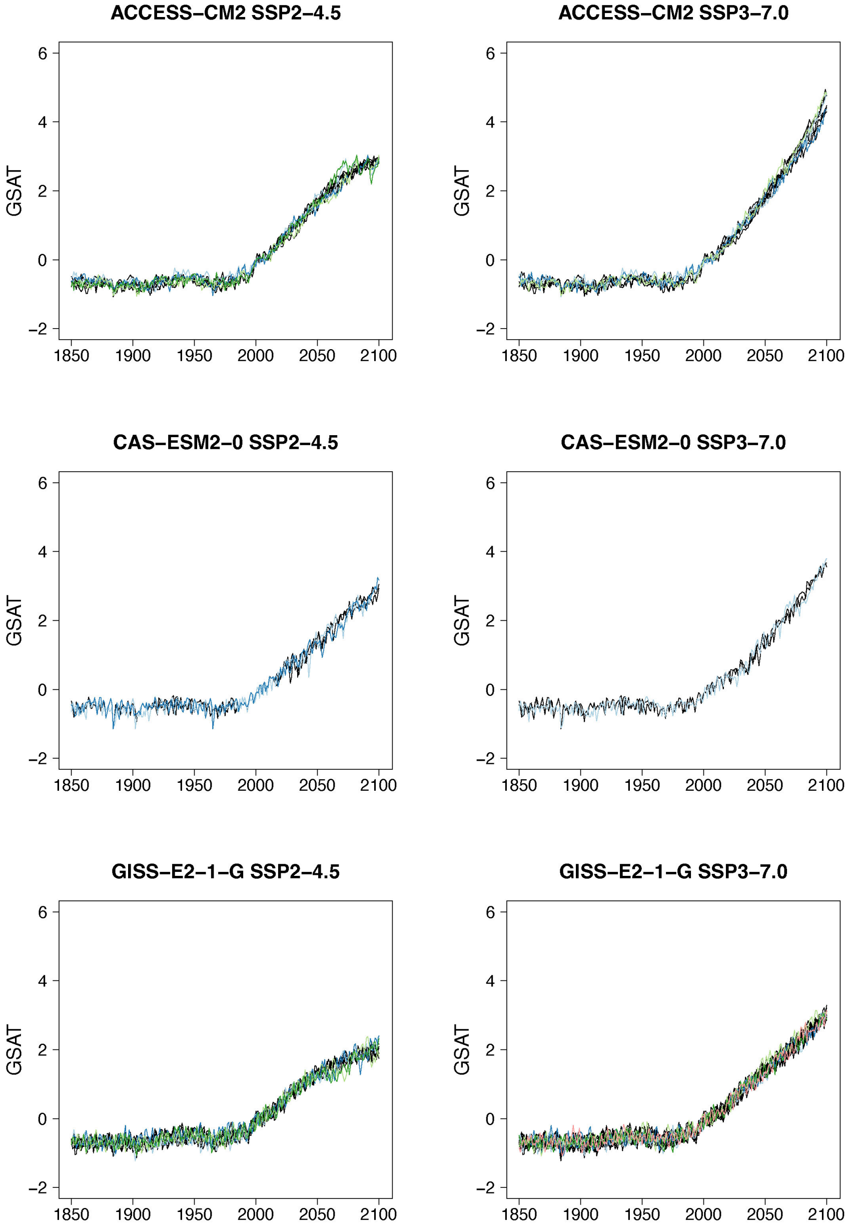

Figure 2. Examples of target (black lines) and stitched (colored) GSAT time series for three ESMs in the PANGEO archive that ran at least one trajectory along the Tier 1 experiments of ScenarioMIP (SSP1-2.6; SSP2-4.5; SSP3-7.0; SSP5-8.5). We choose these three models as they provide differing ensemble sizes (see Table 1) and are characterized by different values of equilibrium climate sensitivity (4.73K, 3.40K and 2.72K respectively). See Figures B1- B7 for further examples.

For all cases when the emulation of GSAT time series (made of annual average values) does not present inconsistencies our hypothesis is that noisier quantities would not suffer from detectable discontinuities either. We have tested this expectation for a range of quantities (temperature, precipitation, and sea level pressure) and scales (from subcontinental to local, i.e. grid-point level). Here, as examples, we compare trends and variability (computed as the standard deviations of the residuals from the trend) between stitched and target time series under the two scenarios (over the 2015-2100 period) for temperature (TAS) and precipitation (PR). All metrics here are computed using time series of gridded output at monthly frequency, covering the entire annual cycle, for the length of the emulated output (2015-2100). In the appendix we show similar results for month-specific output sampling behavior during Boreal winter (January) and Boreal summer (July), addressing the possibility that the emulation could be differently challenged by stronger or weaker forced trends. We use results from the emulation of two models that represent extremes in the PANGEO dataset, in terms of availability of archive trajectories: CAMS-CM1-0 (with only two ensemble members each for SSP1-2.6 and SSP5-8.5) for which we have derived one emulated trajectory per scenario (SSP2-4.5 and SSP3-7.0) and MIROC6 (with 50 ensemble members for each) for which we have emulated three trajectories per scenario. In the trend figures we blacken grid-points where the trends computed from the stitched trajectories are significantly different from those computed from the target trajectory. We use here the same criterion that we applied to the validation of GSAT: trends are significantly different when their 95% confidence intervals do not overlap. For the analysis of monthly variability we show maps of the ratio of the two variances computed from the stitched and target time series, after removing the linear trends. We consider substantially different variances that are not within 20% of one another, i.e. whose ratio is either less than 0.8 or more than 1.2. The color bar is chosen to highlight these two thresholds. Figure 3 shows results for the comparison of TAS and PR trends for CAMS-CM1-0 while Figure C1 through C3 in the appendix show the corresponding analysis for MIROC6. For temperature, as can be assessed in Figure 3, top panels, only isolated patches over the tropical oceans show statistically significant differences in trends. The results for MIROC6, where we can look at three different realizations, show that also for this model's emulation the areas of disagreement consist of isolated patches mostly over ocean regions, and not consistent from realization to realization, suggesting the role of internal variability in producing these results, rather than a systematic problem with STITCHES. Internal variability is likely responsible for an area in the Arctic showing significant discrepancies in two of the three realizations, but effects of ice-free summer intensified warming (Blackport and Kushner, 2016), or behavior of the AMOC could also contribute to this limited area of disagreement. For precipitation the inconsistent areas are barely detectable as smaller scatters of points, mostly over the oceans. These results remain essentially unchanged when considering trends for individual months. Figures C4 and C7 show a sample of plots for January and July temperature and precipitation trends for the two models. As can be assessed, the appearance of statistically significant patches of trend disagreement has the same qualitative characteristics as those in the maps showing the comparison of trends computed using the year-long monthly data.

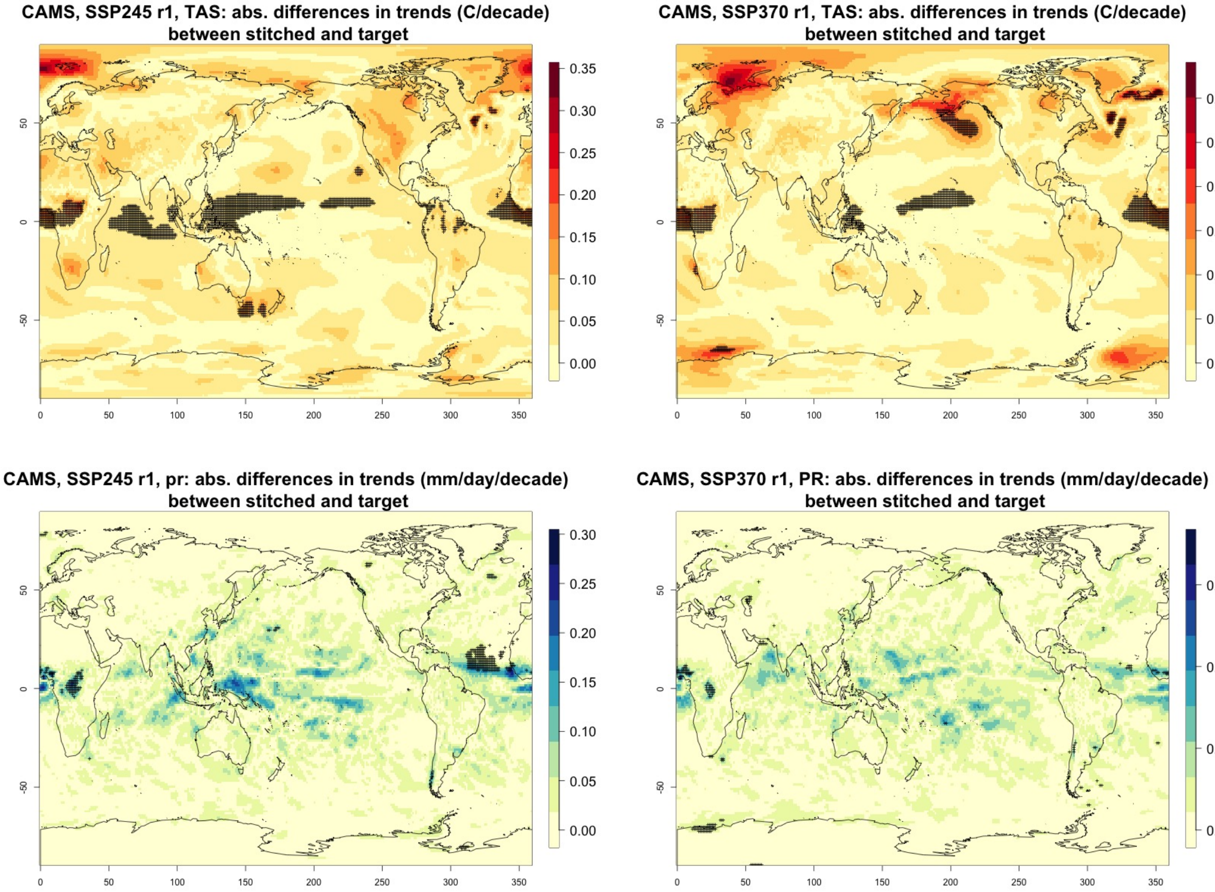

CAMS, SSP245 r1, TAS: abs. differences in trends (C/decade) between stitched and target

CAMS, SSP370 r1, TAS: abs. differences in trends (C/decade) between stitched and target

CAMS, SSP245 r1, pr: abs. differences in trends (mm/day/decade) between stitched and target

CAMS, SSP370 r1, PR: abs. differences in trends (mm/day/decade) between stitched and target

Figure 3. Absolute difference in future trends of monthly temperature (TAS) and precipitation (PR) between stitched and target realizations. The value of the difference is expressed by the color scale and we marked by black crosses those locations where the trends computed from target and stitched time series do not overlap in their 95% confidence intervals, indicating statistically significant differences. Emulation of CAMS-CM1-0 monthly time series for 2015-2100 under SSP2-4.5 and SSP3-7.0.

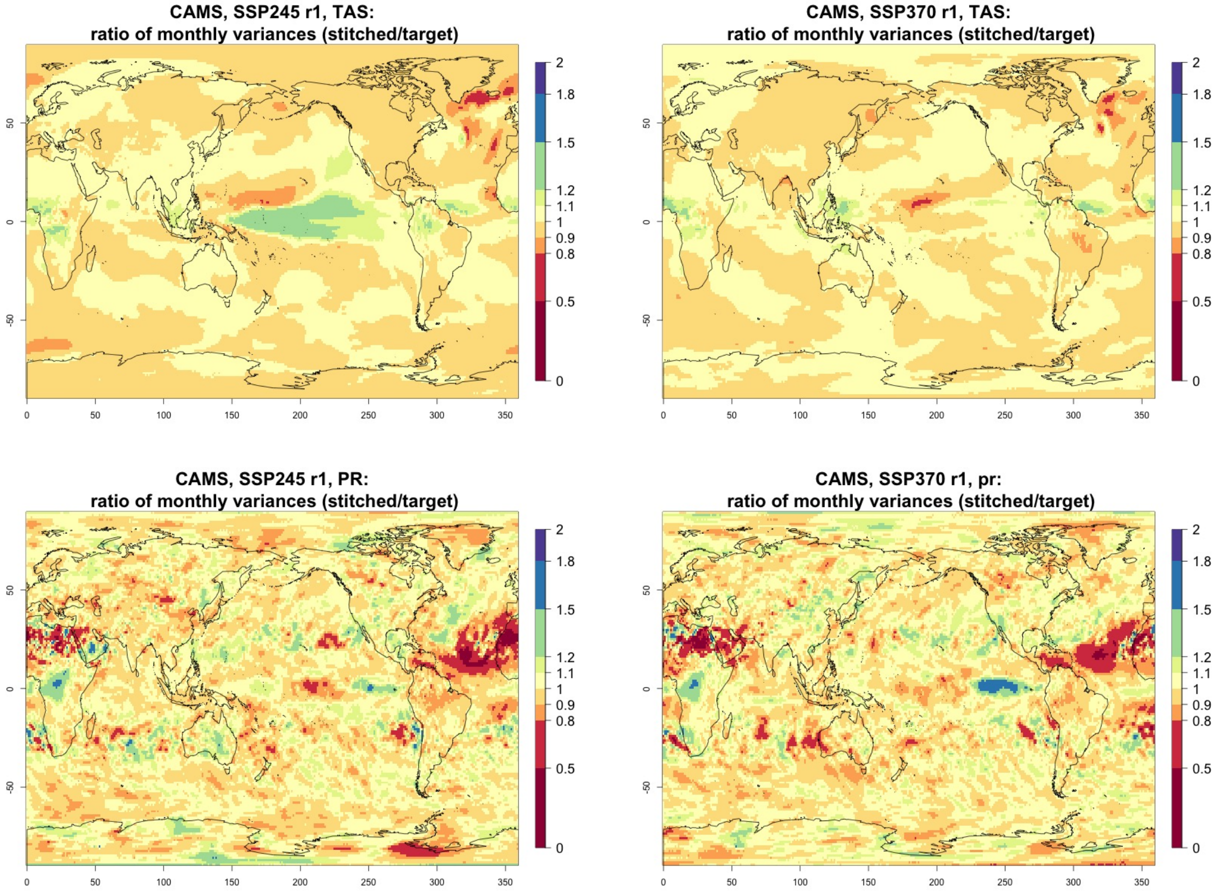
CAMS, SSP245 r1, TAS:
ratio of monthly variances (stitched/target)
CAMS, SSP370 r1, TAS:
ratio of monthly variances (stitched/target)
CAMS, SSP245 r1, PR:
ratio of monthly variances (stitched/target)
CAMS, SSP370 r1, pr:
ratio of monthly variances (stitched/target)
50
0
-50
0
50
100
150
200
250
300
350
2
1.8
1.5
1.2
1.1
1
0.9
0.8
0.5
0

Figure 4. Ratio in monthly variability (standard deviation of residuals from trends) of future temperature (TAS) and precipitation (PR) between stitched (at the numerator) and target (at the denominator) realizations. The value of the ratio is expressed by the color scale which highlights the transition at 0.8 and 1.2. Emulation of CAMS-CM1-0 monthly time series for 2015-2100 under SSP2-4.5 and SSP3-7.0.

Performance in terms of monthly variability of temperature is within 20% of the true variability practically over all the land regions, and over the large majority of the oceans' areas, with the exception of a systematic bias over the west Pacific cold tongue. Rainfall variability appears less homogeneously accurate, until one realizes that the areas where variability appears inconsistent (i.e., areas where the value of the ratio is smaller than 0.8, or larger than 1.2) coincide with climatologically very dry areas of both the Northern and Southern hemispheres. In these regions variability is low, and therefore small differences in the numerator and denominator may cause large variation of the ratio, without implying meaningful differences in rainfall behavior.

Last, still concerned with single time series behavior, we consider a different quantity altogether: the Southern Oscillation Index (SOI), describing the evolution of the El-Niño Southern Oscillation mode of variability. The SOI index is defined as the standardized difference between sea level pressure (SLP) monthly anomalies at Tahiti and Darwin, Australia[4]. The negative or positive sign of this difference indicates abnormally warm or cold ocean waters across the eastern tropical Pacific, associated with El Niño or La Niña episodes. The index, despite being a uni-dimensional time series, reflects the behavior of a coherent spatial field (SLP) at monthly frequency. Its frequency characteristics are important to preserve, as the opposite phases of the SOI have been found to be associated with significant shifts in the weather of regions having strong teleconnections, causing droughts or intense precipitation, and cooler or warmer than average conditions (Mason and Goddard, 2001; Lenssen et al., 2020) . Therefore, for impact analysis, we would not want to produce time series of this index with a spurious behavior, compared to the corresponding continuous output of the emulated ESM. Thus, we perform a comparison of the characteristics of the true and emulated SOI time series using (partial) auto-correlation function and spectral density estimates. Note however that we are not comparing these frequency characteristics to observations, which is not the point of our validation exercise. We consider this validation particularly important, both because of the salience of ENSO behavior for many types of impact, and because the frequency characteristics of this mode of variability are close to our 9-year windows.

Figure 5 presents target and stitched time series of the ENSO index for one of the models (CAMS-CM1-0) and three twenty year windows along the two scenarios emulated. As can be gauged, the three pairs of time series appear similar in magnitude and oscillatory behavior. In order to confirm the latter, we show in Figure 6 the (partial) auto-correlation functions of the corresponding time series. This analysis produces indistinguishable lag patterns, and, importantly, does not reveal any spurious behavior at 9 years' lags. Figures D1 through D6 in the appendix confirm that results are similar for three emulated ensemble members under each scenario for MIROC6. Further, we show in Figure D7 the spectral densities of the entire time series, comparing target and stitched, and showing how the densities of the stitched trajectories have a behavior that is qualitatively and quantitatively (up to what appears as some noisy behavior at very low frequencies) consistent with that of the target trajectories.

[4] https://www.ncdc.noaa.gov/teleconnections/enso/indicators/soi/

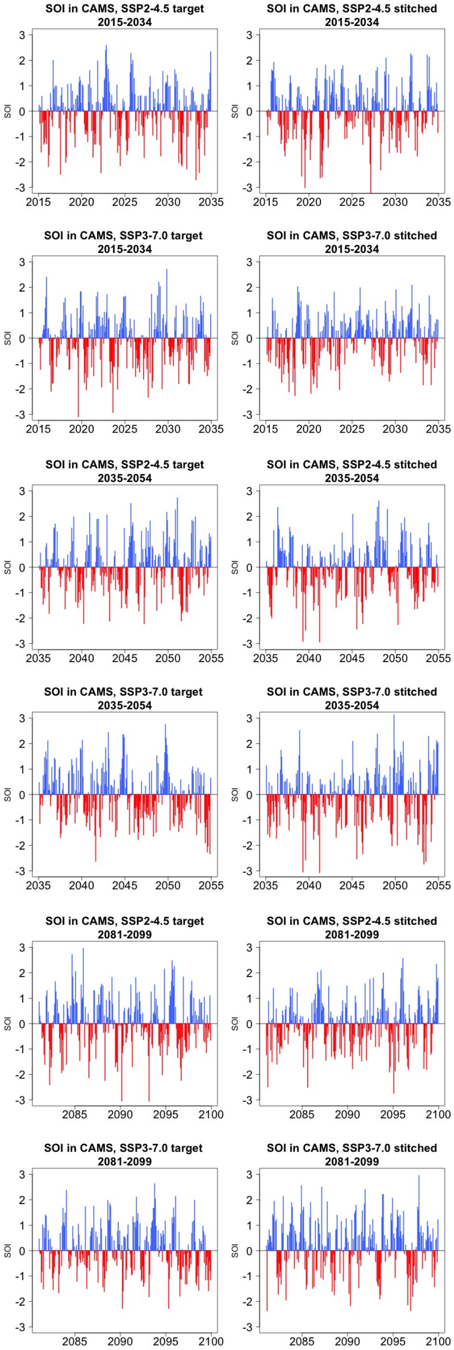

Figure 5. Examples of target (left) and stitched (right) SOI time series for three twenty-year windows along the length of the simulation: 2015-2034 in the top four panels; 2035-2054 in the middle four panels; 2081-2100 in the bottom four panels. Results from emulation of SSP2-4.5 and SSP3-7.0 for CAMS-CM1-0.

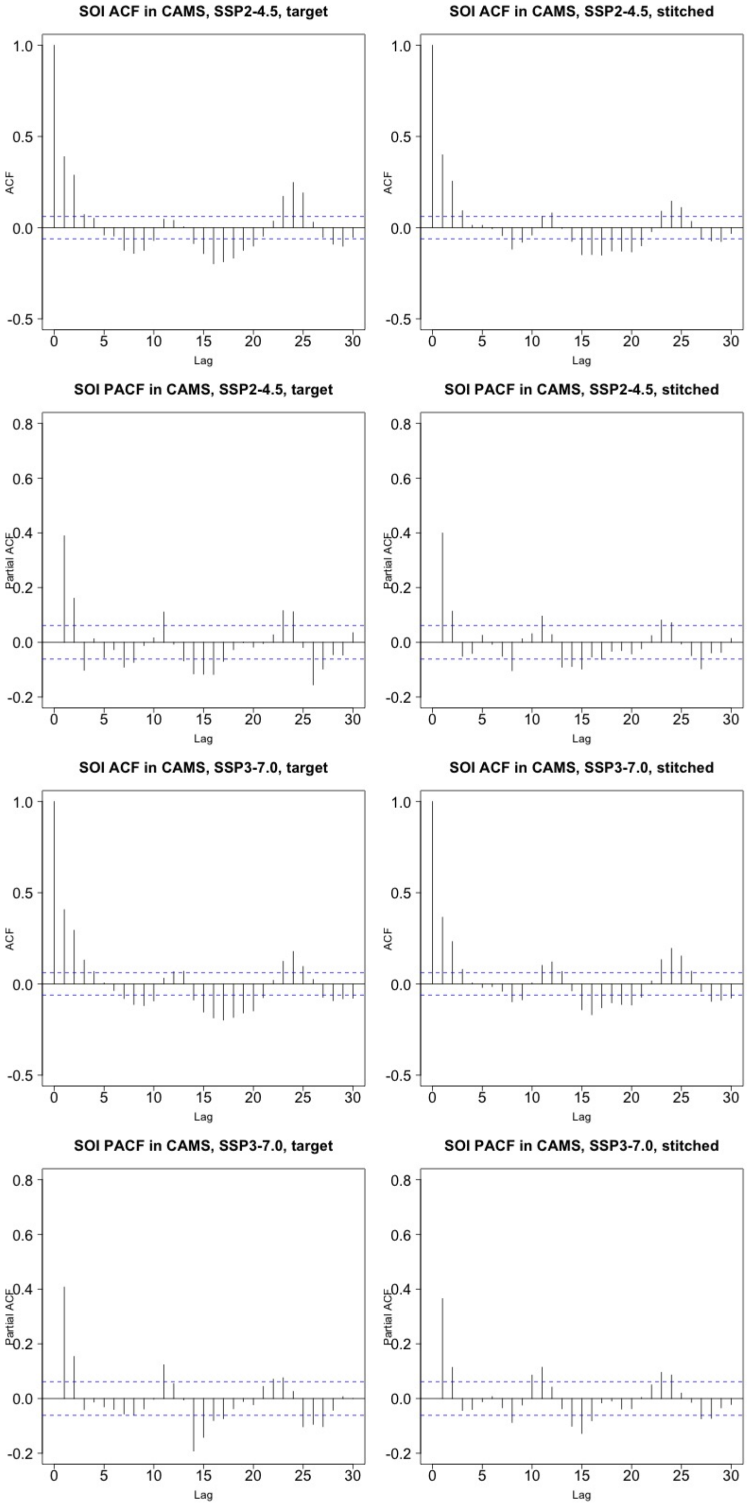

Figure 6. Auto-correlation (ACFs) and Partial auto-correlation functions (PACFs) for real and stitched SOI time series. Top two rows: SSP2-4.5 ACF for target and stitched series and respective PACFS. Bottom two rows: SSP3-7.0 ACF for target and stitched series and respective PACFs. (Our software – R function `acf(..,type="partial")` – does not define the PACF at lag zero.)

On the basis of these results we confirm the correctness of our expectation that, after validating the statistical characteristics of a large scale, low frequency quantity like annual GSAT, further validation of emulated variables at grid-point scale and higher temporal frequency do not seem to present larger challenges. The higher noise of these quantities indeed accommodates the discontinuities introduced by their emulation.

3.1.2 Validation of emulated initial condition members

Our emulator can also be used to provide multiple ensemble members under the same scenario, akin to initial condition ensembles. For this type of application, besides the necessary validation of the individual members according to the above described metrics, we want to validate the properties of the synthetic ensembles as such, comparing their mean behavior and their spread to those of real initial condition ensembles from the same ESM. Figures E1 through E5 show the resulting ensembles for a number of experiments that we conducted over several ESMs and the two scenarios SSP2-4.5 and SSP3-7.0. We chose models that provided at least 5 21^{st} century trajectories of the Tier 1 scenarios. As mentioned in Section 2, this exercise is conducted by using the entire archive available, as we mimic a situation where we are not creating a new scenario, but augmenting the size of an initial condition ensemble run under existing ones.

We adopt the two-dimensional metric of performance introduced by Tebaldi et al. (2020). We indicate by $\mathbf{y}$ a quantity derived from the true ensemble and by $\hat{\mathbf{y}}$ the same quantity derived from the emulated ensemble. Further, we indicate by angle brackets the ensemble average operation. The two dimensional metric is then defined as

$$E_r(\mathbf{y},\hat{\mathbf{y}}) = \left(\frac{|\langle \mathbf{y} \rangle - \langle \hat{\mathbf{y}} \rangle|}{\sqrt{\langle (\mathbf{y} - \langle \mathbf{y} \rangle)^2 \rangle}}, \sqrt{\frac{\langle (\langle \mathbf{y} \rangle - \langle \hat{\mathbf{y}} \rangle)^2 \rangle}{\langle (\mathbf{y} - \langle \mathbf{y} \rangle)^2 \rangle}} \right). \qquad (1)$$

Its first component (which we indicate below as E_1) measures the systematic bias between the means of the true and the synthetic ensembles, normalized by the true ensemble standard deviation. The second, E_2 is defined as the ratio between the synthetic and the true ensemble standard deviations. In a perfect emulation, $E_r = (0,1)$. It is useful to note that the magnitude of these metric components is expressed as a fraction (or multiple) of the true ensemble variance, allowing a judgment of the size of the discrepancies introduced by STITCHES as they compare to the true internal variability of the target ensemble. Here as before we focus on annual series of global mean temperature. Table 4 reports the values of E_1 and E_2. The number under the column labelled "Archive Size" indicates how many 21^{st} century trajectories were available for each of the four scenarios in the archive to create 9-year building blocks for STITCHES. Note that when a model provided numerous trajectories to build from, we tested the performance for increasing sizes of the archive (e.g., for the CanESM5 model we repeat the exercise using 5-,10-,15-,20-,25-members initial condition ensembles for each scenario). The following two columns in the tables list the size of the target ensemble emulated, which is therefore available for validation ($\mathbf{y}$), under "Target Members", and the size of the stitched ensemble, under "Stitched Members", which is the number of additional trajectories created by STITCHES that could be added to the existing ensemble. We choose three years along the 21st century, 2010, 2050 and 2090, and we utilize 9-year windows around those years to compute formula 1 (similar results were obtained by using a shorter 5-year window).

Several outcomes can be gleaned from Table 4. STITCHES trajectories have mean and variability characteristics within a small window of the target ensembles in the great majority of cases. Of course the application should dictate what is the

Table 4. The two components of the E_r metric, E_1 and E_2, computed for several experiments across ESMs, scenarios and number of available archive trajectories from which to create the stitched ensembles. Numbers in columns 4 through 9 represent fractions of the target ensemble standard deviation (see formula 1).

Model	Scenario	Archive	Target	Stitched	E_1			E_2		
		Size	Members	Members	2010	2050	2090	2010	2050	2090
ACCESS-CM2	ssp245	5	5	5	0.00	0.36	0.00	1.03	0.82	1.09
ACCESS-ESM1-5	ssp245	5	10	6	0.29	0.00	0.02	1.16	1.16	1.35
CanESM5	ssp245	5	25	5	0.15	0.13	0.36	0.68	1.26	0.87
MIROC-ES2L	ssp245	5	30	5	0.08	0.50	0.07	0.96	0.95	1.00
MPI-ESM1-2-LR	ssp245	5	10	5	0.01	0.03	0.25	1.07	1.06	1.26
MRI-ESM2-0	ssp245	5	5	4	0.00	0.19	0.11	1.09	1.09	1.21
UKESM1-0-LL	ssp245	5	14	3	0.04	0.51	0.37	1.18	0.99	0.93
ACCESS-ESM1-5	ssp245	10	10	9	0.00	0.02	0.00	1.40	0.99	1.18
MIROC-ES2L	ssp245	10	30	10	0.01	0.00	0.02	1.20	1.17	1.01
MPI-ESM1-2-LR	ssp245	10	10	10	0.00	0.04	0.01	1.06	0.89	0.86
CanESM5	ssp245	10	25	10	0.02	0.01	0.01	1.02	1.13	0.91
CanESM5	ssp245	15	25	15	0.01	0.01	0.01	0.92	0.87	0.99
CanESM5	ssp245	20	25	20	0.01	0.01	0.02	1.02	1.02	0.99
CanESM5	ssp245	25	25	23	0.00	0.00	0.00	0.88	1.02	1.00
ACCESS-CM2	ssp370	5	5	5	0.00	0.00	0.00	0.89	0.91	1.00
ACCESS-ESM1-5	ssp370	5	30	5	0.05	0.14	0.02	1.09	1.04	1.40
CanESM5	ssp370	5	25	4	0.30	0.03	0.00	1.40	0.85	0.90
MIROC-ES2L	ssp370	5	10	5	0.06	0.69	0.01	1.18	1.16	0.90
MPI-ESM1-2-LR	ssp370	5	10	5	0.27	0.30	0.00	1.28	1.15	1.20
MRI-ESM2-0	ssp370	5	5	5	0.00	0.07	0.01	0.90	1.13	1.14
UKESM1-0-LL	ssp370	5	13	3	0.01	0.00	0.09	0.94	1.30	1.03
ACCESS-ESM1-5	ssp370	10	30	11	0.00	0.07	0.01	1.25	0.93	0.91
CanESM5	ssp370	10	25	10	0.11	0.00	0.03	0.87	1.02	1.03
MIROC-ES2L	ssp370	10	10	9	0.11	0.22	0.00	1.11	1.08	0.98
MPI-ESM1-2-LR	ssp370	10	10	9	0.01	0.00	0.01	1.12	1.46	1.05
CanESM5	ssp370	15	25	14	0.01	0.07	0.03	0.94	0.91	1.02
CanESM5	ssp370	20	25	19	0.00	0.00	0.01	0.90	0.96	1.02
CanESM5	ssp370	25	25	23	0.01	0.00	0.00	0.95	1.01	1.01

standard that needs to be met by the synthetic ensembles, but if discrepancies of up to 25 or 30% of the true internal variability are acceptable, most cases described in the table would meet that standard, and in the great majority of cases by a large margin, especially once the ensembles available from which we sample building blocks have at least 10 members. This exercise uses a tolerance value $Z = 0.075$ across the board, but tuning the value to specific ESM characteristics could ameliorate some of the worse performances. A look at the best performances suggests what we should expect, if the tuning was conducted specifically to each ESM characteristics of variability. Section 3.1.3 below further expands on the relation between the tuning parameter Z, the size of the ensembles that STITCHES can create, and the values of the Er metric.

We have performed the same exercise by limiting the archive to the two bracketing scenarios, SSP1-2.6 and SSP5-8.5, and trying to construct ensembles for SSP2-4.5 and SSP3-7.0. In this case STITCHES is significantly challenged: its performance, as measured by the E_r metric, is significantly diminished and, when comparing what happens for the same model and increasing numbers of archive members, unpredictable, due to the fact that the algorithm randomizes both the identity of the archive members and the choice of the nearest neighbors to construct the emulated output. Table F1 reports these discrepancies. A look at Figure 1 may suggest the nature of the challenge here, because of the relatively extreme nature of SSP5-8.5 values compared to SSP2-4.5 in particular. Section 3.1.3 below also discusses this aspect. We argue that this challenge could be lessened by a more deliberate design of ESM experiments in relation to the $(T, X * dT)$ space. Additionally, as it has been argued recently, SSP5-8.5 may represent an obsolete or at least improbable scenario (Hausfather and Peters, 2020) and therefore the range to be explored by future scenarios could be narrower in the next phase of CMIP experiments.

3.1.3 Trade-offs between generated ensemble size and Z

The size of a stitched ensemble targeting a given experiment is directly related to the number of ESM ensemble members present in the archive, as well as the tolerance for matching, Z. Larger values of Z result in larger numbers of stitched ensemble members, until the archive is exhausted. It is unlikely that a closed form relationship between $(\text{archive size}, Z)$ and size of the stitched ensemble exists, as another factor in the success of the emulation is how similar the GSAT trajectories in the archive are to the target and archive scenarios, not only in median value but in rate of warming, the two dimensions of our neighborhood. Instead, we present empirical estimates, for each ESM separately, of a conservative cutoff value for Z, Z_{cutoff} that should safely result in generated ensemble members satisfying our validation criteria presented in the above Sections 3.1.1 and 3.1.2. Specifically, we will identify the Z_{cutoff} at which the generated ensemble size appears to saturate while still maintaining small Er values. Thus, using Z values beyond the provided Z_{cutoff} provides no additional benefit.

To identify Z_{cutoff} for each experiment of each ESM, we conduct a sweep of Z values ranging from 0.04 to 0.3°C. As noted in step 6 of the algorithm, the actual matches within each Z neighborhood are drawn randomly for stitching a trajectory. Therefore, at each Z value tested, we perform 50 of these random draws of the STITCHES algorithm for generating the largest possible collapse-free ensemble, targeting each of experiment SSP2-4.5 and SSP3-7.0, and using the full archive for that ESM (see Table 1). We calculate the same Er statistics above for both GSAT and the GSAT differences "at the seams" computed over the annual time series of stitched GSAT, for each draw of a full generated ensemble. Z_{cutoff} is identified as the largest tolerance value that keeps the average value across draws of the two pairs of these metrics for each target ensemble below 10%. Generally, it is the E_2 dimension of the GSAT differences at the seams when targeting SSP2-4.5 that is largest of the four error metrics across both target experiments: i.e., the standard deviation of the generated interannual jumps differs from the standard deviation of the target interannual jumps of the target. This exercise should be repeated for other values of X (number of years in a window), particularly for values substantially further away from the $X = 9$ value considered in this work. The metarepository for this paper (see code and data availability) includes the experiment scripts used for this exploration, which users may adapt.

Z_{cutoff} values and the corresponding draw-averaged generated ensemble size for each experiment-ESM combination are reported in Table 5. Increasing the tolerance beyond these Z_{cutoff} can increase the generated ensemble size, but with larger errors, meaning potentially the stitched realizations at that point may not behave well. For example, at $Z_{cutoff} = 0.25$, ACCESS-CM2 can stitch seven realizations targeting SSP2-4.5 but at max error of 11.6% (E_2 of the GSAT differences in this case). Values of E_2 of the GSAT differences this large may correspond to stitched GSAT trajectories that clearly feature abrupt switching between windows of distinctly SSP1-2.6 and SSP5-8.5 behavior, rather than actually emulating an SSP2-4.5 trajectory. Finally, if one wishes to select a single tolerance to use for emulation of both SSP2-4.5 and SSP3-7.0 (and likely for similar, novel, intermediate scenarios), the larger Z_{cutoff} should be used. For example, if one wished for a single Z_{cutoff} value for CanESM5, $Z_{cutoff} = 0.13$ would provide generated ensemble sizes of 25 each for both SSP2-4.5 and SSP3-7.0 (with a draw-averaged max Er of 5.1% rather than 4.3%).

By comparing the generated ensemble size from Table 5 with the CMIP6 archive sizes outlined in Table 1, we see that for most ESMs, STITCHES can generate a stitched ensemble of the same size as the target ensemble. The cases with large archive sizes (CanESM5, MIROC-ES2L, MIROC6, and MPI-ESM1-LR) however, make it clear that the size of the stitched ensemble is not necessarily a direct function of the availability of runs in the archive or the size of the target ensemble, but depends on the proximity in $(T, dT * X)$ space of the target windows to the archive windows. A look at the panels in Figure 1 gives a good representation of the challenges, as SSP370 appears to lie comfortably within the envelope of the SSP585 runs, whereas SSP126 and SSP245 appear more isolated. We will discuss the implications of this in Section 4. The Z_{cutoff} values in Table 5 are also not the final limits on where good matches may be generated. Specifically, because we start the matching neighborhood for each target point by finding the nearest neighbor in the archive first and then adding the tolerance to that distance (step 5 of the algorithm), there is a heterogeneity of matching neighborhood size for each target point even within a single trajectory. A different choice could uncover further results, however the choice to begin with nearest neighbors was made for convenience: at $Z = 0$, the stitched trajectory returned is simply made up of the nearest neighbor points in the archive. Finally, there is utility in the stochastic draws used in this exercise as well. Multiple draws of generated ensembles fed through impacts models may lead to new insights, despite the fact that appending multiple draws together into a single “super"-generated ensemble is not advised as it will bypass the restriction on generated ensemble envelope collapse enforced in step 6 of our constructive algorithm.

Table 5. For each ESM and the two scenarios targeted by the emulation, we show the size of the archive, the number of trajectories used as target, and the number of stitched trajectories obtained from them, for the value of Z_{cutoff} which keeps the metric Er, when averaged across 50 draws, at the maximum value indicated. We refer to Section 3.1.3 for details.

Model	Target Scenario	Archive size	Target size	Stitched size	Z_{cutoff}	$Er*$
ACCESS-CM2	SSP2-4.5	16	3	5	0.175	5.4 %
BCC-CSM2-MR	SSP2-4.5	4	1	1	0.04	0.49%
CanESM5	SSP2-4.5	100	25	25	0.105	4.3%
CAS-ESM2-0	SSP2-4.5	8	2	3	0.265	4.6%
CESM2-WACCM	SSP2-4.5	10	3	3	0.115	5.4%
CMCC-CM2-SR5	SSP2-4.5	4	1	1	0.04	1.7%
CMCC-ESM2	SSP2-4.5	4	1	1	0.04	0.78%
FGOALS-g3	SSP2-4.5	16	4	5	0.105	3.5%
FIO-ESM-2-0	SSP2-4.5	9	3	3	0.09	3.4%
HadGEM3-GC31-LL	SSP2-4.5	9	4	1	0.04	2.2%
MCM-UA-1-0	SSP2-4.5	4	1	1	0.04	1.1%
MIROC-ES2L	SSP2-4.5	60	30	66	0.215	5.9%
MIROC6	SSP2-4.5	123	20	19	0.21	6.7%
MPI-ESM1-2-HR	SSP2-4.5	16	2	3	0.075	3.2%
MPI-ESM1-2-LR	SSP2-4.5	40	10	12	0.135	5.5%
NorESM2-LM	SSP2-4.5	7	3	4	0.125	4.6%
NorESM2-MM	SSP2-4.5	5	2	4	0.15	5.7%
UKESM1-0-LL	SSP2-4.5	37	6	13	0.18	4.7%
ACCESS-CM2	SSP3-7.0	16	5	5	0.13	4.5 %
BCC-CSM2-MR	SSP3-7.0	4	1	1	0.04	0.36%
CanESM5	SSP3-7.0	100	25	25	0.13	5.0%
CAS-ESM2-0	SSP3-7.0	8	2	3	0.26	5.4%
CESM2-WACCM	SSP3-7.0	10	3	1	0.04	0.67%
CMCC-CM2-SR5	SSP3-7.0	4	1	1	0.04	0.31%
CMCC-ESM2	SSP3-7.0	4	1	1	0.04	0.75%
FGOALS-g3	SSP3-7.0	16	4	5	0.12	0.54%
MCM-UA-1-0	SSP3-7.0	4	1	1	0.04	0.3%
MIROC-ES2L	SSP3-7.0	60	10	28	0.255	3.9%
MIROC6	SSP3-7.0	123	3	51	0.22	6.0%
MPI-ESM1-2-HR	SSP3-7.0	16	10	9	0.07	4.4%
MPI-ESM1-2-LR	SSP3-7.0	40	10	12	0.14	5.2%
NorESM2-LM	SSP3-7.0	7	3	1	0.04	2.1%
NorESM2-MM	SSP3-7.0	5	1	1	0.04	0.33%
UKESM1-0-LL	SSP3-7.0	37	13	13	0.16	5.4%

4 Discussion and conclusions

We have proposed an algorithm, STITCHES, that exploits available simulations of future scenarios to deliver fully consistent and complete ESM-like output according to a new scenario, based on the trajectory of global temperature that the new scenario produces. STITCHES works by stitching together decade-long windows (we use 9 years to be precise, but the length of the window is a tunable parameter) of existing 21$^{\mathrm{st}}$ century ESM simulation output. These windows are chosen on the basis of their corresponding GSAT absolute value and derivative, identified to match those of subsequent windows of the GSAT time series derived from the scenario to be emulated. The same algorithm can also be used to enrich the size of existing initial condition ensembles. We have demonstrated the algorithm performance using the PANGEO CMIP6/ScenarioMIP archive of the four Tier 1 experiments, SSP1-2.6, SSP2-4.5, SSP3-7.0, SSP5-8.5, targeting the emulation of the two intermediate scenarios.

Our numerous validation tests have shown that the stitched time series do not reveal in the great majority of cases spurious behavior, even when the matching criteria are set without being specifically tailored to the internal variability of the ESM to be emulated. We have shown that jumps or discontinuities are seldom created at global scale, when considering surface temperature. Since surface temperature is the smoothest quantity among the variables commonly used to drive impact models, our hypothesis has been that any other variable at global or regional scale, and for yearly frequencies or higher, would be even better-behaved at the seams, since the larger internal variability would even more easily overwhelm discontinuities introduced by STITCHES. We have confirmed this hypothesis with case studies for gridded temperature and precipitation at the monthly frequency. We have also shown that for ENSO, a salient mode of variability for many natural and human systems, a 9-year window does not introduce odd frequency artifacts in the SOI time series. This should reassure modelers of impacts sensitive to ENSO teleconnections. Synthetic "large ensembles" created to enrich initial condition experiments show an ensemble behavior within a small neighborhood of the truth (in most cases much narrower than $\pm 25 - 30\%$ of the target ensemble variability) in terms of ensemble mean and ensemble variance.

Our exploration of the performance of the algorithm as a function of the available archive size suggests that five 21st century trajectories ensure an acceptable performance (according to our metrics) and even smaller archive sizes often - if not always – deliver acceptable stitched new trajectories. Thus, for modeling centers choosing to invest resources in future scenario simulations, running a well-chosen small set of trajectories that span what the community considers the plausible range of GSAT absolute change and rates of change, or radiative forcing, could suffice, and the center could be better served by focusing on running a few initial condition ensemble members for each trajectory, rather than investing in multiple similarly shaped scenarios. This also entails savings for the community that provides the direct forcing inputs to ESMs by translating IAM output into spatially and time resolved forcing fields for scenario simulations. Resources in post-processing of model output, extending to the need of downscaling and bias-correcting, will be saved as well, as the emulated scenarios can be built from those post-processed ones.

Of course, our proposal does come with caveats. ENSO frequencies are right around the timescale that is preserved by 9-year windows, but there exist slower modes of variability in the climate system whose single phases may instead align with such time span, and whose coherent behavior would be broken by our window splitting and stitching together. Thus, any investigation of impacts that are known to be sensitive to low-frequency variability at decadal time scales needs to proceed with caution, try lengthening the window X, or not use STITCHES output at all. Similarly, any impact that depends on quantities whose integral is important, rather than their instantaneous value, cannot use the output from STITCHES if such integral frequently, or by definition, extends over the window size. Pre-eminently, sea level rise derived from ocean heat content, which is a path dependent quantity, cannot use the ocean heat content that comes with a STITCHES scenario, which would not be coherent with the scenario path. Similarly, mega-droughts lasting over a decade cannot be coherently represented in a scenario emulated by STITCHES.

There are more subtle aspects of stitched scenarios that may pose questions of fidelity and representativeness. We have not addressed the challenges that short but intense forcing episodes, like volcanic eruptions, may pose, since we have focused the application of STITCHES on future scenarios, which do not represent them. A careful look at Figure 1 can highlight a region of the space populated by grey dots (the historical part of the simulations) showing a peculiar pairing of absolute temperature anomalies and rate of change in the region around $T = -0.01$ compared to that around $T = 0.01$. This would suggest a specific behavior of GSAT while recovering from volcanic eruptions that is not easily emulated by finding analogs in the historical period (away from volcanic episodes). One other possible challenge to STITCHES has to do with regional and/or short-lived forcers like land-use and aerosols, which usually vary across scenarios. STITCHES would not represent closely these forcers if the scenario to be emulated contained different regional patterns or histories for them, compared to the scenarios used to generate the pieces. Thus, if those regional, short-lived forcers create climate signals that significantly alter the nature of the output they appear in, STITCHES would not replicate those signals. This is, however, not different from what happened in any analysis using time-sampling (King et al., 2018), or simple pattern scaling. Thus, here we work under the assumption that – amidst the uncertainties of different ESM responses and impact modeling affecting regional climate and impact outcomes – the signals introduced by regional and/or short-lived forcers would not be consequential to the results. We do encourage deeper exploration of these questions.

Last, some technical aspects of our algorithm will benefit from further analysis/considerations: possibly some applications may be able to relax the tolerance parameter, and thus set the conditions for easier matching and more numerous stitched realizations. This might be true of applications that would not be too sensitive to interannual differences. On the contrary, tightening the tolerance to match specific ESMs' internal variability will be beneficial in eliminating spurious behavior that we have documented in some cases, especially when the archive of available runs is poor. More generally we could choose a difference distance measure in the $(T, X * dT)$ space, or a completely different space over which to look for nearest neighbors, but the necessity of conforming to what a simple model can produce on the basis of a new emission scenario needs to be kept as a consideration.

We would have liked to make more than just a rule-of-thumb recommendation for the number of ensemble members that modeling centers should run, and link that formally to the number of expected trajectories created by STITCHES. That said, the last phases of CMIP have shown that, ultimately, modeling centers will commit what they can to running future scenarios. Our proposal shifts those energies and resources away from running a number of scenarios of similar shapes. One additional possibility that we have not explored is utilizing idealized experiments like 1% CO_2 among the building blocks, consistently with our discussion of the secondary relevance (until proved wrong) of forcing agents other than well-mixed greenhouse gases.

In addition to stabilized scenarios, which were not systematically explored by the last set of simulations and that therefore would pose a challenge to STITCHES, STITCHES cannot emulate at this time another type of scenario that is becoming more and more prominent in the policy discourse: the overshoot, i.e., a scenario that presents a peak and decline in forcing and therefore global average temperature. If a range of overshoots are sought, there is the need to run with ESMs some cases with different steepness and length in order to provide building blocks of decreasing temperature at different rates.

Despite the warranted caveats, we believe that our proposal has desirable outcomes for the research communities occupied with climate, scenario and impact modeling. Impact and IAM modelers that want to assess impacts for scenarios other than those that have been generated by ESMs, including endogenously generate forcing pathways within IAMs, could rely on STITCHES to fill the gaps, acquiring the same type of output, in all its complexity and refinement, that an ESM would provide. An 'on-line' application of STITCHES within an IAM simulation could allow modeling climate impacts within the evolving system that the IAM is modeling, and therefore represent fully consistent feedback loops between climate change drivers (emissions) and climate change impacts. The wider impact research community could choose from a larger set of trajectories, and possibly, a larger set of initial condition ensembles than ESM ran. Climate modelers can reduce the effort devoted to preparing inputs for, setting up, running and post-processing future scenarios. We acknowledge here the richness of climate model output archives already at our disposal (CMIP5, CMIP6, SMILES) which right now provide a wide variety of building blocks. The next phases of CMIP could complement what is available now by deliberately exploring types of scenarios that are not well represented in the current archives, like stabilized trajectories and overshoots. The challenge would lie in choosing the best set of runs to optimally populate the $(T, X * dT)$ space to maximize the number and shape of attainable new trajectories from the existing ones. The deployment of STITCHES, in concert with other emulators like MESMER-M and X (Nath et al., 2022; Quilcaille et al., 2022) and PREMU (Liu et al., 2022), which are intended to produce new realizations of internal variability could then complement and enrich the effort of the ESM community.

Code and data availability. The STITCHES software is available via GitHub (https://github.com/JGCRI/stitches/releases/tag/v0.9.0) and is frozen on zenodo (https://doi.org/10.5281/zenodo.6463264). Note that at the time of archiving, GitHub-zenodo integration was not functioning and so the pre-release STITCHES files were uploaded to zenodo directly. The code using the STITCHES software to generate data and the code analyzing data for this paper is available at a GitHub metarepository (https://github.com/JGCRI/Tebaldi_etal_2022_ESD) and is frozen on zenodo(https://doi.org/10.5281/zenodo.6463270). All our ESM data is from the CMIP6 archive available through PANGEO (http://gallery.pangeo.io/repos/pangeo-gallery/cmip6/). The data generated using the STITCHES package and analyzed in this paper is archived (https://doi.org/10.5281/zenodo.6461693).

Appendix A: A diagram of the STITCHES algorithm

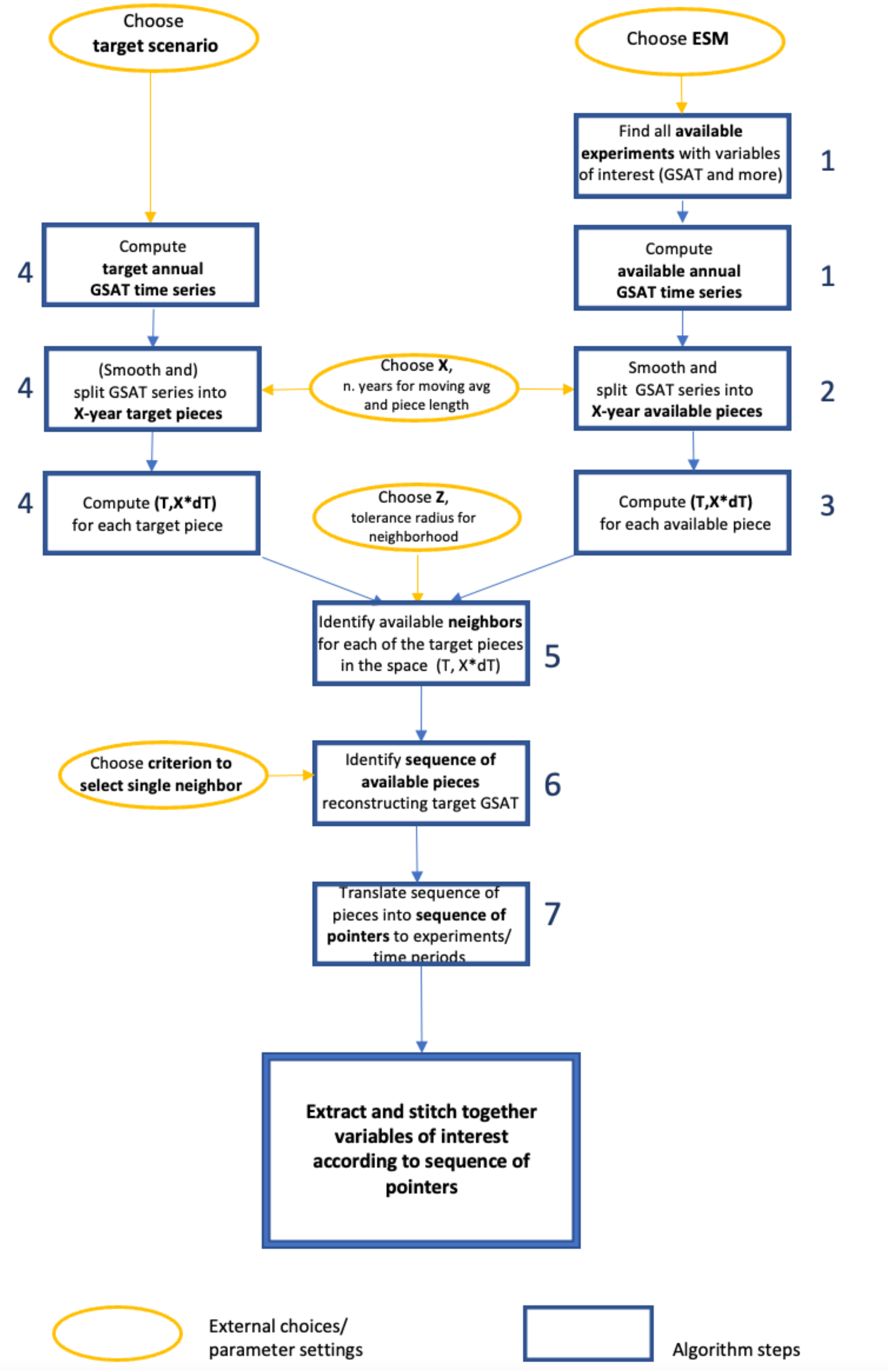
Choose target scenario
Choose ESM
Find all available experiments with variables of interest (GSAT and more)
1
Compute target annual GSAT time series
4
Compute available annual GSAT time series
1
(Smooth and) split GSAT series into X-year target pieces
4
Choose X, n. years for moving avg and piece length
Smooth and split GSAT series into X-year available pieces
2
Compute (T,X*dT) for each target piece
4
Choose Z, tolerance radius for neighborhood
Compute (T,X*dT) for each available piece
3
Identify available neighbors for each of the target pieces in the space (T, X*dT)
5
Choose criterion to select single neighbor
Identify sequence of available pieces reconstructing target GSAT
6
Translate sequence of pieces into sequence of pointers to experiments/ time periods
7
Extract and stitch together variables of interest according to sequence of pointers
External choices/ parameter settings
Algorithm steps

Figure A1. Numbers to the side of the boxes refer to the algorithm steps detailed in section 2.

Appendix B: Additional GSAT time series for intermediate scenarios

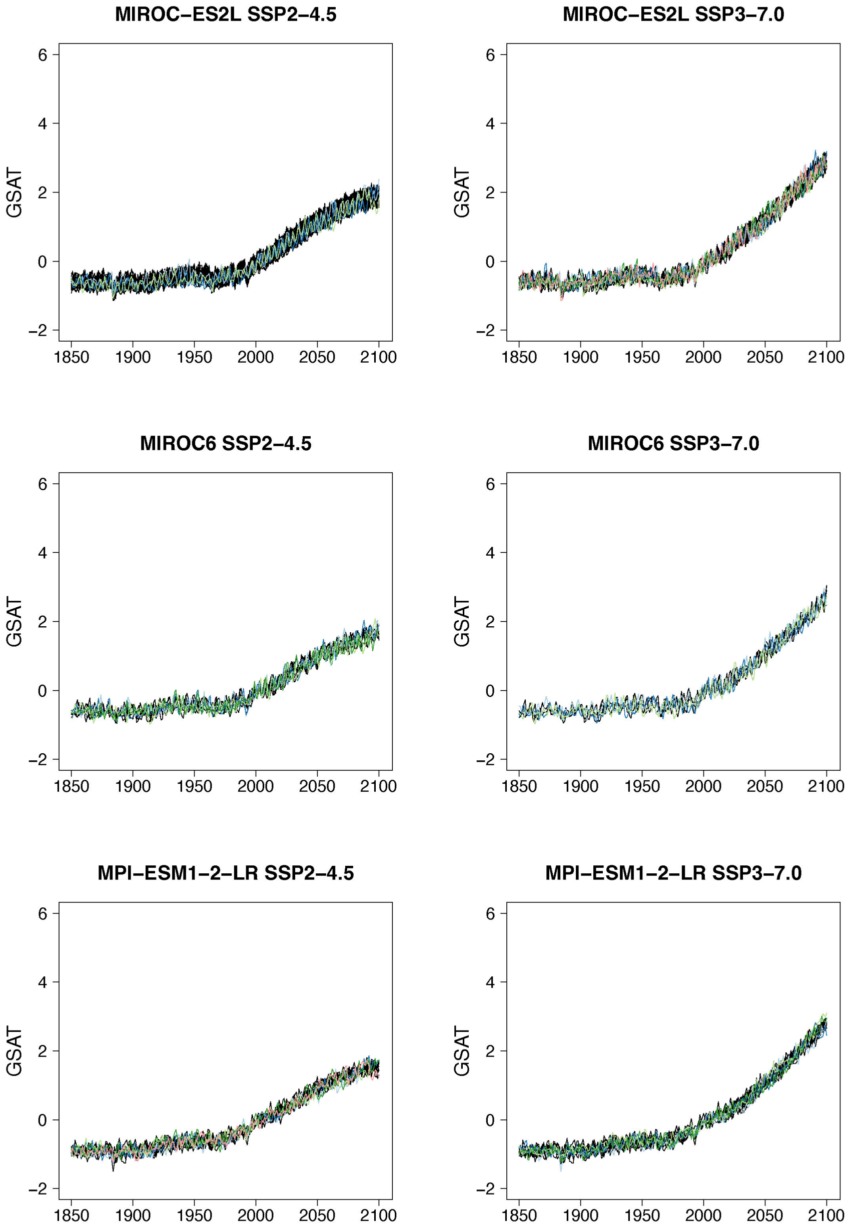

Figure B1. Examples of target (black lines) and stitched (colored) GSAT time series for ESMs in the PANGEO archive that ran at least one trajectory along the Tier 1 experiments of ScenarioMIP (SSP1-2.6; SSP2-4.5; SSP3-7.0; SSP5-8.5). We use the two bracketing scenarios and emulate trajectories that follow the two intermediate scenarios.

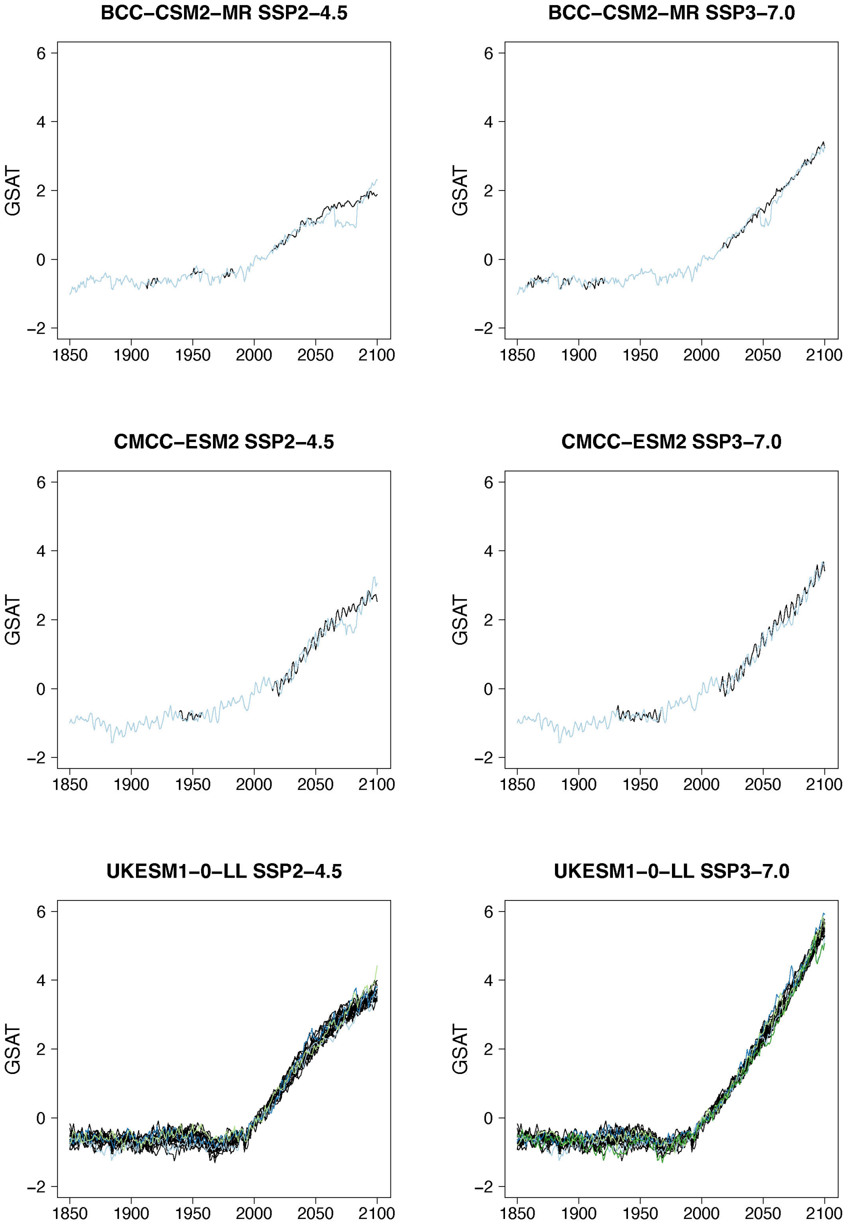

Figure B2. Examples of target (black lines) and stitched (colored) GSAT time series for ESMs in the PANGEO archive that ran at least one trajectory along the Tier 1 experiments of ScenarioMIP (SSP1-2.6; SSP2-4.5; SSP3-7.0; SSP5-8.5). We use the two bracketing scenarios and emulate trajectories that follow the two intermediate scenarios.

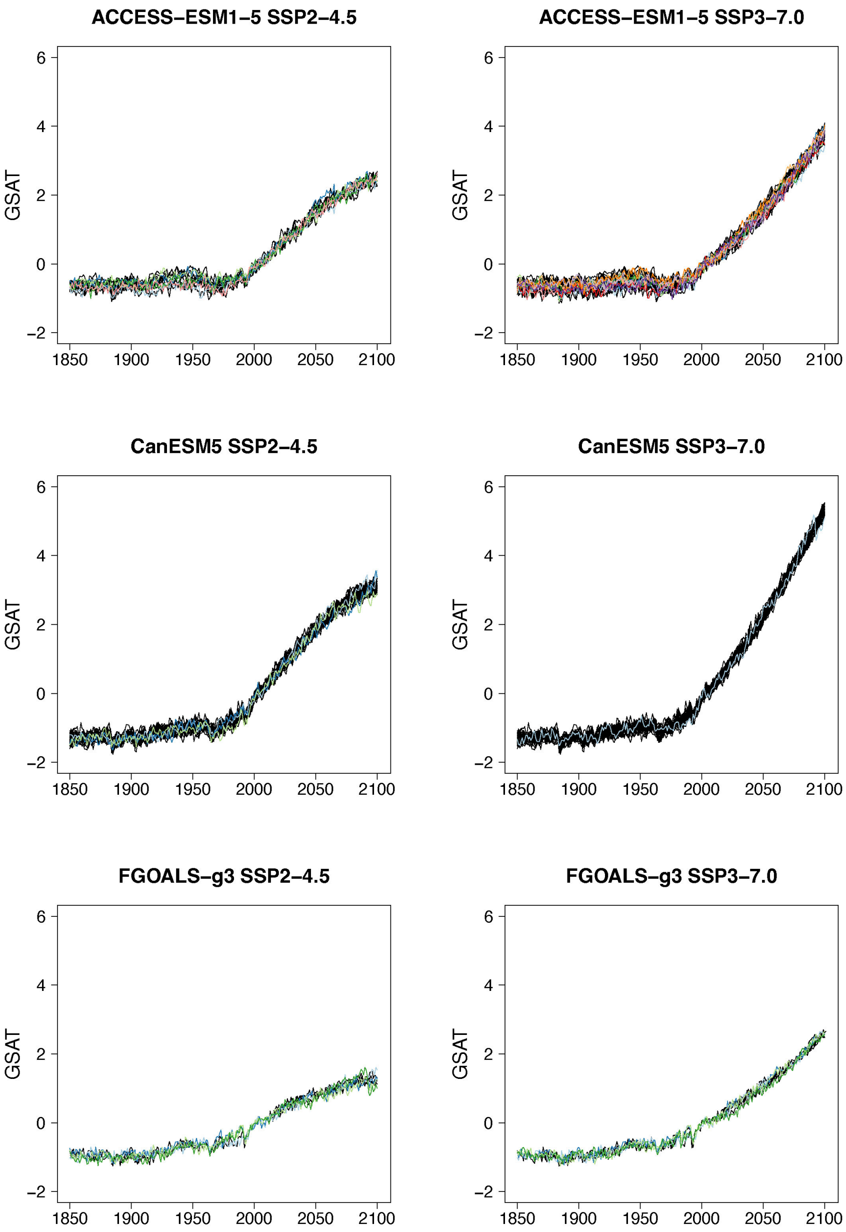

Figure B3. Examples of target (black lines) and stitched (colored) GSAT time series for ESMs in the PANGEO archive that ran at least one trajectory along the Tier 1 experiments of ScenarioMIP (SSP1-2.6; SSP2-4.5; SSP3-7.0; SSP5-8.5). We use the two bracketing scenarios and emulate trajectories that follow the two intermediate scenarios.

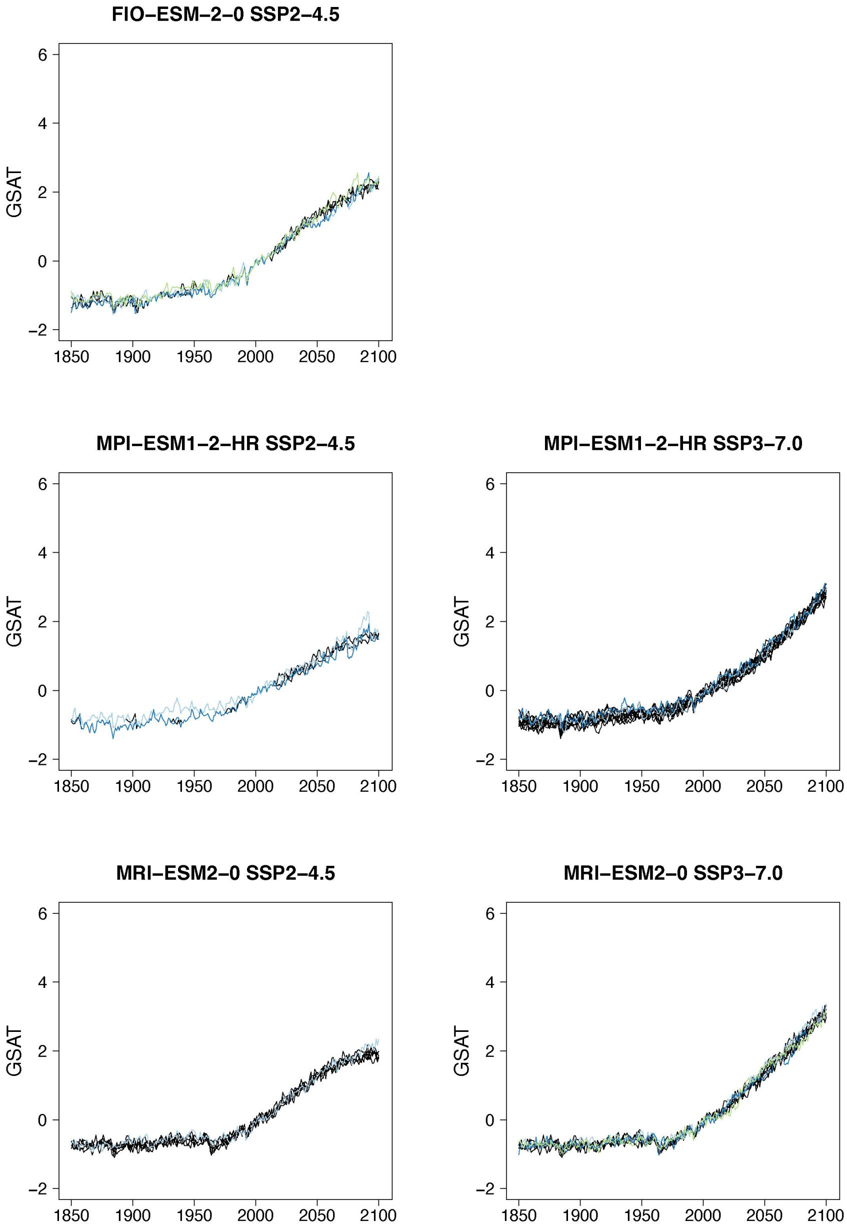

Figure B4. Examples of target (black lines) and stitched (colored) GSAT time series for ESMs in the PANGEO archive that ran at least one trajectory along the Tier 1 experiments of ScenarioMIP (SSP1-2.6; SSP2-4.5; SSP3-7.0; SSP5-8.5). We use the two bracketing scenarios and emulate trajectories that follow the two intermediate scenarios.

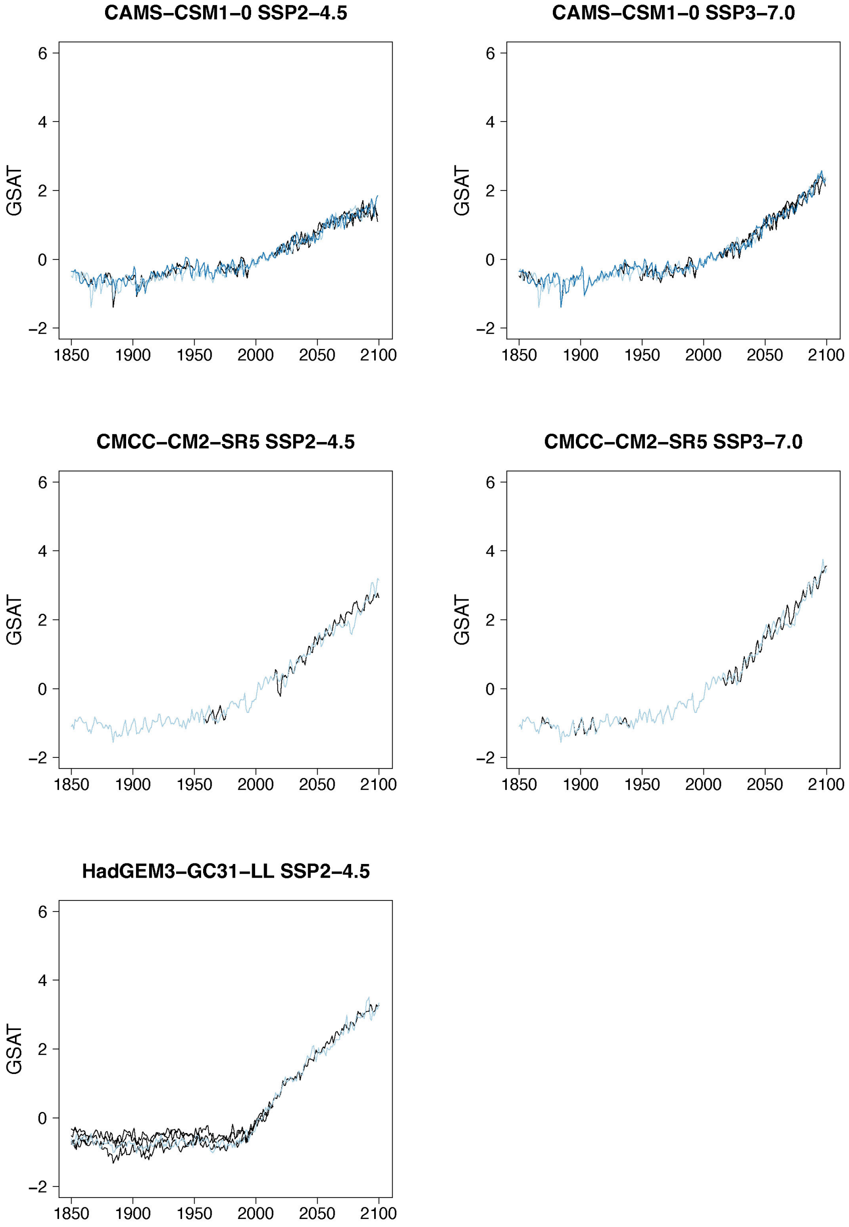

Figure B5. Examples of target (black lines) and stitched (colored) GSAT time series for ESMs in the PANGEO archive that ran at least one trajectory along the Tier 1 experiments of ScenarioMIP (SSP1-2.6; SSP2-4.5; SSP3-7.0; SSP5-8.5). We use the two bracketing scenarios and emulate trajectories that follow the two intermediate scenarios.

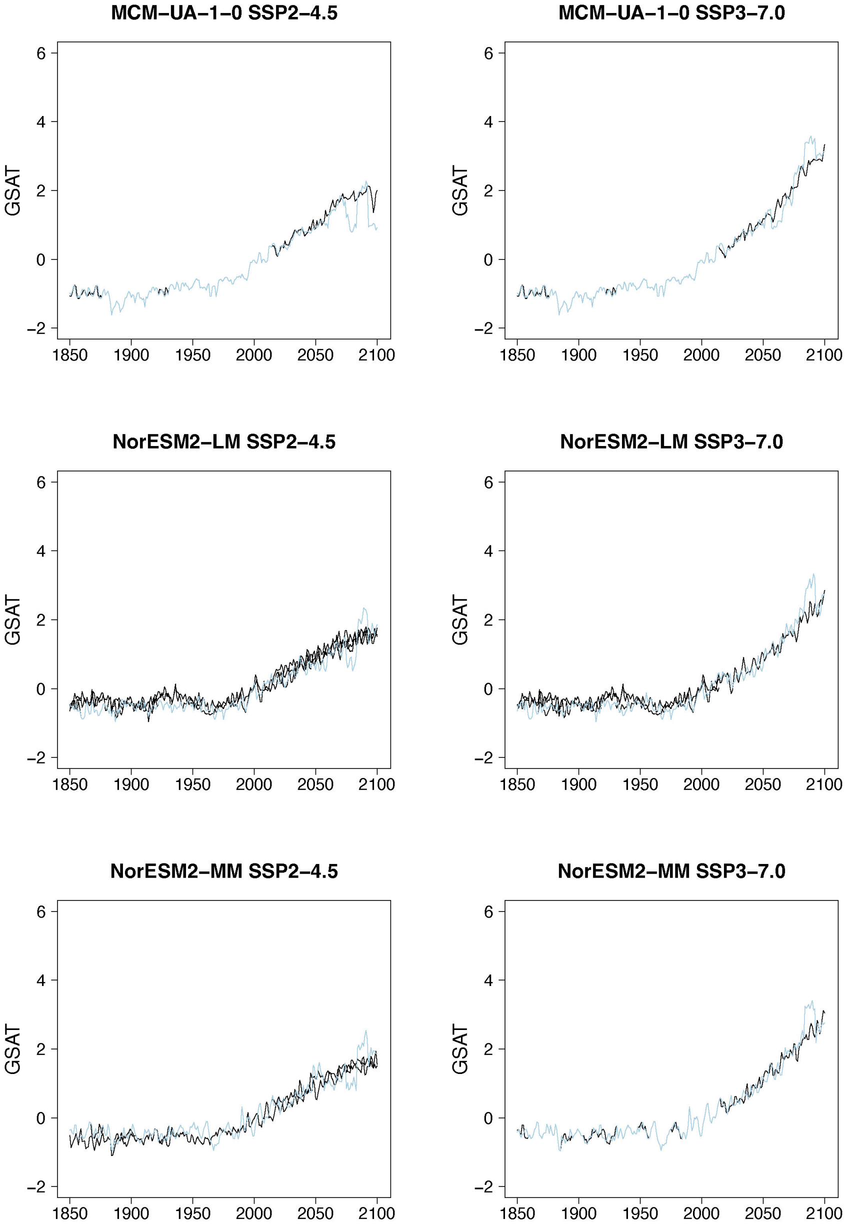

Figure B6. Examples of target (black lines) and stitched (colored) GSAT time series for ESMs in the PANGEO archive that ran at least one trajectory along the Tier 1 experiments of ScenarioMIP (SSP1-2.6; SSP2-4.5; SSP3-7.0; SSP5-8.5). We use the two bracketing scenarios and emulate trajectories that follow the two intermediate scenarios.

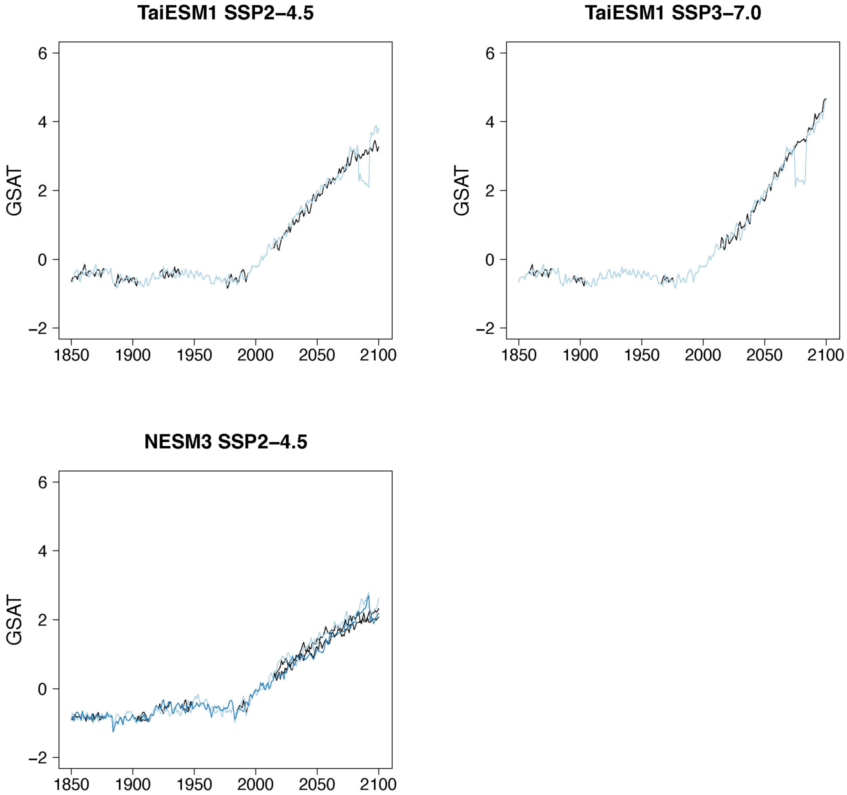

Figure B7. Examples of target (black lines) and stitched (colored) GSAT time series for ESMs in the PANGEO archive that ran at least one trajectory along the Tier 1 experiments of ScenarioMIP (SSP1-2.6; SSP2-4.5; SSP3-7.0; SSP5-8.5). We use the two bracketing scenarios and emulate trajectories that follow the two intermediate scenarios.

Appendix C: Additional trend and variability analysis of gridded data

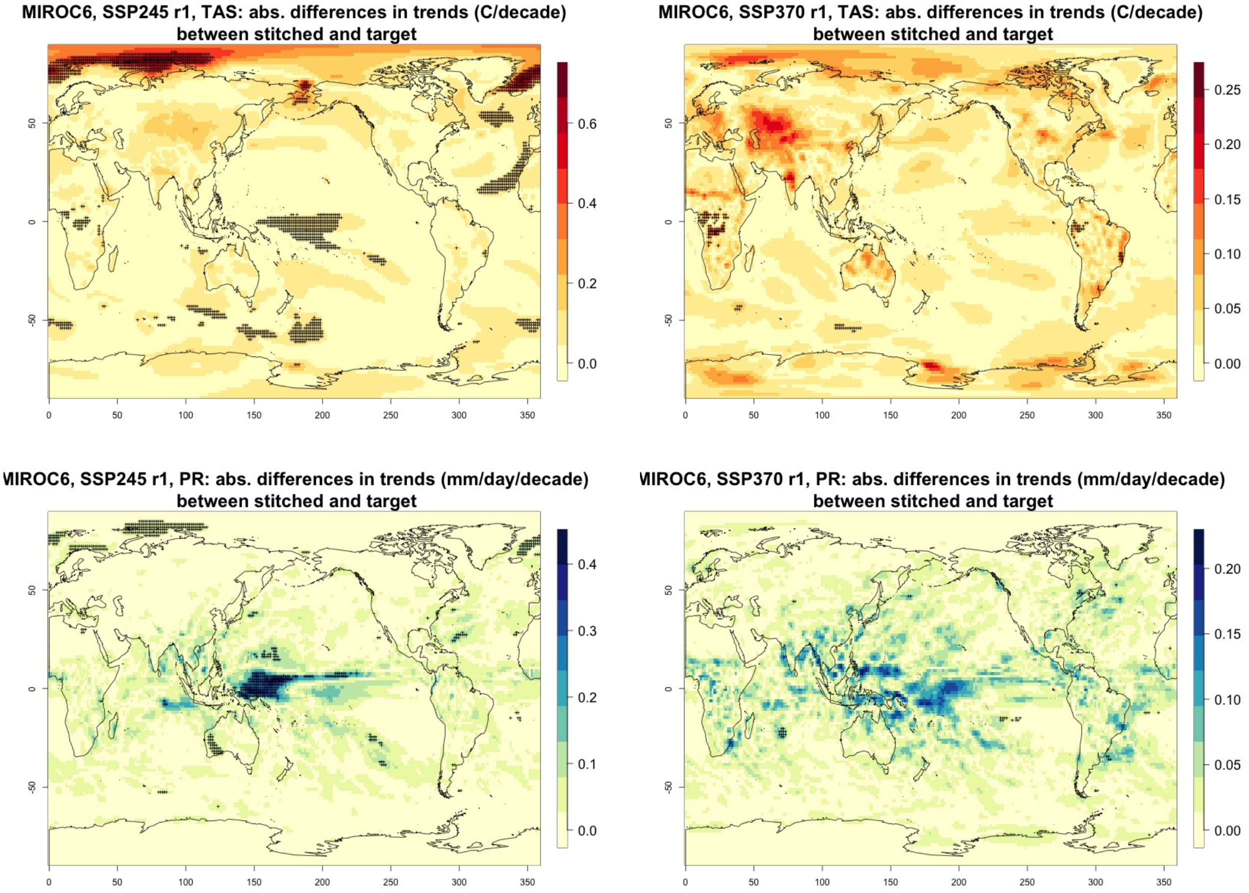
MIROC6, SSP245 r1, TAS: abs. differences in trends (C/decade) between stitched and target
MIROC6, SSP370 r1, TAS: abs. differences in trends (C/decade) between stitched and target
MIROC6, SSP245 r1, PR: abs. differences in trends (mm/day/decade) between stitched and target
MIROC6, SSP370 r1, PR: abs. differences in trends (mm/day/decade) between stitched and target
50
0
-50
0
50
100
150
200
250
300
350
0.0
0.2
0.4
0.6
0.00
0.05
0.10
0.15
0.20
0.25
0.0
0.1
0.2
0.3
0.4
0.00
0.05
0.10
0.15
0.20

Figure C1. Absolute difference in decadal trends of temperature (TAS) and precipitation (PR) between stitched and target realizations. The value of the difference is expressed by the color scale and we marked as significant by black crosses those locations where the 95% confidence intervals of the trends computed from target and stitched time series do not overlap, indicating statistically significant differences. Emulation of MIROC6, monthly time series over 2015-2100, for SSP2-4.5 and SSP3-7.0. First realization.

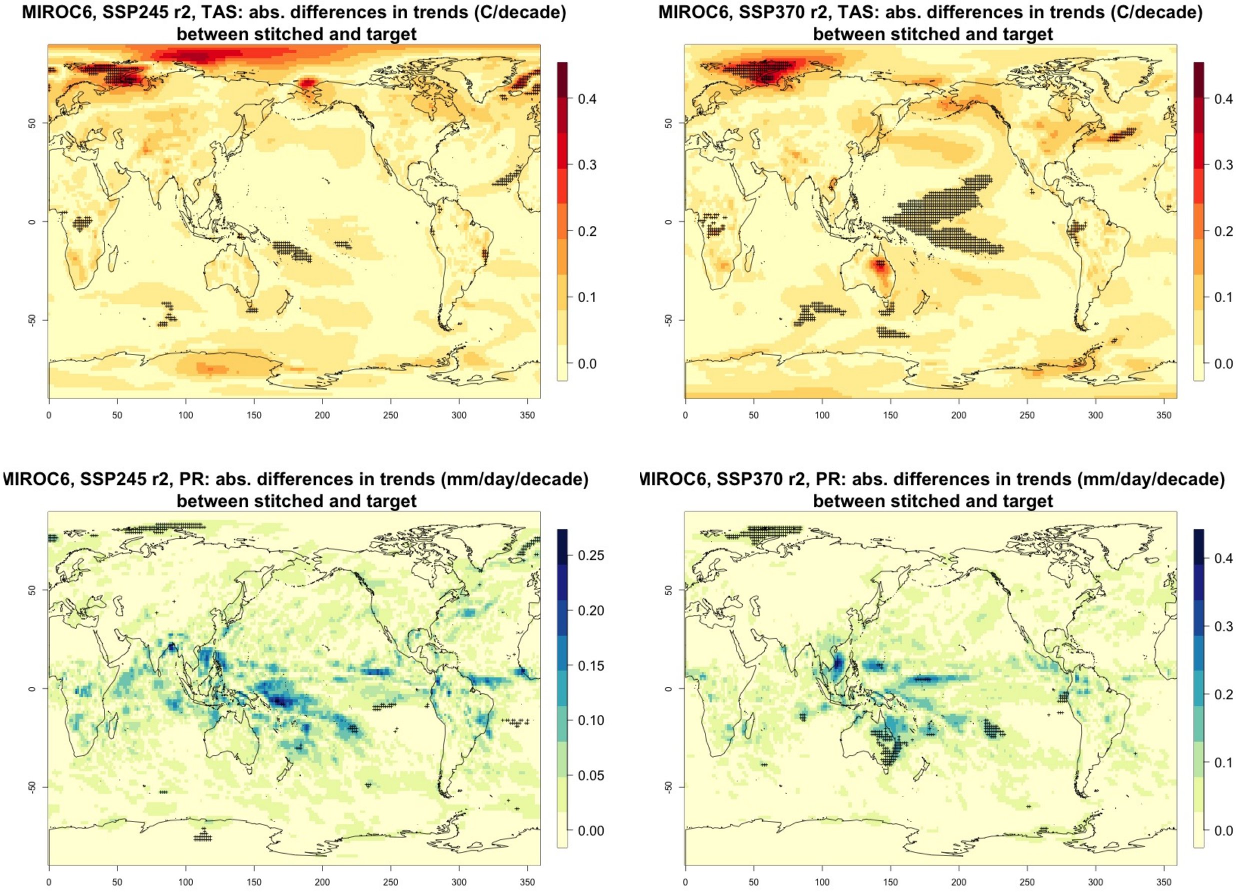
MIROC6, SSP245 r2, TAS: abs. differences in trends (C/decade)
between stitched and target
MIROC6, SSP370 r2, TAS: abs. differences in trends (C/decade)
between stitched and target
MIROC6, SSP245 r2, PR: abs. differences in trends (mm/day/decade)
between stitched and target
MIROC6, SSP370 r2, PR: abs. differences in trends (mm/day/decade)
between stitched and target
-50
0
50
0
50
100
150
200
250
300
350
0.0
0.1
0.2
0.3
0.4
0.00
0.05
0.10
0.15
0.20
0.25

Figure C2. Absolute difference in decadal trends of temperature (TAS) and precipitation (PR) between stitched and target realizations. The value of the difference is expressed by the color scale and we marked as significant by black crosses those locations where the 95% confidence intervals of the trends computed from target and stitched time series do not overlap, indicating statistically significant differences. Emulation of MIROC6, monthly time series over 2015-2100, for SSP2-4.5 and SSP3-7.0. Second realization.

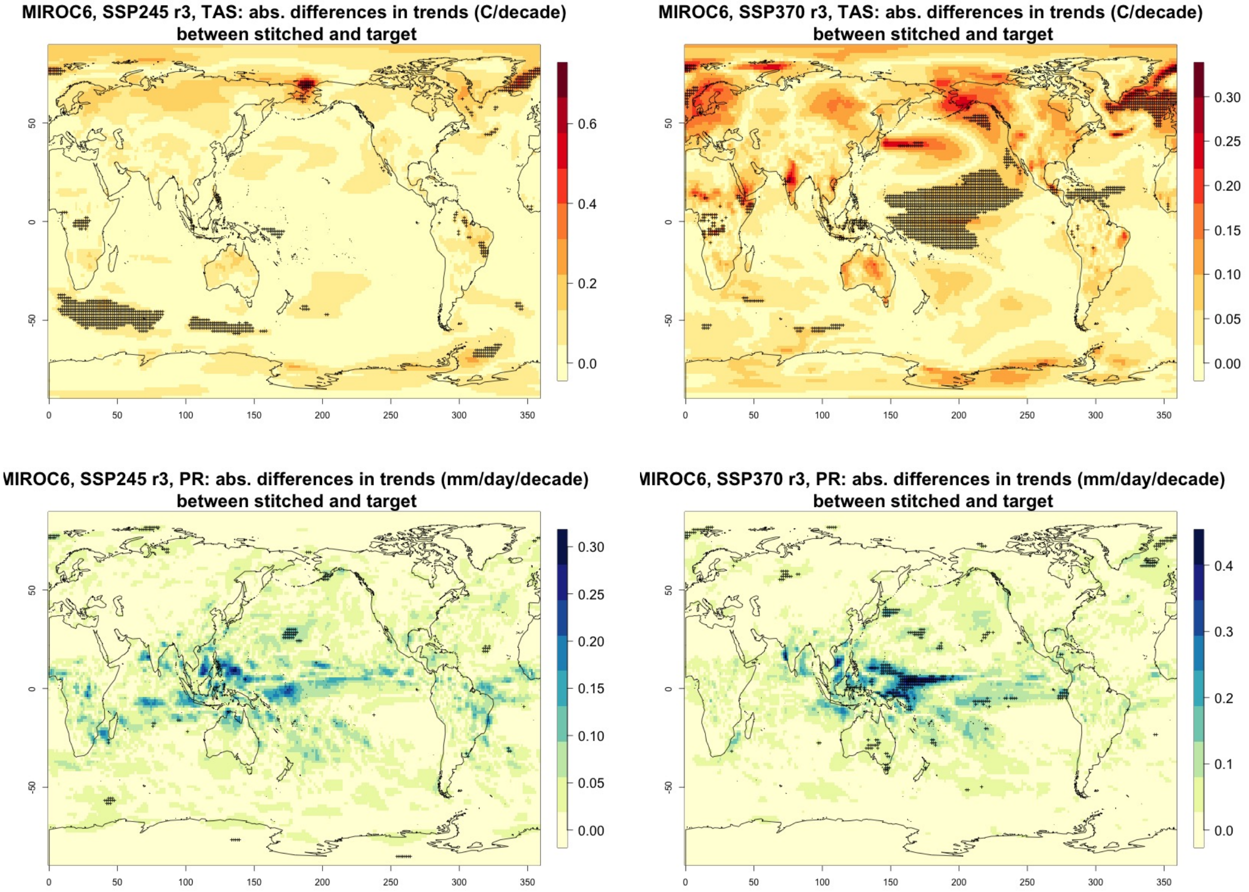
MIROC6, SSP245 r3, TAS: abs. differences in trends (C/decade) between stitched and target

MIROC6, SSP370 r3, TAS: abs. differences in trends (C/decade) between stitched and target

MIROC6, SSP245 r3, PR: abs. differences in trends (mm/day/decade) between stitched and target

MIROC6, SSP370 r3, PR: abs. differences in trends (mm/day/decade) between stitched and target

Figure C3. Absolute difference in decadal trends of temperature (TAS) and precipitation (PR) between stitched and target realizations. The value of the difference is expressed by the color scale and we marked as significant by black crosses those locations where the 95% confidence intervals of the trends computed from target and stitched time series do not overlap, indicating statistically significant differences. Emulation of MIROC6, monthly time series over 2015-2100, for SSP2-4.5 and SSP3-7.0. Third realization.

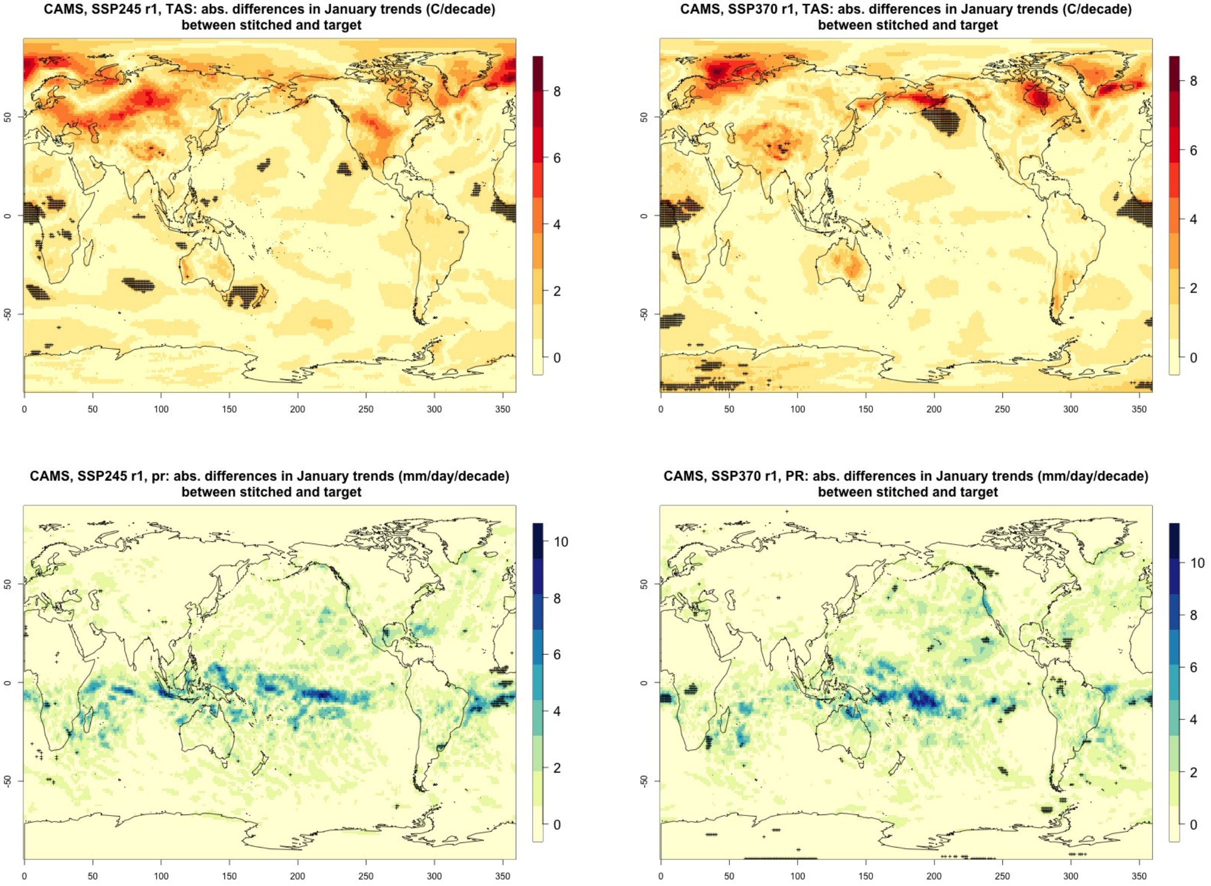
CAMS, SSP245 r1, TAS: abs. differences in January trends (C/decade)
between stitched and target
CAMS, SSP370 r1, TAS: abs. differences in January trends (C/decade)
between stitched and target
CAMS, SSP245 r1, pr: abs. differences in January trends (mm/day/decade)
between stitched and target
CAMS, SSP370 r1, PR: abs. differences in January trends (mm/day/decade)
between stitched and target
50
0
-50
0
50
100
150
200
250
300
350
0
2
4
6
8
10

Figure C4. Absolute difference in decadal trends of January temperature (TAS) and precipitation (PR) between stitched and target realizations. The value of the difference is expressed by the color scale and we marked as significant by black crosses those locations where the 95% confidence intervals of the trends computed from target and stitched time series do not overlap, indicating statistically significant differences. Emulation of CAMS, January time series over 2015-2100, for SSP2-4.5 and SSP3-7.0.

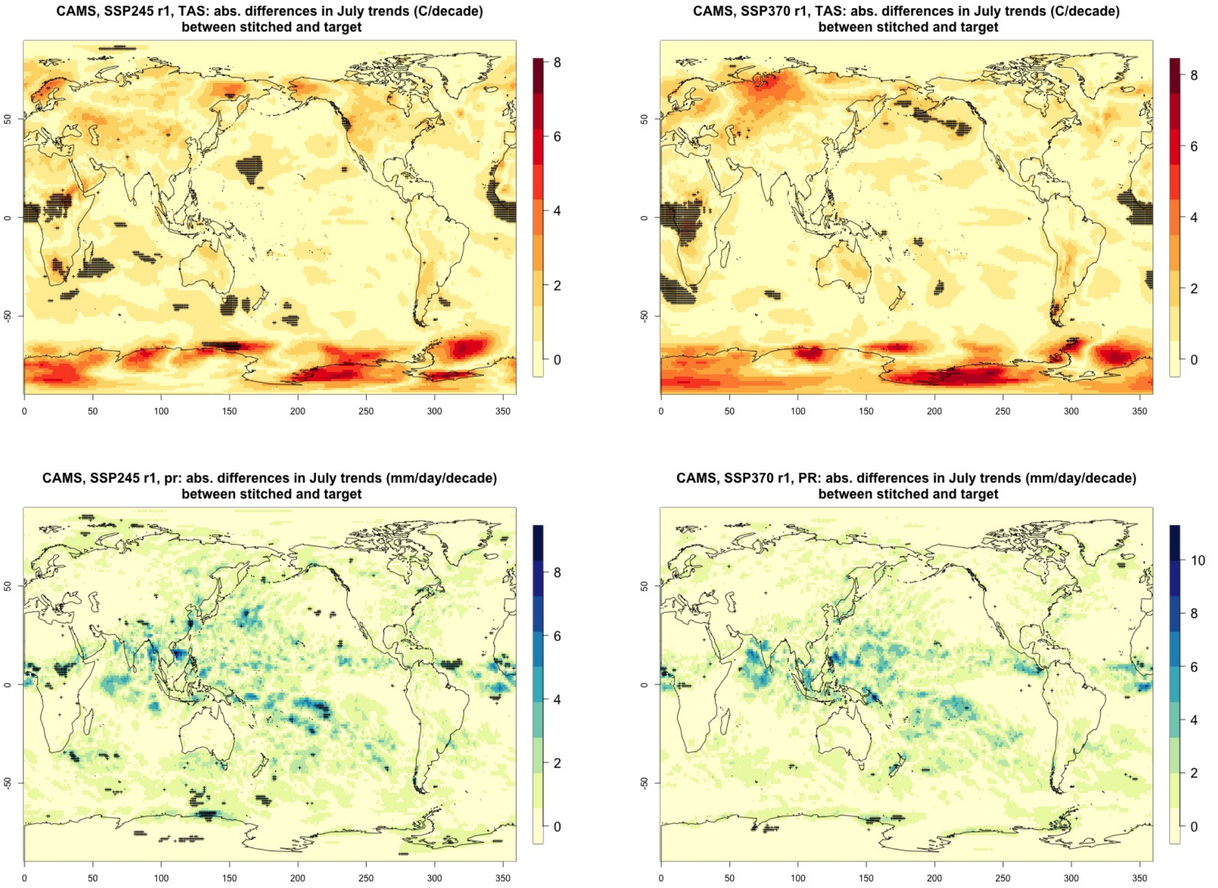

CAMS, SSP245 r1, TAS: abs. differences in July trends (C/decade) between stitched and target

CAMS, SSP370 r1, TAS: abs. differences in July trends (C/decade) between stitched and target

CAMS, SSP245 r1, pr: abs. differences in July trends (mm/day/decade) between stitched and target

CAMS, SSP370 r1, PR: abs. differences in July trends (mm/day/decade) between stitched and target

Figure C5. Absolute difference in decadal trends of July temperature (TAS) and precipitation (PR) between stitched and target realizations. The value of the difference is expressed by the color scale and we marked as significant by black crosses those locations where the 95% confidence intervals of the trends computed from target and stitched time series do not overlap, indicating statistically significant differences. Emulation of CAMS, July time series over 2015-2100, for SSP2-4.5 and SSP3-7.0.

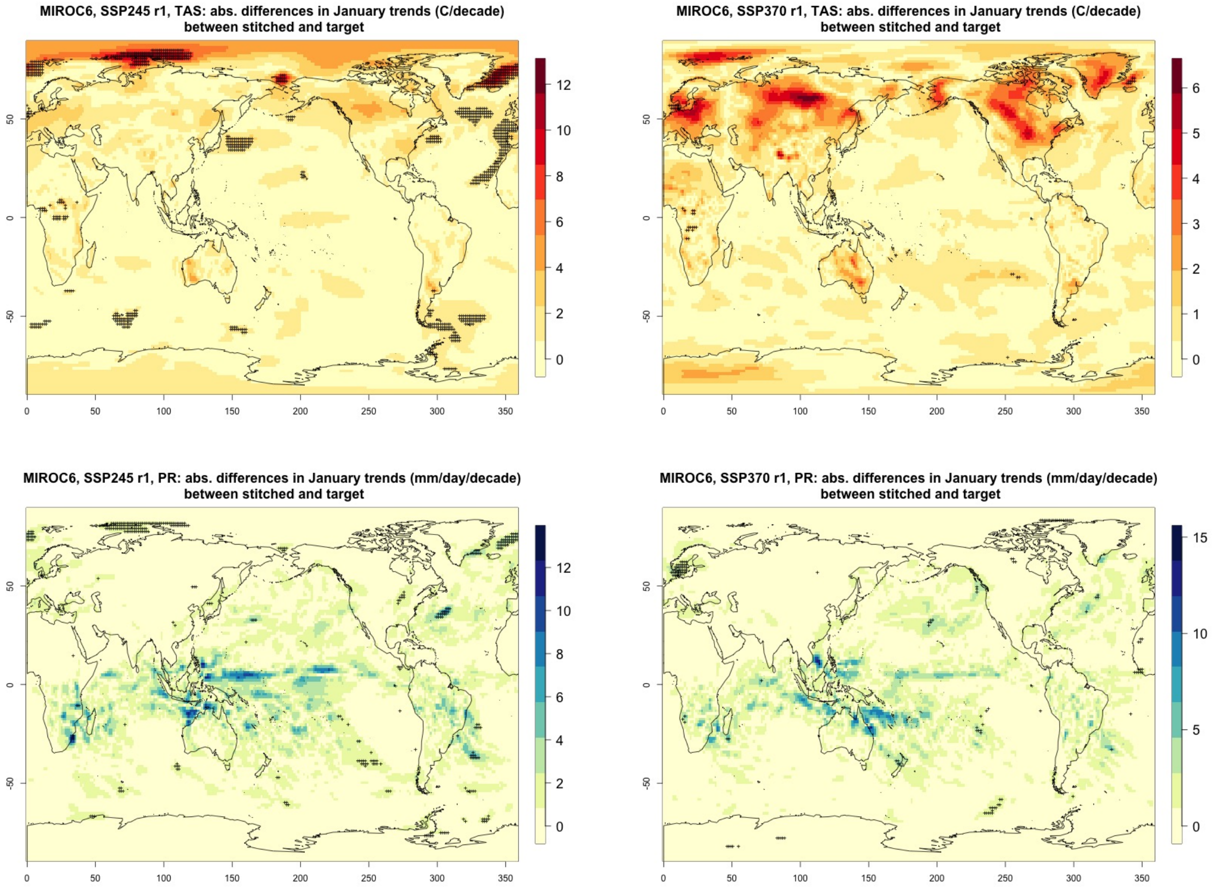
MIROC6, SSP245 r1, TAS: abs. differences in January trends (C/decade)
between stitched and target
MIROC6, SSP370 r1, TAS: abs. differences in January trends (C/decade)
between stitched and target
MIROC6, SSP245 r1, PR: abs. differences in January trends (mm/day/decade)
between stitched and target
MIROC6, SSP370 r1, PR: abs. differences in January trends (mm/day/decade)
between stitched and target
12
10
8
6
4
2
0
6
5
4
3
2
1
0
12
10
8
6
4
2
0
15
10
5
0
50
0
-50
0
50
100
150
200
250
300
350

Figure C6. Absolute difference in decadal trends of January temperature (TAS) and precipitation (PR) between stitched and target realizations. The value of the difference is expressed by the color scale and we marked as significant by black crosses those locations where the 95% confidence intervals of the trends computed from target and stitched time series do not overlap, indicating statistically significant differences. Emulation of MIROC6, January time series over 2015-2100, for SSP2-4.5 and SSP3-7.0. First realization.

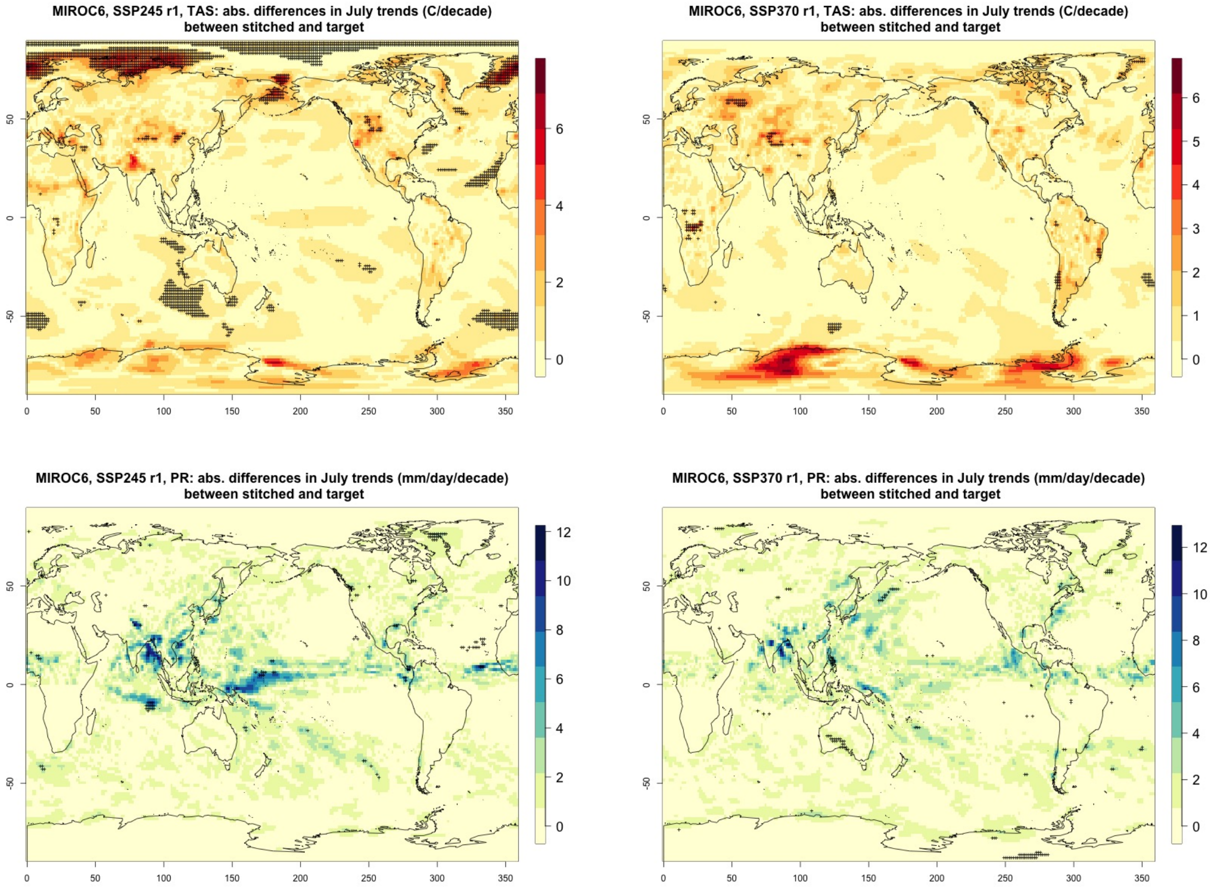
MIROC6, SSP245 r1, TAS: abs. differences in July trends (C/decade)
between stitched and target
MIROC6, SSP370 r1, TAS: abs. differences in July trends (C/decade)
between stitched and target
MIROC6, SSP245 r1, PR: abs. differences in July trends (mm/day/decade)
between stitched and target
MIROC6, SSP370 r1, PR: abs. differences in July trends (mm/day/decade)
between stitched and target
50
0
-50
0
50
100
150
200
250
300
350
0
2
4
6
0
1
2
3
4
5
6
0
2
4
6
8
10
12

Figure C7. Absolute difference in decadal trends of July temperature (TAS) and precipitation (PR) between stitched and target realizations. The value of the difference is expressed by the color scale and we marked as significant by black crosses those locations where the 95% confidence intervals of the trends computed from target and stitched time series do not overlap, indicating statistically significant differences. Emulation of MIROC6, July time series over 2015-2100, for SSP2-4.5 and SSP3-7.0. First realization.

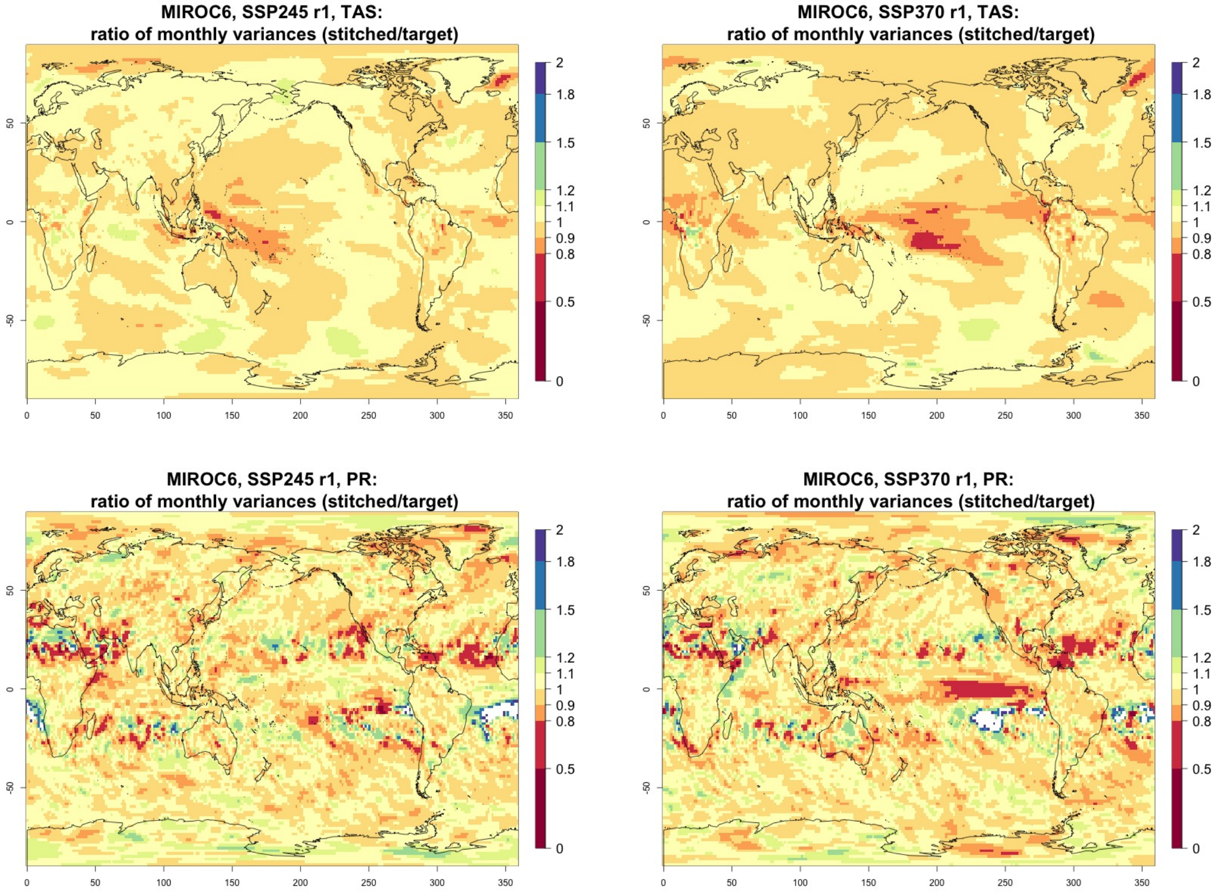

MIROC6, SSP245 r1, TAS:
ratio of monthly variances (stitched/target)

MIROC6, SSP370 r1, TAS:
ratio of monthly variances (stitched/target)

MIROC6, SSP245 r1, PR:
ratio of monthly variances (stitched/target)

MIROC6, SSP370 r1, PR:
ratio of monthly variances (stitched/target)

Figure C8. Ratio in monthly variability (standard deviation of residuals from trends) of temperature (TAS) and precipitation (PR) between stitched (at the numerator) and target (at the denominator) time series. The value of the ratio is expressed by the color scale which highlights the transitions at 0.8 and 1.2. Emulation of MIROC6, monthly time series over 2015-2100, for SSP2-4.5 and SSP3-7.0. First realization.

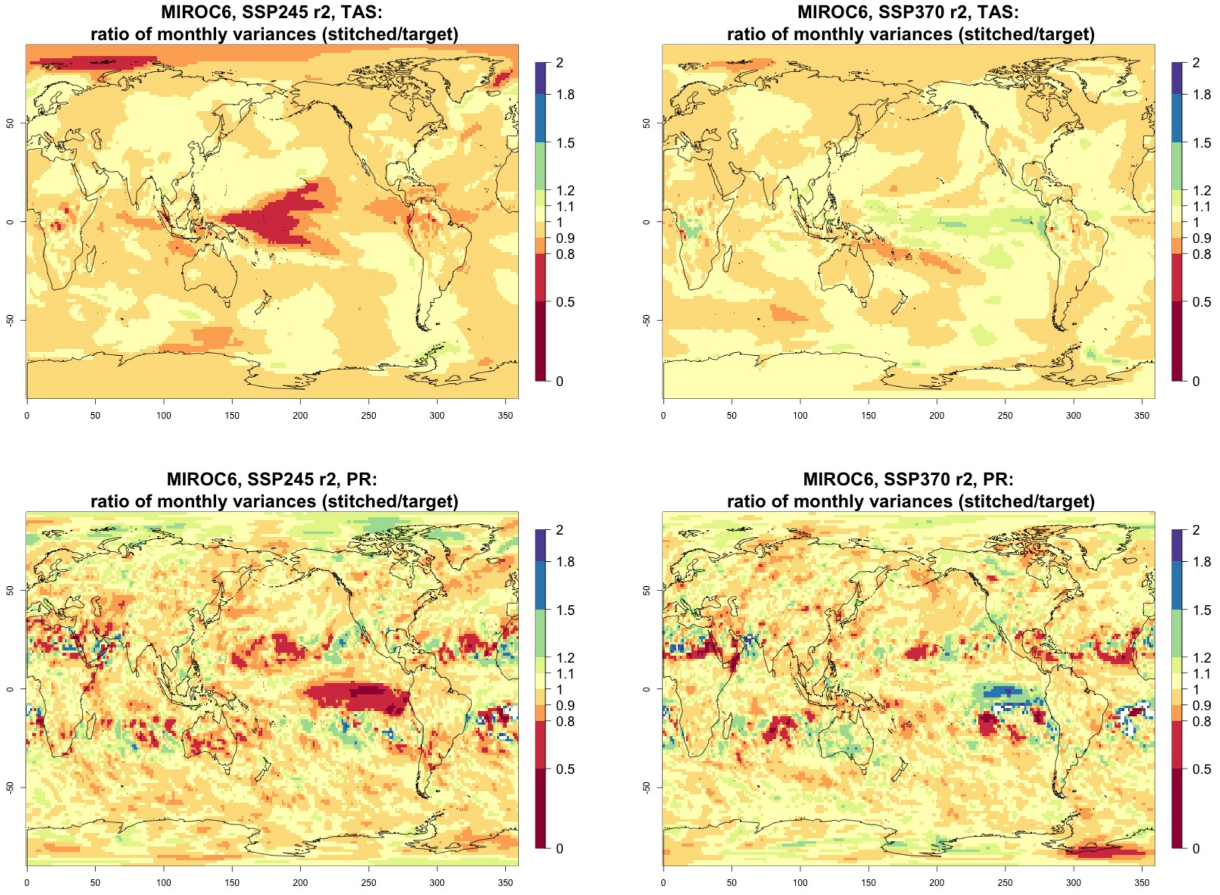
MIROC6, SSP245 r2, TAS:
ratio of monthly variances (stitched/target)
MIROC6, SSP370 r2, TAS:
ratio of monthly variances (stitched/target)
MIROC6, SSP245 r2, PR:
ratio of monthly variances (stitched/target)
MIROC6, SSP370 r2, PR:
ratio of monthly variances (stitched/target)
50
0
-50
0
50
100
150
200
250
300
350
2
1.8
1.5
1.2
1.1
1
0.9
0.8
0.5
0

Figure C9. Ratio in monthly variability (standard deviation of residuals from trends) of temperature (TAS) and precipitation (PR) between stitched (at the numerator) and target (at the denominator) time series. The value of the ratio is expressed by the color scale which highlights the transitions at 0.8 and 1.2. Emulation of MIROC6, monthly time series over 2015-2100, for SSP2-4.5 and SSP3-7.0. Second realization.

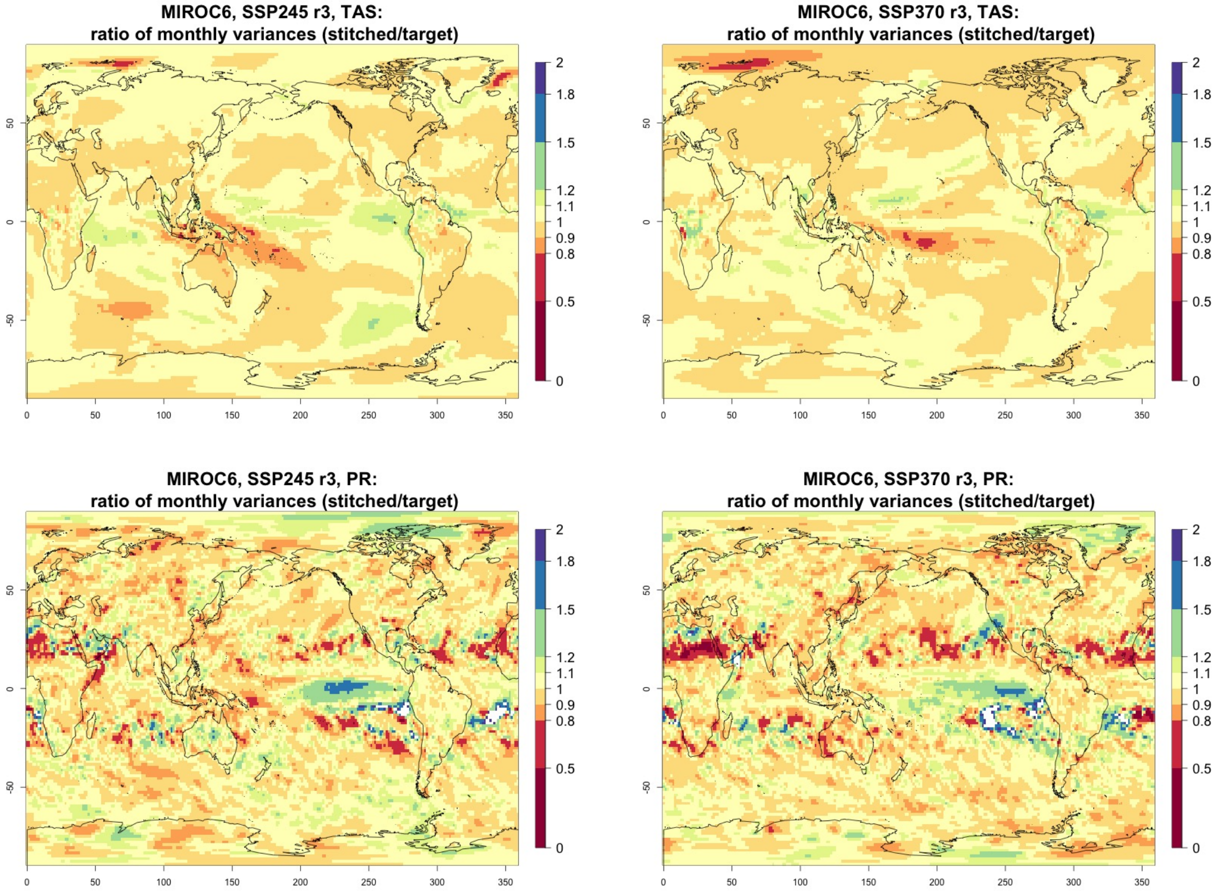

MIROC6, SSP245 r3, TAS:
ratio of monthly variances (stitched/target)

MIROC6, SSP370 r3, TAS:
ratio of monthly variances (stitched/target)

MIROC6, SSP245 r3, PR:
ratio of monthly variances (stitched/target)

MIROC6, SSP370 r3, PR:
ratio of monthly variances (stitched/target)

Figure C10. Ratio in monthly variability (standard deviation of residuals from trends) of temperature (TAS) and precipitation (PR) between stitched (at the numerator) and target (at the denominator) time series. The value of the ratio is expressed by the color scale which highlights the transitions at 0.8 and 1.2. Emulation of MIROC6, monthly time series over 2015-2100, for SSP2-4.5 and SSP3-7.0. Third realization.

Appendix D: Additional SOI analysis for MIROC6

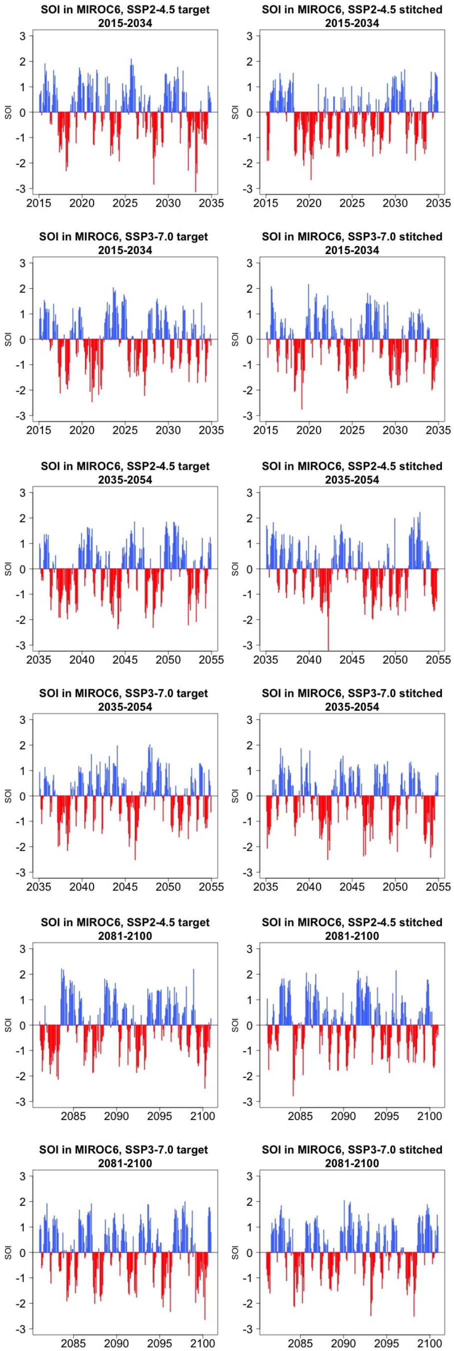

Figure D1. Examples of target (left) and stitched (right) SOI time series for three twenty-year windows along the length of the simulation: 2015-2034 in the top four panels; 2035-2054 in the middle four panels; 2081-2100 in the bottom four panels. Results from emulation of SSP2-4.5 and SSP3-7.0 for one of three ensemble members emulated under each scenario for MIROC6.

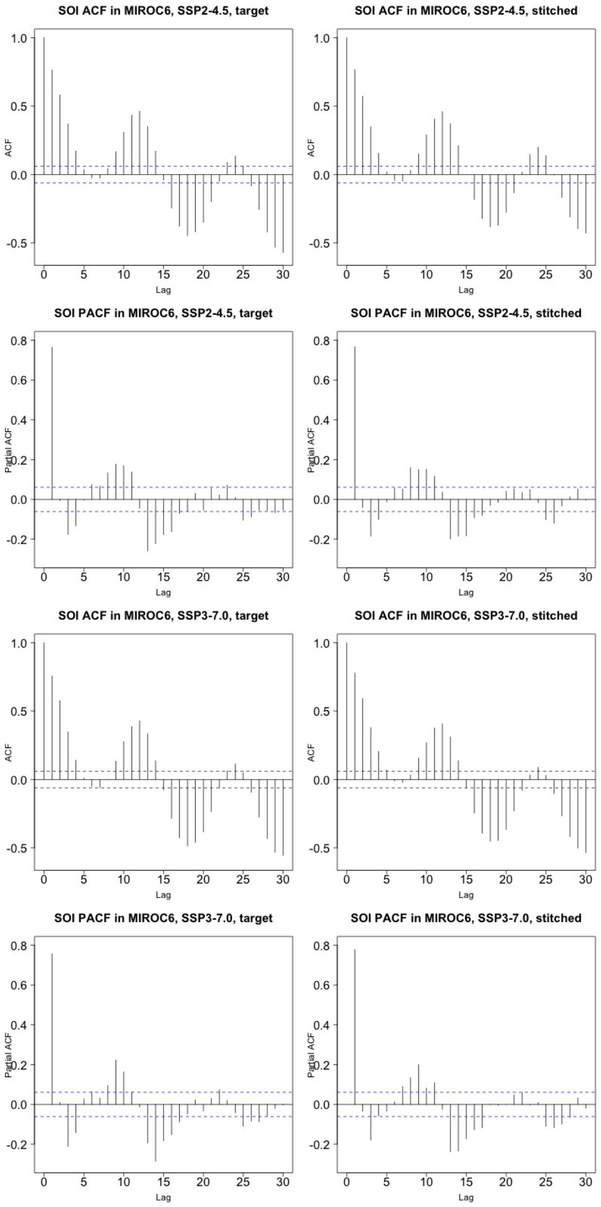

Figure D2. Auto-correlation (ACFs) and Partial auto-correlation functions (PACFs) for real and stitched SOI time series. Top two rows: SSP2-4.5 ACF for target and stitched series and respective PACFS. Bottom two rows: SSP3-7.0 ACF for target and stitchedseries and respective PACFs. Results from emulation of one of three ensemble members emulated under each scenario for MIROC6. (Our software – R function `acf(..,type="partial")` – does not define the PACF at lag zero.)

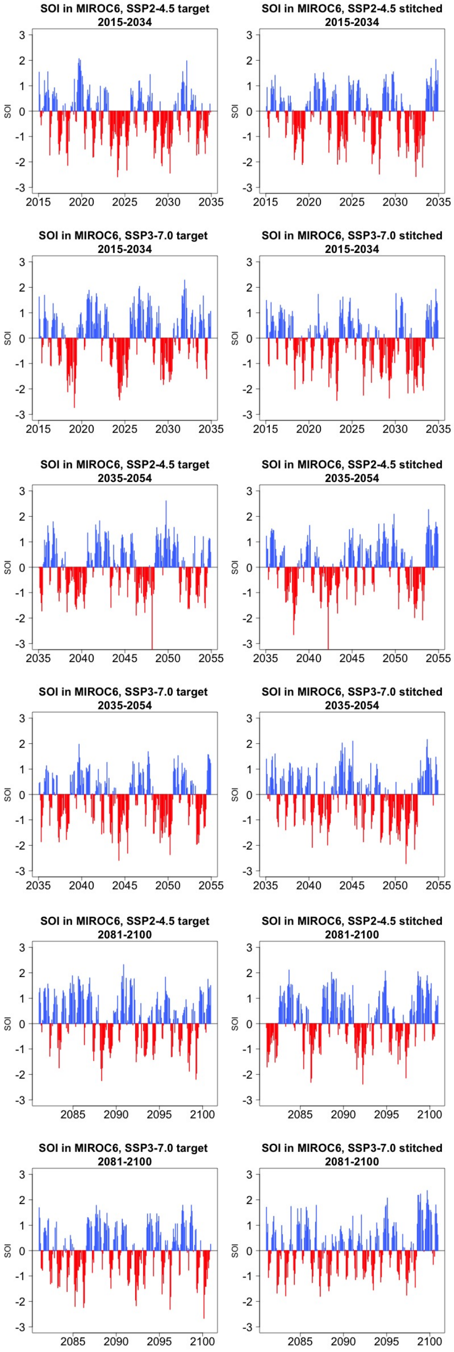

SOI in MIROC6, SSP2-4.5 target 2015-2034

SOI in MIROC6, SSP2-4.5 stitched 2015-2034

SOI in MIROC6, SSP3-7.0 target 2015-2034

SOI in MIROC6, SSP3-7.0 stitched 2015-2034

SOI in MIROC6, SSP2-4.5 target 2035-2054

SOI in MIROC6, SSP2-4.5 stitched 2035-2054

SOI in MIROC6, SSP3-7.0 target 2035-2054

SOI in MIROC6, SSP3-7.0 stitched 2035-2054

SOI in MIROC6, SSP2-4.5 target 2081-2100

SOI in MIROC6, SSP2-4.5 stitched 2081-2100

SOI in MIROC6, SSP3-7.0 target 2081-2100

SOI in MIROC6, SSP3-7.0 stitched 2081-2100

Figure D3. Examples of target (left) and stitched (right) SOI time series for three twenty-year windows along the length of the simulation: 2015-2034 in the top four panels; 2035-2054 in the middle four panels; 2081-2100 in the bottom four panels. Results from emulation of SSP2-4.5 and SSP3-7.0 for one of three ensemble members emulated under each scenario for MIROC6.

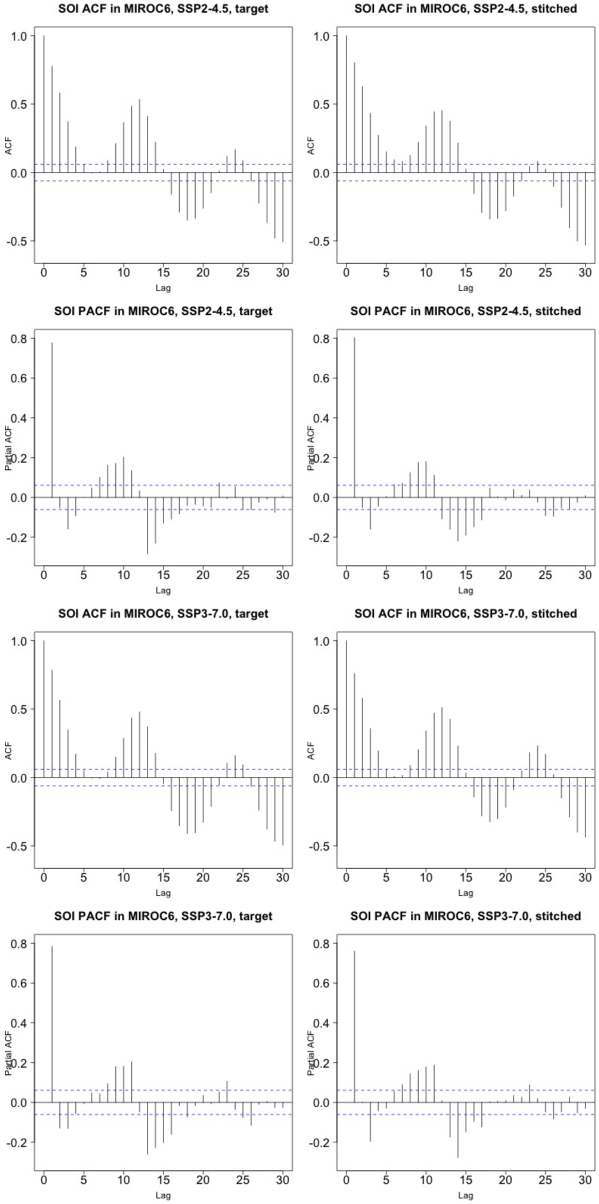

Figure D4. Auto-correlation (ACFs) and Partial auto-correlation functions (PACFs) for real and stitched SOI time series. Top two rows: SSP2-4.5 ACF for target and stitched series and respective PACFS. Bottom two rows: SSP3-7.0 ACF for target and stitchedseries and respective PACFs. Results from emulation of one of three ensemble members emulated under each scenario for MIROC6. (Our software – R function `acf(..,type="partial")` – does not define the PACF at lag zero.)

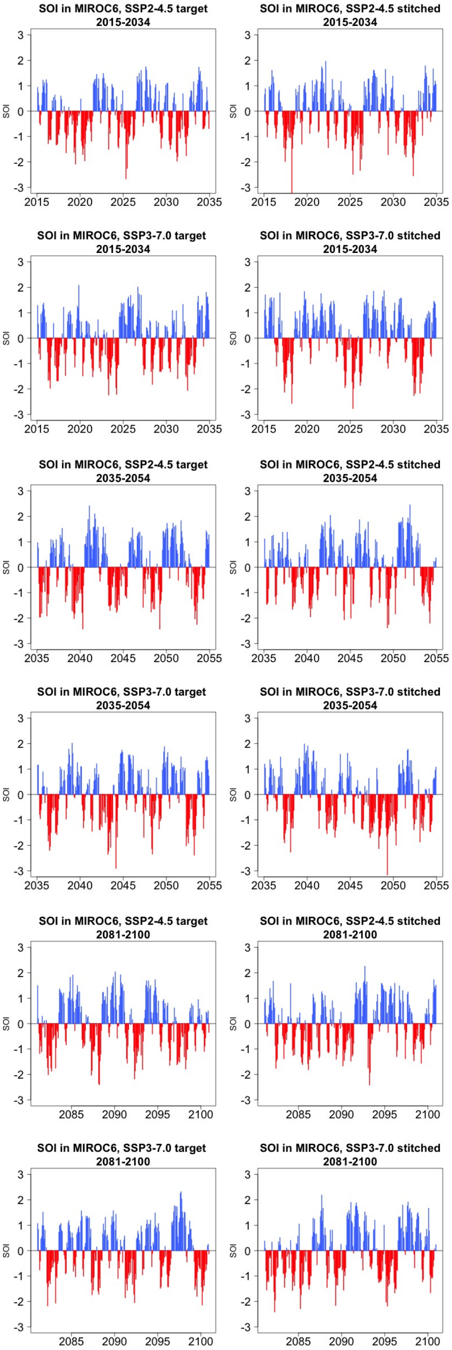

Figure D5. Examples of target (left) and stitched (right) SOI time series for three twenty-year windows along the length of the simulation: 2015-2034 in the top four panels; 2035-2054 in the middle four panels; 2081-2100 in the bottom four panels. Results from emulation of SSP2-4.5 and SSP3-7.0 for one of three ensemble members emulated under each scenario for MIROC6.

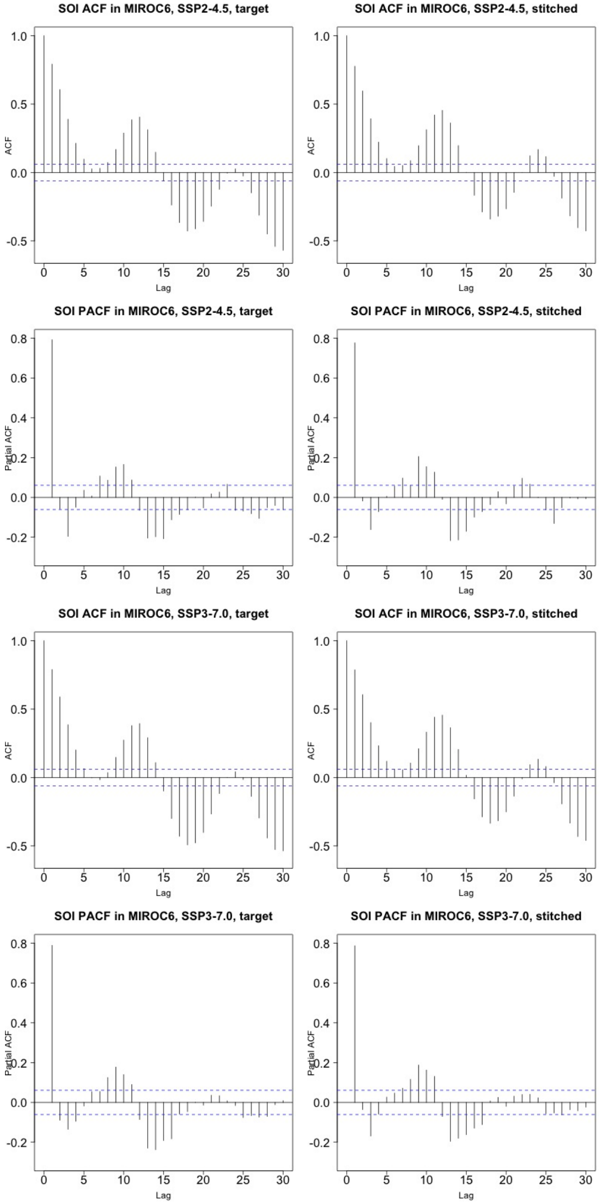
SOI ACF in MIROC6, SSP2-4.5, target

SOI ACF in MIROC6, SSP2-4.5, stitched

SOI PACF in MIROC6, SSP2-4.5, target

SOI PACF in MIROC6, SSP2-4.5, stitched

SOI ACF in MIROC6, SSP3-7.0, target

SOI ACF in MIROC6, SSP3-7.0, stitched

SOI PACF in MIROC6, SSP3-7.0, target

SOI PACF in MIROC6, SSP3-7.0, stitched

Figure D6. Auto-correlation (ACFs) and Partial auto-correlation functions (PACFs) for real and stitched SOI time series. Top two rows: SSP2-4.5 ACF for target and stitched series and respective PACFS. Bottom two rows: SSP3-7.0 ACF for target and stitchedseries and respective PACFs. Results from emulation of one of three ensemble members emulated under each scenario for MIROC6. (Our software – R function `acf(..,type="partial")` – does not define the PACF at lag zero.)

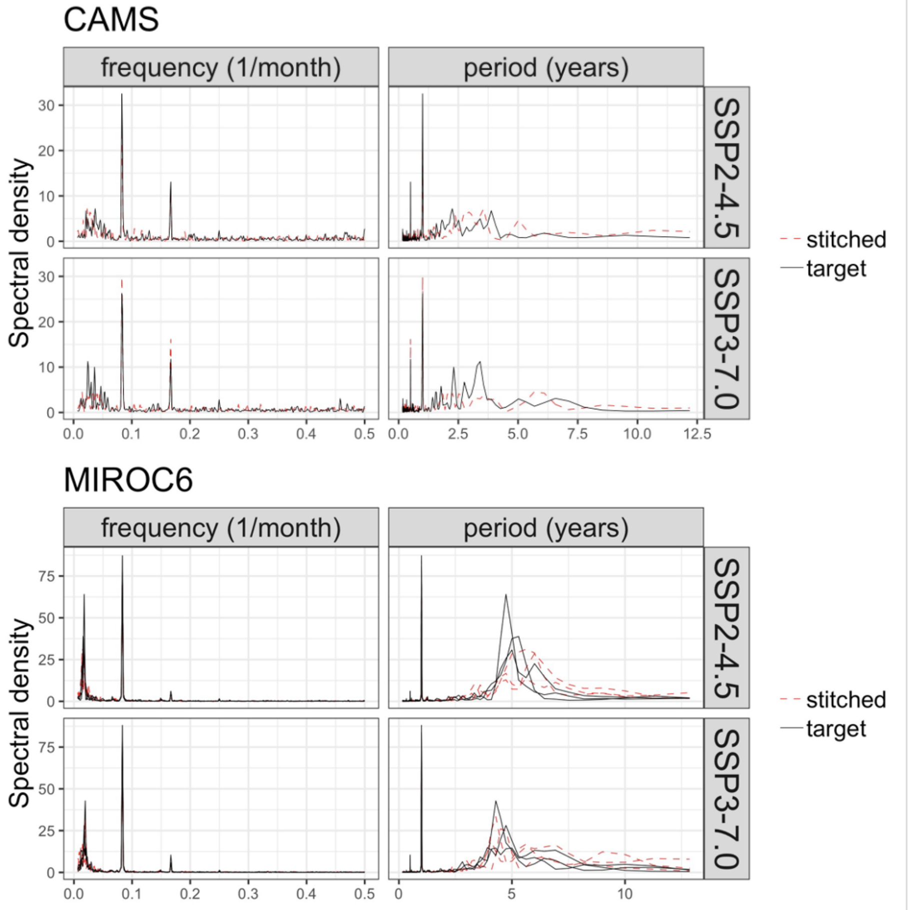

Figure D7. Spectral densities computed from target (solid lines) and stitched (dashed lines) SOI time series, for both models and one (for CAMS-CM-0, top 4 plots) and three (for MIROC6, bottom 4 plots) realizations.

Appendix E: GSAT time series for enriched ensembles

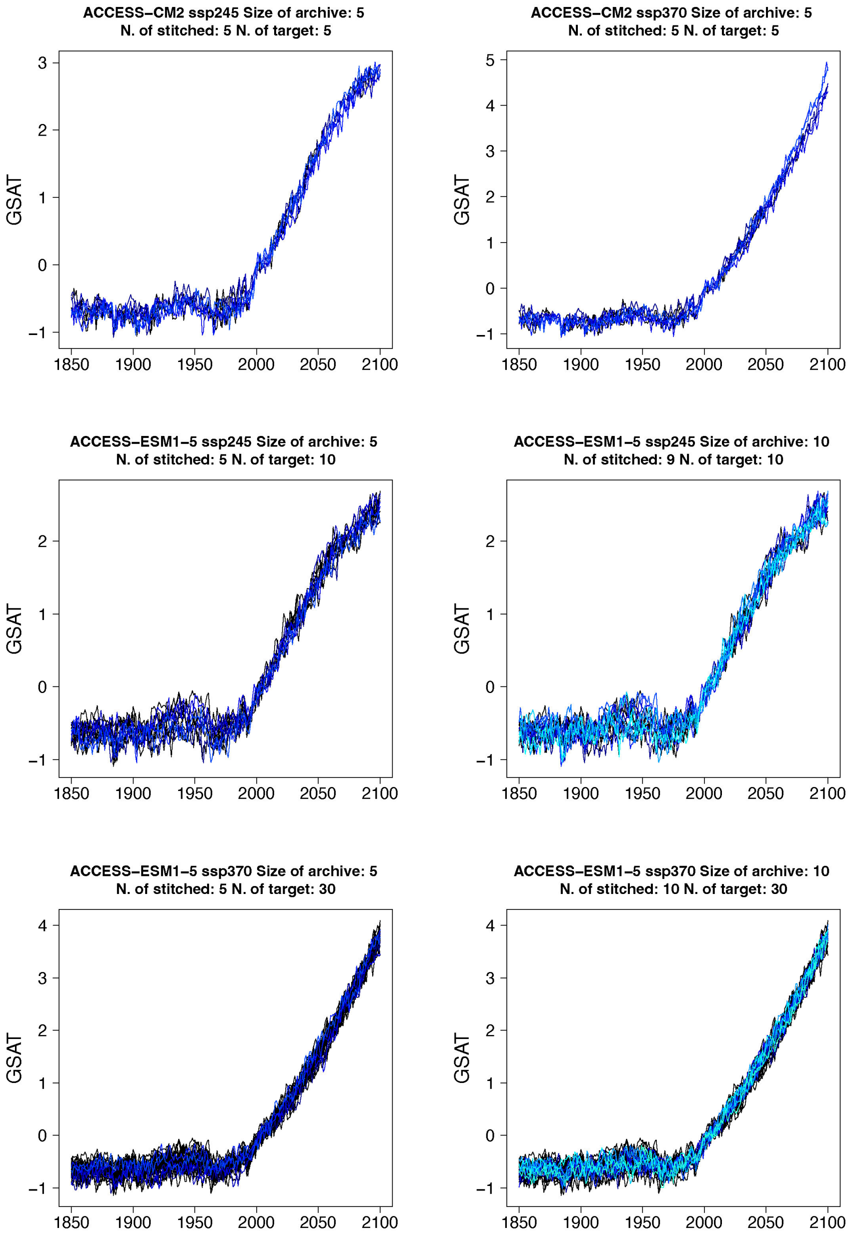

Figure E1. Examples of enriched ensembles of GSAT time series for ESMs in the PANGEO archive that have at least 5 trajectories available over the 21$^{\text{st}}$ century. As in the figures in Appendix A, warmer colors indicate a larger number of stitched trajectories in the figure, as the title also describes.

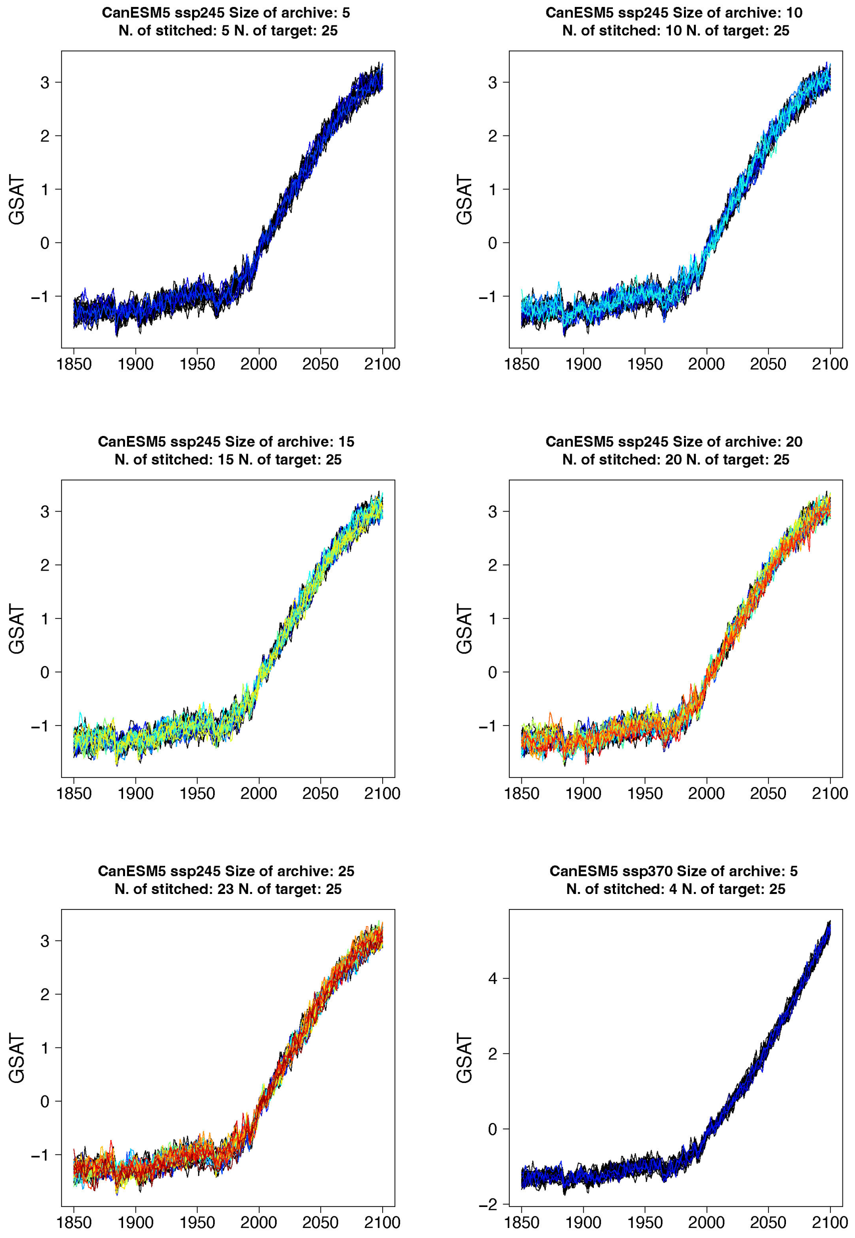

Figure E2. Examples of enriched ensembles of GSAT time series for ESMs in the PANGEO archive that have at least 5 trajectories available over the 21$^{\text{st}}$ century. As in the figures in Appendix A, warmer colors indicate a larger number of stitched trajectories in the figure, as the title also describes.

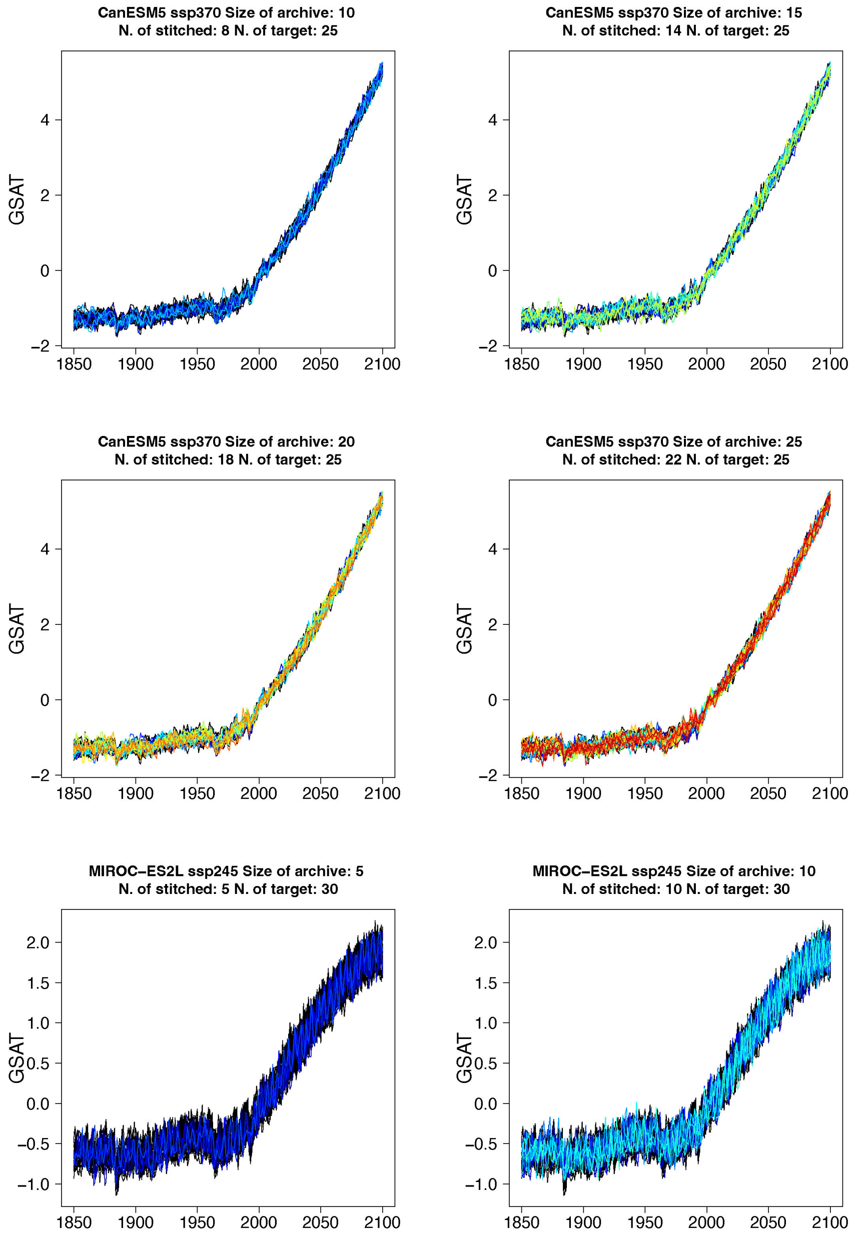

Figure E3. Examples of enriched ensembles of GSAT time series for ESMs in the PANGEO archive that have at least 5 trajectories available over the 21$^{\text{st}}$ century. As in the figures in Appendix A, warmer colors indicate a larger number of stitched trajectories in the figure, as the title also describes.

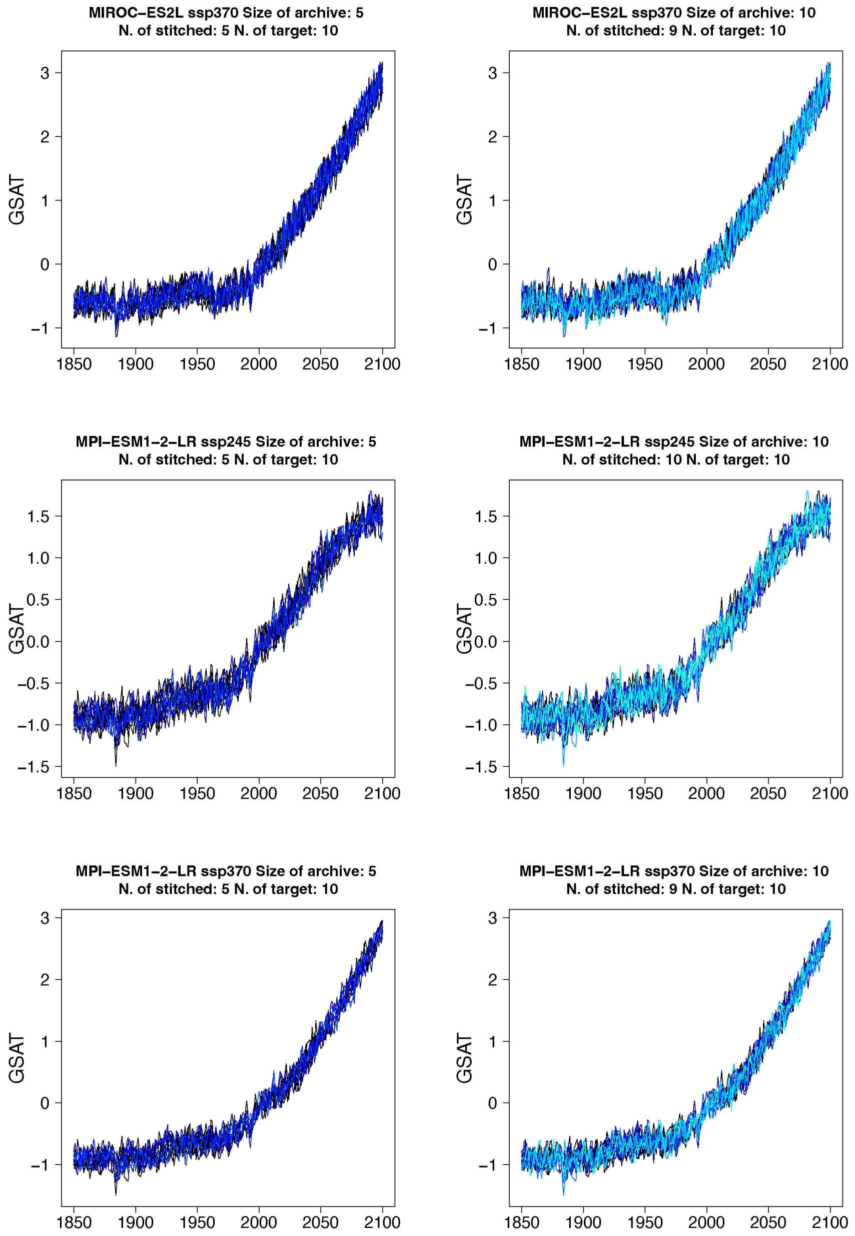

Figure E4. Examples of enriched ensembles of GSAT time series for ESMs in the PANGEO archive that have at least 5 trajectories available over the 21$^{\text{st}}$ century. As in the figures in Appendix A, warmer colors indicate a larger number of stitched trajectories in the figure, as the title also describes.

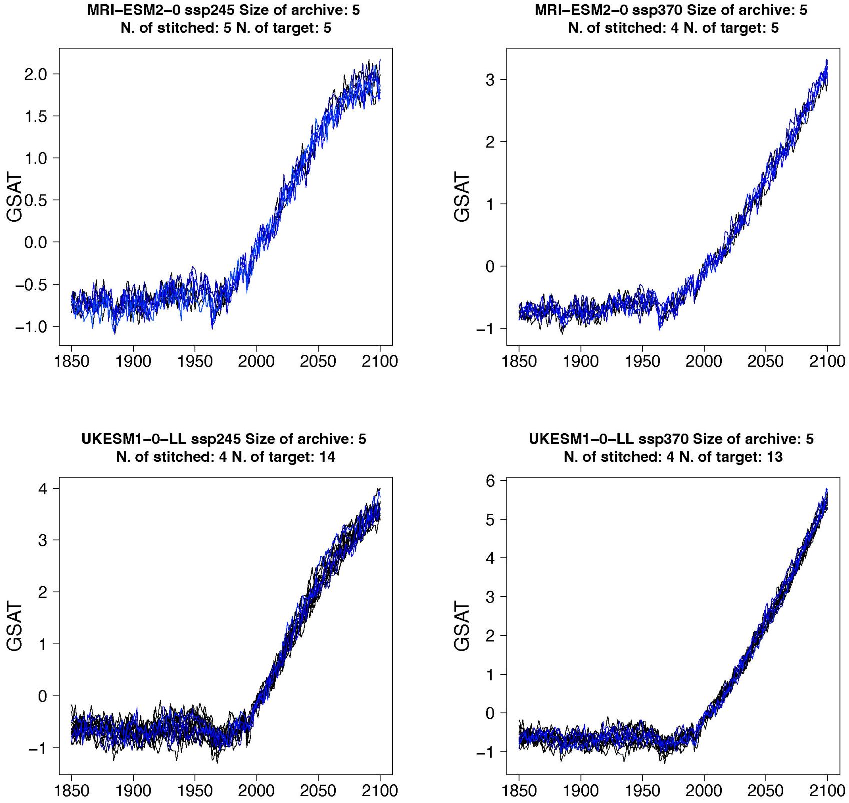

Figure E5. Examples of enriched ensembles of GSAT time series for ESMs in the PANGEO archive that have at least 5 trajectories available over the 21$^{\mathrm{st}}$ century. As in the figures in Appendix A, warmer colors indicate a larger number of stitched trajectories in the figure, as the title also describes.

Appendix F: Table of E_1 and E_2 metrics for enriched ensemble exercise performed using only bracketing scenarios SSP1-2.6 and SSP5-8.5.

Table F1. The two components of the Er metric, E_1 and E_2, computed for several experiments across ESMs, scenarios and number of available archive trajectories from which to create the stitched ensembles. Numbers in columns 4 through 9 represent fractions of the target ensemble standard deviation (see formula 1).

Model	Scenario	Archive	Target	Stitched		E_1			E_2	
		Size	Members	Members	2010	2050	2090	2010	2050	2090
ACCESS-CM2	ssp245	5	5	4	0.07	0.12	0.38	1.05	0.50	2.01
ACCESS-ESM1-5	ssp245	5	10	1	0.68	0.18	0.02	1.20	0.67	0.75
CanESM5	ssp245	5	25	2	0.10	0.44	1.24	1.20	1.09	6.94
MIROC-ES2L	ssp245	5	30	2	0.00	2.57	0.61	0.96	1.43	0.70
MPI-ESM1-2-LR	ssp245	5	10	2	0.47	0.06	1.22	1.31	1.50	0.77
MRI-ESM2-0	ssp245	5	5	1	0.50	0.09	6.34	0.75	1.76	2.49
UKESM1-0-LL	ssp245	5	14	1	0.04	0.00	6.57	0.47	0.56	1.69
ACCESS-ESM1-5	ssp245	10	10	3	0.06	0.06	0.55	0.55	1.57	1.43
CanESM5	ssp245	10	25	5	0.00	0.00	3.19	1.41	0.81	7.67
MIROC-ES2L	ssp245	10	30	2	1.53	0.90	0.24	0.82	1.06	2.06
MPI-ESM1-2-LR	ssp245	10	10	5	0.06	0.09	0.42	0.84	1.10	2.43
CanESM5	ssp245	15	25	3	0.48	0.01	0.16	1.35	1.03	3.66
CanESM5	ssp245	20	25	6	0.01	0.18	5.27	1.07	1.09	5.22
CanESM5	ssp245	25	25	7	0.01	0.05	4.30	0.84	1.00	4.34
ACCESS-CM2	ssp370	5	5	3	0.07	0.06	0.06	1.90	2.61	1.34
ACCESS-ESM1-5	ssp370	5	30	4	0.07	0.52	0.11	0.51	1.23	1.13
CanESM5	ssp370	5	25	2	0.00	1.85	0.22	1.12	0.28	2.48
MIROC-ES2L	ssp370	5	10	3	1.41	0.27	0.14	0.91	1.63	1.57
MPI-ESM1-2-LR	ssp370	5	10	4	0.40	0.07	0.02	0.81	1.73	2.39
MRI-ESM2-0	ssp370	5	5	3	0.12	0.12	0.08	1.27	1.24	1.63
UKESM1-0-LL	ssp370	5	13	2	0.21	0.30	0.09	0.70	0.84	1.78
ACCESS-ESM1-5	ssp370	10	30	5	0.07	0.00	0.01	0.96	1.24	2.06
CanESM5	ssp370	10	25	2	1.29	0.16	1.13	1.53	0.89	0.68
MIROC-ES2L	ssp370	10	10	4	0.29	0.00	0.05	1.06	1.16	1.08
MPI-ESM1-2-LR	ssp370	10	10	4	0.03	0.24	0.05	1.23	1.84	1.87
CanESM5	ssp370	15	25	8	0.00	0.15	0.81	0.67	2.07	1.94
CanESM5	ssp370	20	25	7	0.02	0.31	0.00	1.08	1.32	2.53
CanESM5	ssp370	25	25	6	0.00	0.00	1.04	1.04	1.31	0.84

Author contributions. CT conceived the general approach. AS and KD significantly refined it, trouble-shot it and implemented it in Python. All authors collaborated in testing the results. CT led this paper write-up with AS and KD contributing to it.

Competing interests. All authors declare no conflict of interest.

Acknowledgements. This work was conducted with the support of the U.S. Department of Energy, Office of Science, as part of research in MultiSector Dynamics, Earth and Environmental System Modeling Program. CT was also supported by the CASCADE project, funded by the U.S. Department of Energy, Office of Science, Office of Biological and Environmental Research, as part of the Regional and Global Modeling and Analysis Program. The Pacific Northwest National Laboratory is operated by Battelle for the US Department of Energy (contract no. DE-AC05-76RLO1830). Lawrence Berkeley National Laboratory is operated by the US Department of Energy (contract no. DE340AC02-05CH11231).

References

Beusch, L., Gudmundsson, L., and Seneviratne, S. I.: Emulating Earth system model temperatures with MESMER: from global mean temperature trajectories to grid-point-level realizations on land, Earth System Dynamics, 11, 139–159, https://doi.org/10.5194/esd-11-139-2020, 2020.

Beusch, L., Nicholls, Z., Gudmundsson, L., Hauser, M., Meinshausen, M., and Seneviratne, S. I.: From emission scenarios to spatially resolved projections with a chain of computationally efficient emulators: MAGICC (v7.5.1) – MESMER (v0.8.1) coupling, Geoscientific Model Development Discussions, 2021, 1–26, https://doi.org/10.5194/gmd-2021-252, 2021.

Blackport, R. and Kushner, P. J.: The Transient and Equilibrium Climate Response to Rapid Summertime Sea Ice Loss in CCSM4, Journal of Climate, 29, 401 – 417, https://doi.org/10.1175/JCLI-D-15-0284.1, 2016.

Castruccio, S., McInerney, D., Stein, M. L., Liu Crouch, F., Jacob, R., and Moyer, E.: Statistical emulation of climate model projections based on precomputed GCM runs, Journal of Climate, 27, 1829–1844, https://doi.org/https://doi.org/10.1175/JCLI-D-13-00099.1, 2014.

Chen, D., Rojas, M., Samset, B., Cobb, K., Diongue Niang, A., Edwards, P., Emori, S., Faria, S., Hawkins, E., Hope, P., Huybrechts, P., Meinshausen, M., Mustafa, S., Plattner, G.-K., and Tréguier, A.-M.: Framing, Context, and Methods., in: Climate Change 2021: The Physical Science Basis. Contribution of Working Group I to the Sixth Assessment Report of the Intergovernmental Panel on Climate Change, edited by Masson-Delmotte, V., Zhai, P., Pirani, A., Connors, S., Pèan, C., Berger, S., Caud, N., Chen, Y., Goldfarb, L., Gomis, M., Huang, M., Leitzell, K., Lonnoy, E., Matthews, J., Maycock, T. B., Waterfield, T. an Yelekci, O., Yu, R., and Zhou, B., Intergovernmental Panel on Climate Change, p. in press, Cambridge University Press, United Kingdom, 2021.

Eyring, V., Bony, S., Meehl, G. A., Senior, C. A., Stevens, B., Stouffer, R. J., and Taylor, K. E.: Overview of the Coupled Model Intercomparison Project Phase 6 (CMIP6) experimental design and organization, Geoscientific Model Development, 9, 1937–1958, https://doi.org/10.5194/gmd-9-1937-2016, 2016.

Gidden, M. J., Riahi, K., Smith, S. J., Fujimori, S., Luderer, G., Kriegler, E., van Vuuren, D. P., van den Berg, M., Feng, L., Klein, D., Calvin, K., Doelman, J. C., Frank, S., Fricko, O., Harmsen, M., Hasegawa, T., Havlik, P., Hilaire, J., Hoesly, R., Horing, J., Popp, A., Stehfest, E., and Takahashi, K.: Global emissions pathways under different socioeconomic scenarios for use in CMIP6: a dataset of harmonized emissions trajectories through the end of the century, Geoscientific Model Development, 12, 1443–1475, https://doi.org/10.5194/gmd-12-1443-2019, 2019.

Gutiérrez, J., Jones, R., Narisma, G., Alves, L., Amjad, M., Gorodetskaya, I. V., Grose, M., Klutse, N., Krakovska, S., Li, J., Martínez-Castro, D., Mearns, L., Mernild, S., Ngo-Duc, T., van den Hurk, B., and Yoon, J.-H.: Atlas., in: Climate Change 2021: The Physical Science Basis. Contribution of Working Group I to the Sixth Assessment Report of the Intergovernmental Panel on Climate Change, edited by Masson-Delmotte, V., Zhai, P., Pirani, A., Connors, S., Pèan, C., Berger, S., Caud, N., Chen, Y., Goldfarb, L., Gomis, M., Huang, M., Leitzell, K., Lonnoy, E., Matthews, J., Maycock, T. B., Waterfield, T. an Yelekci, O., Yu, R., and Zhou, B., Intergovernmental Panel on Climate Change, p. in press, Cambridge University Press, United Kingdom, 2021.

Hartin, C. A., Patel, P., Schwarber, A., Link, R. P., and Bond-Lamberty, B. P.: A simple object-oriented and open-source model for scientific and policy analyses of the global climate system: Hector v1.0, Geoscientific Model Development, 8, 939–955, https://doi.org/10.5194/gmd-8-939-2015, 2015.

Hausfather, Z. and Peters, G. P.: Emissions–the 'business as usual'story is misleading, Nature, pp. 618–620, https://doi.org/https://doi.org/10.1038/d41586-020-00177-3, 2020.

Hawkins, E. and Sutton, R.: The Potential to Narrow Uncertainty in Regional Climate Predictions, Bulletin of the American Meteorological Society, 90, 1095 – 1108, https://doi.org/10.1175/2009BAMS2607.1, 2009.

Huntingford, C. and Cox, P. M.: An analogue model to derive additional climate change scenarios from existing GCM simulations, Climate Dynamics, 16, 575–586, https://doi.org/10.1007/s003820000067, 2000.

Hurtt, G. C., Chini, L., Sahajpal, R., Frolking, S., Bodirsky, B. L., Calvin, K., Doelman, J. C., Fisk, J., Fujimori, S., Klein Goldewijk, K., Hasegawa, T., Havlik, P., Heinimann, A., Humpenöder, F., Jungclaus, J., Kaplan, J. O., Kennedy, J., Krisztin, T., Lawrence, D., Lawrence, P., Ma, L., Mertz, O., Pongratz, J., Popp, A., Poulter, B., Riahi, K., Shevliakova, E., Stehfest, E., Thornton, P., Tubiello, F. N., van Vuuren, D. P., and Zhang, X.: Harmonization of global land use change and management for the period 850–2100 (LUH2) for CMIP6, Geoscientific Model Development, 13, 5425–5464, https://doi.org/10.5194/gmd-13-5425-2020, 2020.

James, R., Washington, R., Schleussner, C.-F., Rogelj, J., and Conway, D.: Characterizing half-a-degree difference: a review of methods for identifying regional climate responses to global warming targets, Wiley Interdisciplinary Reviews: Climate Change, 8, e457, 2017.

King, A. D., Knutti, R., Uhe, P., Mitchell, D. M., Lewis, S. C., Arblaster, J. M., and Freychet, N.: On the Linearity of Local and Regional Temperature Changes from 1.5°C to 2°C of Global Warming, Journal of Climate, 31, 7495–7514, https://doi.org/10.1175/JCLI-D-17-0649.1, 2018.

King, A. D., Lane, T. P., Henley, B. J., and Brown, J. R.: Global and regional impacts differ between transient and equilibrium warmer worlds, Nature Climate Change, 10, 42–47, https://doi.org/10.1038/s41558-019-0658-7, 2020.

Lange, S.: Trend-preserving bias adjustment and statistical downscaling with ISIMIP3BASD (v1.0), Geoscientific Model Development, 12, 3055–3070, https://doi.org/10.5194/gmd-12-3055-2019, 2019.

Lee, J.-Y., Marotzke, J., Bala, G., Cao, L., Corti, S., Dunne, J., Engelbrecht, F., Fischer, E., Fyfe, J., Jones, C., Maycock, A., Mutemi, J., Ndiaye, O., Panickal, S., and Zhou, T.: Future Global Climate: Scenario-Based Projections and Near-Term Information., in: Climate Change 2021: The Physical Science Basis. Contribution of Working Group I to the Sixth Assessment Report of the Intergovernmental Panel on Climate Change, edited by Masson-Delmotte, V., Zhai, P., Pirani, A., Connors, S., Pèan, C., Berger, S., Caud, N., Chen, Y., Goldfarb, L., Gomis, M., Huang, M., Leitzell, K., Lonnoy, E., Matthews, J., Maycock, T. B., Waterfield, T. an Yelekci, O., Yu, R., and Zhou, B., Intergovernmental Panel on Climate Change, p. in press, Cambridge University Press, United Kingdom, 2021.

Lehner, F., Deser, C., Maher, N., Marotzke, J., Fischer, E. M., Brunner, L., Knutti, R., and Hawkins, E.: Partitioning climate projection uncertainty with multiple large ensembles and CMIP5/6, Earth System Dynamics, 11, 491–508, https://doi.org/10.5194/esd-11-491-2020, 2020.

Lenssen, N. J. L., Goddard, L., and Mason, S.: Seasonal Forecast Skill of ENSO Teleconnection Maps, Weather and Forecasting, 35, 2387 – 2406, https://doi.org/10.1175/WAF-D-19-0235.1, 2020.

Link, R., Snyder, A., Lynch, C., Hartin, C., Kravitz, B., and Bond-Lamberty, B.: Fldgen v1. 0: an emulator with internal variability and space–time correlation for Earth system models, Geoscientific Model Development (Online), 12, 1477–1489, 2019.

Liu, G., Peng, S., Huntingford, C., and Xi, Y.: A new precipitation emulator (PREMU v1.0) for lower complexity models, Geoscientific Model Development Discussions, 2022, 1–30, https://doi.org/10.5194/gmd-2022-144, 2022.

Manabe, S., Stouffer, R. J., Spelman, M. J., and Bryan, K.: Transient Responses of a Coupled Ocean–Atmosphere Model to Gradual Changes of Atmospheric CO2. Part I. Annual Mean Response, Journal of Climate, 4, 785 – 818, https://doi.org/10.1175/1520-0442(1991)004<0785:TROACO>2.0.CO;2, 1991.

Mason, S. J. and Goddard, L.: Probabilistic precipitation anomalies associated with ENSO, Bull. Amer. Meteor. Soc., 82, 619–638, 2001.

Masson-Delmotte, V., Zhai, P., Pörtner, H., Roberts, D., Skea, J., Shukla, P., and et al., eds.: IPCC (2018). Global warming of 1.5°C. An IPCC Special Report on the impacts of global warming of 1.5°C above pre-industrial levels and related global greenhouse gas emission pathways, in the context of strengthening the global response to the threat of climate change, sustainable development, and efforts to eradicate poverty, World Meteorological Organization, Geneva, Switzerland, 2018.

Meinshausen, M., Raper, S. C. B., and Wigley, T. M. L.: Emulating coupled atmosphere-ocean and carbon cycle models with a simpler model, MAGICC6 Part 1: Model description and calibration, Atmospheric Chemistry and Physics, 11, 1417–1456, https://doi.org/10.5194/acp-11-1417-2011, 2011.

Meinshausen, M., Nicholls, Z. R. J., Lewis, J., Gidden, M. J., Vogel, E., Freund, M., Beyerle, U., Gessner, C., Nauels, A., Bauer, N., Canadell, J. G., Daniel, J. S., John, A., Krummel, P. B., Luderer, G., Meinshausen, N., Montzka, S. A., Rayner, P. J., Reimann, S., Smith, S. J., van den Berg, M., Velders, G. J. M., Vollmer, M. K., and Wang, R. H. J.: The shared socio-economic pathway (SSP) greenhouse gas concentrations and their extensions to 2500, Geoscientific Model Development, 13, 3571–3605, https://doi.org/10.5194/gmd-13-3571-2020, 2020.

Nath, S., Lejeune, Q., Beusch, L., Seneviratne, S. I., and Schleussner, C.-F.: MESMER-M: an Earth system model emulator for spatially resolved monthly temperature, Earth System Dynamics, 13, 851–877, https://doi.org/10.5194/esd-13-851-2022, 2022.

O'Neill, B. C., Tebaldi, C., van Vuuren, D. P., Eyring, V., Friedlingstein, P., Hurtt, G., Knutti, R., Kriegler, E., Lamarque, J.-F., Lowe, J., Meehl, G. A., Moss, R., Riahi, K., and Sanderson, B. M.: The Scenario Model Intercomparison Project (ScenarioMIP) for CMIP6, Geoscientific Model Development, 9, 3461–3482, https://doi.org/10.5194/gmd-9-3461-2016, 2016.

Quilcaille, Y., Gudmundsson, L., Beusch, L., Hauser, M., and Seneviratne, S. I.: Showcasing MESMER-X: Spatially resolved emulation of annual maximum temperatures of Earth System Models, Earth and Space Science Open Archive, p. 18, https://doi.org/10.1002/essoar.10511207.1, 2022.

Santer, B. D., Wigley, T. M. L., Schlesinger, M. E., and Mitchell, J.: DEVELOPING CLIMATE SCENARIOS FROM EQUILIBRIUM GCM RESULTS, Report of the Max Plank Institut f ur Meteorologie, 47, 29, 1990.

Schlosser, C. A., Gao, X., Strzepek, K., Sokolov, A., Forest, C. E., Awadalla, S., and Farmer, W.: Quantifying the Likelihood of Regional Climate Change: A Hybridized Approach, Journal of Climate, 26, 3394–3414, https://doi.org/10.1175/JCLI-D-11-00730.1, 2013.

Seneviratne, S., Zhang, X., Adnan, M., Badi, W., Dereczynski, C., Di Luca, A., Ghosh, S., Iskandar, I., Kossin, J., Lewis, S., Otto, F., Pinto, I., Satoh, M., Vicente-Serrano, S., Wehner, M., and Zhou, B.: Weather and Climate Extreme Events in a Changing Climate., in: Climate Change 2021: The Physical Science Basis. Contribution of Working Group I to the Sixth Assessment Report of the Intergovernmental Panel on Climate Change, edited by Masson-Delmotte, V., Zhai, P., Pirani, A., Connors, S., Pèan, C., Berger, S., Caud, N., Chen, Y., Goldfarb, L., Gomis, M., Huang, M., Leitzell, K., Lonnoy, E., Matthews, J., Maycock, T. B., Waterfield, T. an Yelekci, O., Yu, R., and Zhou, B., Intergovernmental Panel on Climate Change, p. in press, Cambridge University Press, United Kingdom, 2021.

Tebaldi, C., Armbruster, A., Engler, H. P., and Link, R.: Emulating climate extreme indices, Environmental Research Letters, 15, 074 006, https://doi.org/10.1088/1748-9326/ab8332, 2020.

Tebaldi, C., Debeire, K., Eyring, V., Fischer, E., Fyfe, J., Friedlingstein, P., Knutti, R., Lowe, J., O'Neill, B., Sanderson, B., van Vuuren, D., Riahi, K., Meinshausen, M., Nicholls, Z., Tokarska, K. B., Hurtt, G., Kriegler, E., Lamarque, J.-F., Meehl, G., Moss, R., Bauer, S. E., Boucher, O., Brovkin, V., Byun, Y.-H., Dix, M., Gualdi, S., Guo, H., John, J. G., Kharin, S., Kim, Y., Koshiro, T., Ma, L., Olivié, D., Panickal, S., Qiao, F., Rong, X., Rosenbloom, N., Schupfner, M., Séférian, R., Sellar, A., Semmler, T., Shi, X., Song, Z., Steger, C., Stouffer, R., Swart, N., Tachiiri, K., Tang, Q., Tatebe, H., Voldoire, A., Volodin, E., Wyser, K., Xin, X., Yang, S., Yu, Y., and Ziehn, T.: Climate model projections from the Scenario Model Intercomparison Project (ScenarioMIP) of CMIP6, Earth System Dynamics, 12, 253–293, https://doi.org/10.5194/esd-12-253-2021, 2021.

van Vuuren, D. P., Kriegler, E., O'Neill, B. C., Ebi, K. L., Riahi, K., Carter, T. R., Edmonds, J., Hallegatte, S., Kram, T., Mathur, R., and Winkler, H.: A new scenario framework for Climate Change Research: scenario matrix architecture, Climatic Change, 122, 373–386, https://doi.org/10.1007/s10584-013-0906-1, 2014.